# KNOWLEDGEABLE LANGUAGE MODELS AS BLACK-BOX OPTIMIZERS FOR PERSONALIZED MEDICINE

**Anonymous authors**Paper under double-blind review

000

001

002003004

010 011

012

013

014

015

016

017

018

019

021

025

026

027 028 029

030

032

033

034

035

036

037

040

041

042

043

044

046

047

051

052

#### **ABSTRACT**

The goal of personalized medicine is to discover a treatment regimen that optimizes a patient's clinical outcome based on their personal genetic and environmental factors. However, candidate treatments cannot be arbitrarily administered to the patient to assess their efficacy; we often instead have access to an in silico surrogate model that approximates the true fitness of a proposed treatment. Unfortunately, such surrogate models have been shown to fail to generalize to previously unseen patient-treatment combinations. We hypothesize that domainspecific prior knowledge—such as medical textbooks and biomedical knowledge graphs—can provide a meaningful alternative signal of the fitness of proposed treatments. To this end, we introduce LLM-based Entropy-guided Optimization with kNowledgeable priors (LEON), a mathematically principled approach to leverage large language models (LLMs) as black-box optimizers without any taskspecific fine-tuning, taking advantage of their ability to contextualize unstructured domain knowledge to propose personalized treatment plans in natural language. In practice, we implement LEON via 'optimization by prompting,' which uses LLMs as stochastic engines for proposing treatment designs. Experiments on real-world optimization tasks show LEON outperforms both traditional and LLMbased methods in proposing individualized treatments for patients.

## 1 Introduction

**Personalized medicine** is a clinical strategy that seeks to individualize treatment strategies based on a patient's unique genetic and environmental features (Gutowski et al., 2023; Mizan & Taghipour, 2022; Adams et al., 2022; Consortium, 2009). Through reasoning about a patient, previously observed patients, and existing medical knowledge and literature, clinicians seek to determine an optimal treatment (Mehandru et al., 2025). Such a task can be framed as a conditional optimization problem, where the goal is to design a treatment regimen—conditioned on the patient's unique features—that optimizes their clinical outcome. However, applying traditional optimization methods in this setting presents significant challenges. First, ground-truth design evaluations are costly; it is infeasible to assess the efficacy of novel treatment options directly in human subjects. Evaluating newly proposed treatment regimens may therefore be difficult or even impossible. To overcome this limitation, a common approach is to instead leverage feedback from a surrogate for the ground-truth objective, such as a machine learning model or digital twin, to estimate the quality of a proposed treatment for the patient (Kuang et al., 2024; Katsoulakis et al., 2024). However, such surrogate models are frequently imperfect and used on out-of-distribution patients (De Domenico et al., 2025). Certain populations are systematically under-enrolled in clinical studies (Costa et al., 2023; Walker et al., 2022; Islam et al., 2024; Casey et al., 2022; Pittell et al., 2023), and so black-box surrogate functions often fail to accurately predict design fitness for different patient populations (Taylor et al., 2022; Kirtane & Lee, 2017; Smith-Graziani & Flowers, 2021; Larkin et al., 2022).

A natural question is whether designing better surrogate models can overcome these limitations, with the hope that more accurate proxies of the ground-truth objective will yield better optimized therapeutic proposals. For example, Kuang et al. (2024) enforce a physics-based prior on a learned digital twin model, and Yu et al. (2021) assume the objective is locally smooth over the design space. However, in many real-world applications we cannot specify the surrogate model—the underlying mechanisms behind patient responses to treatment may be under-specified or even entirely unknown (Kuang et al., 2024), and building accurate digital twin models is often limited by the availability of

055

056

058

060

061

062

063

064 065

067

068

069

070 071 072

073

074

075

076

077

079

081 082

084

085

090

092

093

094

095

096

097

098

099

102

103

105

106

107

Figure 1: <u>LLM</u>-based <u>Entropy-guided Optimization with kNowledgeable priors (LEON).</u> We use LLMs as zero-shot conditional optimizers to propose personalized treatment designs at the patient level. (a) The LLM is prompted with prior knowledge and the history of previously proposed designs and their predicted scores to (b) propose a new batch of designs. (c) These candidates are evaluated using LEON, and then (d) cached as context to the LLM in subsequent iterations.

real patient data and patient privacy concerns (De Domenico et al., 2025). In these settings, we may only think of both the surrogate and underlying ground-truth functions as **black-box models**.

Recent work (Reinhart & Statt, 2024; Yang et al., 2024a; Chen et al., 2025a; Ma et al., 2024a; Nasir et al., 2024; Song et al., 2024) on large language models (LLMs) have explored their emerging capabilities in *black-box optimization*, where the goal is to propose a design x that maximizes a black-box objective function f(x). In particular, modern LLMs have been shown to solve zero-shot optimization problems in domains such as mathematics (Nadkarni et al., 2021; Novikov et al., 2025) and computer science (Garg et al., 2022; Guo et al., 2024c; Fu et al., 2024; Ma et al., 2024b). However, in these settings the objective function is almost always evaluable with minimal cost (i.e., using a code interpreter or formal verification tools)—unlike in clinical patient-centered tasks.

In this work, we introduce a method to leverage LLMs as black-box optimizers in clinical medicine. Our core hypothesis is that by leveraging domain-specific prior knowledge, LLM-based optimizers can overcome the limitations associated with out-of-distribution surrogate model predictions during optimization. More explicitly, our contributions are as follows:

- 1. **Formulating personalized medicine as a black-box optimization problem.** We propose a mathematically principled approach to formulate personalized medicine as a conditional black-box optimization problem, where the goal is to find an optimal treatment strategy conditioned on a set of input patient covariates that optimizes a target outcome metric.
- 2. **Constraining the optimization problem.** Existing surrogate models are often imperfect proxies of costly ground-truth objectives in personalized medicine. To overcome this, we introduce a set of intuitive constraints to our initial black-box optimization problem. Our constraints limit the optimization trajectory to treatment designs that (1) are likely to have reliable predictions from the surrogate model; and (2) are consistently proposed by the LLM as high-quality treatments according to relevant domain knowledge.
- 3. **Deriving a solution to the constrained optimization problem.** We derive a computationally tractable solution to our proposed re-formulation of personalized medicine as a constrained black-box optimization problem. Our approach fundamentally relies on the statistical analysis of the distribution of proposed designs and the use of an adversarial source critic model during optimization. We refer to our method as <u>LLM-based Entropy-guided Optimization with kNowledgeable priors (LEON)</u> (Fig. 1). We implement LEON via 'optimization-by-prompting' (Yang et al., 2024a), using the LEON-defined objective to score candidate designs. In this setting, the LLM functions as a stochastic treatment recommendation system that seeks to iteratively propose higher scoring designs.
- 4. **Using LEON to solve real-world personalized medicine tasks.** We demonstrate how LEON can be used to solve conditional optimization problems over both discrete and continuous search spaces. Comparing with 10 other baseline methods, we find that LEON achieves an average rank of <u>1.2</u> on 5 representative treatment design problems.

# 2 RELATED WORK

**LLMs as optimizers.** A growing body of work has explored the ability of generalist LLMs to solve domain-specific optimization tasks (Reinhart & Statt, 2024; Liu et al., 2024b; Yang et al., 2024a; Ma et al., 2024a; Song et al., 2024). For instance, Chen et al. (2025a) fine-tune language models for antibody protein design. However, unlike in medicine, accurate molecular dynamic simulations (Albaugh & Gingrich, 2022; Ho et al., 2024), state-of-the-art foundation models (Novikov et al., 2025; Wang et al., 2024b), and scalable experimental setups (Yang et al., 2025; Rix et al., 2020; Johnston et al., 2024) have made online optimization methods empirically effective in this domain. Similarly, methods like those introduced by Shojaee et al. (2025); Shypula et al. (2024); Ma et al. (2024b) introduce methods to use LLMs for code optimization according to an objective that is easily verifiable by modern computer systems. Novikov et al. (2025) and Romera-Paredes et al. (2024) use LLMs to propose new solutions to resource allocation and extremal combinatoric problems. Chen et al. (2023a); Nasir et al. (2024); Ji et al. (2025); Chiquier et al. (2024) separately use LLMs to design new machine learning models for neural architecture search, Zeng et al. (2024); Hong et al. (2025) for tensor network design, and Akioyamen et al. (2024) for database query optimization without any model fine-tuning. However, unlike the problem of personalized treatment design, these applications are all examples of *unconditional* optimization tasks.

**Optimization under distribution shift.** A separate body of work has considered the problem of leveraging traditional (i.e., non-LLM-based) optimizers under distribution shift. Trabucco et al. (2021) leverages gradient data to update the surrogate model over the course of an optimization experiment to act as a conservative lower bound of the ground-truth function, Yu et al. (2021) imposes a smoothness prior on the surrogate model over the design space, and Chen et al. (2023b) leverages a retrieval-based approach to build a more robust surrogate model. However, such methods assume control over the design of the surrogate model—an assumption that fails in black-box optimization. Other techniques forgo learning a surrogate model altogether Mashkaria et al. (2023); Krishnamoorthy et al. (2023); however, such methods rely on learning from multiple design observations in a single context, which do not exist in *conditional* optimization tasks like those in personalized medicine. Finally, Angermueller et al. (2020) and Williams (1992) formulate optimization as a reinforcement learning problem; however, we do not consider sequential decision-making tasks in our work.

## 3 BACKGROUND AND PRELIMINARIES

Entropy and equivalence classes. Entropy is a fundamental concept in information theory that quantifies the relative uncertainty associated with the variables of a system. Prior work from Qiu et al. (2025); Farquhar et al. (2024); Kuhn et al. (2023) has examined how the entropy of the distribution of an LLM's outputs can be used to estimate the model's epistemic uncertainty. Briefly, if a non-deterministic model consistently returns equivalent responses to the same prompt—corresponding to a low-entropy distribution of outputs—we can be more confident in its own certainty of its response. Such methods have been shown to improve question answering (Nikitin et al., 2024; Kuhn et al., 2023), hallucination detection (Farquhar et al., 2024), and document retrieval (Qiu et al., 2025).

Crucially, the definition of what constitutes a set of 'equivalent' responses is predicated on the existence of an **equivalence relation**  $\sim$ : two outputs x, x' are equivalent iff  $x \sim x'$ . Any valid equivalence relation partitions the input space into a set of N disjoint *equivalence classes*  $[x]_i$ , where  $[x]_i = \{x' \in \mathcal{X} : x' \sim x\}$  and  $\bigcup_{i=1}^N [x]_i = \mathcal{X}^1$ . We denote this *quotient set* of these N equivalence classes by  $\mathcal{X}/\sim$ . The entropy with respect to  $\sim$  is given by  $\mathcal{H}_{\sim} := -\sum_{i=1}^N p_i \log p_i$ , where  $p_i := |[x]_i|/|\mathcal{X}|$  is the fractional occupancy of equivalence class  $[x]_i$ .

Adversarial supervision in optimization. A central challenge in optimization under distribution shift lies in the absence of direct access to the ground-truth objective function during optimization. In practice, optimization can instead be performed against a surrogate model, which may be inaccurate in out-of-distribution (OOD) regions inevitably explored during the optimization process. Naïvely optimizing against a surrogate model can therefore produce candidate solutions that appear promising according to the surrogate, but perform poorly when ultimately evaluated using the ground-truth

 $<sup>^{1}</sup>$ In this work, we assume that the number of equivalence classes N is finite. This is a relatively weak assumption for most real-world, computable optimization problems (Kozen, 1997).

objective. To mitigate this, recent works bound the 1-Wasserstein distance between the distribution of real designs used to train the surrogate model and that of generated candidates (Yao et al., 2025b; 2024). Such a constraint provides theoretical guarantees on the generalization error of the surrogate model, effectively reducing the extent of extrapolation (**Supplementary Theorem D.1**).

However, directly computing the 1-Wasserstein distance between probability distributions poses significant computational challenges, as classical algorithms can scale as  $\mathcal{O}(n^3)$  in the number of samples (Kuhn, 1955). To address this, one can exploit Kantorovich & Rubinstein (1958) to recast the 1-Wasserstein distance as a supremum over a class of Lipschitz functions:

$$W_1(p,q) := \mathbb{E}_{x \sim p(x)}[c^*(x)] - \mathbb{E}_{x \sim q(x)}[c^*(x)]$$
(1)

where p(x) (resp., q(x)) is the (empirical) distribution of the real (resp., generated) designs and  $c^*(x) := \arg\max_{\|c\|_L \le 1} \left[ \mathbb{E}_{x \sim p(x)}[c^*(x)] - \mathbb{E}_{x \sim q(x)}[c^*(x)] \right]$ . One can think of the function  $c^*$  as an adversarial source critic that learns to discriminate the source distribution of an input x. The learned function  $c^*(x)$  thereby assigns high (resp., low) value to inputs that are likely to have been sampled from p(x) (resp., q(x)). Such an approach has been shown to reduce the extrapolation of learned models in generative adversarial learning (Arjovsky et al., 2017; Yao et al., 2025b; 2024).

## 4 Entropy-Guided Optimization with Knowledgeable Priors

#### 4.1 PROBLEM FORMULATION

The task of finding an optimal patient treatment strategy can be formulated as an conditional black-box optimization problem, where the goal is to find an optimal distribution q(x) according to

$$\arg\max_{q(x)\in p(\mathcal{X})} \quad \mathbb{E}_{x\sim q(x)}[f(x;z)] \tag{2}$$

where  $\mathcal{X}$  is the set of all possible treatments,  $p(\mathcal{X})$  the set of all valid probability measures over  $\mathcal{X}$ , x any particular treatment design, and  $z \in \mathcal{Z}$  the patient  $conditioning\ vector$ . For example,  $\mathcal{X}$  might be a set of medications, z a patient's personal health data sampled from a distribution p(z), and f the patient's therapeutic response to a medication. In this setting, the objective is not to find a universally optimal design, but rather to identify an optimal treatment x given a specific context z.

In many real-world applications, the ground-truth objective function f is inaccessible during optimization. We instead only have access to a surrogate function  $\hat{f}: \mathcal{X} \times \mathcal{Z} \to \mathbb{R}$  trained on a distribution of observations whose z-marginal is not equal to p(z). The surrogate  $\hat{f}$  may be a patient simulator (Man et al., 2014; Evans et al., 2015), a digital twin (Katsoulakis et al., 2024; De Domenico et al., 2025; Kuang et al., 2024), or a machine learning model trained to approximate f. Importantly, we highlight the mismatch between p(z) and the source distribution of the training set of  $\hat{f}$ ; for example,  $\hat{f}$  may only be learned from patients at one hospital, and our patient  $z \sim p(z)$  is sampled from a different hospital. A natural strategy in this setting is to instead solve the related problem

$$\arg\max_{q(x)\in p(\mathcal{X})} \quad \mathbb{E}_{x\sim q(x)}[\hat{f}(x;z)] \tag{3}$$

with the hope that optimizing against  $\hat{f}$  admits a distribution over  $\mathcal{X}$  that also maximizes f in expectation. Importantly, the *conditional* problem formulation in (3) diverges from the related unconditional problem commonly considered in prior work (Trabucco et al., 2022; 2021; Yu et al., 2021). In practice, solving (3) is ineffective (Trabucco et al., 2021; Yu et al., 2021). This is because the out-of-distribution surrogate function  $\hat{f}$  frequently exhibits detrimental biases and performance degradations on a target distribution of patients, leading to worse outcomes according to the ground-truth objective function f in clinical settings (Taylor et al., 2022; Kirtane & Lee, 2017; Larkin et al., 2022). To overcome this limitation, we follow Yao et al. (2025b; 2024) and assume access to a dataset  $\mathcal{D}_{\rm src} \subseteq \mathcal{X}$  of previous treatment designs (e.g., the full treatment-patient dataset used to learn  $\hat{f}$  projected onto  $\mathcal{X}$ ); we show in our work how to use  $\mathcal{D}_{\rm src}$  to solve a modified instance of (3).

## 4.2 CONSTRAINED CONDITIONAL OPTIMIZATION

We first modify the original problem in (3) by introducing two constraints:

$$\arg\max_{q(x)\in p(\mathcal{X})} \quad \mathbb{E}_{x\sim q(x)}[\hat{f}(x;z)]$$
s.t. 
$$\mathbb{E}_{x'\sim \mathcal{D}_{sc}}[c^*(x')] - \mathbb{E}_{x\sim q(x)}[c^*(x)] \leq W_0, \quad \text{and} \quad \mathcal{H}_{\sim}(q(x)) \leq H_0$$
(4)

Following (1), the first constraint imposes an upper bound  $W_0$  on the 1-Wasserstein distance between the empirical distribution of proposed treatment designs q(x) and a dataset  $\mathcal{D}_{src}$  of previously proposed designs in the real world. Leveraging an auxiliary source critic model  $c^*: \mathcal{X} \to \mathbb{R}$ , this constraint ensures that the distribution of proposed designs is not too dissimilar to the distribution of historically reported designs, implicitly constraining the allowed degree of extrapolation against  $\hat{f}$  during optimization (Supplementary Theorem D.1). This mitigates the risk of proposing spurious candidates that appear favorable under the surrogate objective  $\hat{f}$  but are unlikely to perform well in practice (Yao et al., 2025b; 2024). Importantly, the domain of  $c^*$  is restricted to  $\mathcal{X}$ ; this means that no patient observations z from the source dataset  $\mathcal{D}_{src}$  are required. In other words, patient privacy of individuals in  $\mathcal{D}_{src}$  is explicitly preserved in (2). The second constraint places an upper bound  $H_0$  on the  $\sim$ -coarse-grained entropy of the distribution of designs q(x), defined below:

**Definition 4.1** ( $\sim$ -Coarse-Grained Entropy). Let  $\sim$  be an equivalence relation over the input space  $\mathcal{X}$ , and assume that the set of equivalence classes  $\mathcal{X}/\sim$  imposed by  $\sim$  is finite. Let  $N:=|\mathcal{X}/\sim|$  be the number of equivalence classes and q(x) be a valid probability distribution over the input space  $\mathcal{X}$ . Denote  $[x]_i$  as the ith equivalence class in  $\mathcal{X}/\sim$ , and  $\bar{q}_i:=\int_{[x]_i}dx\,q(x)$  to be the probability of drawing an element from the ith equivalence class. Then, the  $\sim$ -coarse-grained entropy  $\mathcal{H}_{\sim}:p(\mathcal{X})\to\mathbb{R}_+$  is defined as  $\mathcal{H}_{\sim}(q(x)):=-\sum_{i=1}^N \bar{q}_i\log\bar{q}_i$ .

The second constraint therefore enforces an upper bound on the entropy of the distribution of designs with respect to the equivalence relation  $\sim$ , encouraging sampling strategies (such as those that leverage domain-specific prior knowledge) that increase the certainty of the optimizer's proposals. In general, solving (4) exactly is highly intractable; both  $\hat{f}$  and  $c^*$  can be arbitrarily non-convex black-box functions, and the  $\sim$ -coarse-grained entropy may be highly sensitive to perturbations in the input space. To address this, we first show using **Lemma 4.2** how to derive an ansatz to the constrained problem in (4). We then show how to algorithmically solve for the free parameters of the solution class as applied to a suite of real-world optimization tasks for personalized medicine.

**Lemma 4.2** (Design Collapse Within Equivalence Classes). *Using the method of Lagrange multi*pliers, we can rewrite (4) as a function of the partial Lagrangian  $\mathcal{L}_{\lambda}(q)$  for some constant  $\lambda \in \mathbb{R}_{+}$ :

$$\arg\max_{q(x)\in p(\mathcal{X})} \quad \mathcal{L}_{\lambda}(q) := \mathbb{E}_{x\sim q(x)}[\hat{f}(x;z)] + \lambda(W_0 - \mathbb{E}_{x\sim\mathcal{D}_{src}}[c^*(x)] + \mathbb{E}_{x\sim q(x)}[c^*(x)])$$
s.t.  $\mathcal{H}_{\sim}(q(x)) \le H_0$  (5)

Suppose there exists a distribution q(x) that satisfies the remaining constraint in (5). Furthermore, assume that the function  $\hat{f}(x;z) + \lambda c^*(x)$  is continuous everywhere and coercive in  $\mathcal{X}$ . For all N equivalence classes, we can then define  $x_i^*$  (not necessarily unique) according to

$$x_i^*(\lambda) := \arg\max_{x \in [x]_i} \left( \hat{f}(x; z) + \lambda c^*(x) \right)$$
(6)

Then, the alternative distribution  $q^*(x) = \sum_{i=1}^N \bar{q}_i \, \delta(x - x_i^*)$ , where  $\bar{q}_i$  is as in **Definition 4.1**, also satisfies the constraint and simultaneously achieves a non-inferior value  $\mathcal{L}_{\lambda}(q^*) \geq \mathcal{L}_{\lambda}(q)$ .

The proof for this result is shown in **Appendix A**. Intuitively, **Lemma 4.2** shows that any feasible distribution q(x) cannot be superior to an alternative distribution  $q^*(x)$  that is both feasible and places all of its probability mass on each of the optimal designs within each equivalence class. We remark that each  $x_i^*$  need not be unique within the corresponding equivalence class  $[x]_i$ : it is easy to show that any solution to (6) within the same  $\sim$ -equivalence class (or an appropriately weighted combination of multiple optimal solutions) still admits a feasible distribution  $q^*(x)$ . **Lemma 4.2** allows us to restrict the search space of optimal distributions within  $p(\mathcal{X})$ . In particular, note that for a given  $\lambda$  and equivalence class  $\sim$ , the optimal policy is exactly specified by the choice of equivalence class probabilities  $\bar{q}_i$ . The original problem in (4) is therefore equivalent to

$$\arg\max_{\bar{q}\in\Delta(N)} \sum_{i=1}^{N} \bar{q}_{i}\hat{f}(x_{i}^{*})$$
s.t.  $\mathbb{E}_{x\sim\mathcal{D}_{\text{src}}}[c^{*}(x)] - \sum_{i=1}^{N} \bar{q}_{i}[c^{*}(x_{i}^{*})] \leq W_{0}$ , and  $\mathcal{H}(\bar{q}) \leq H_{0}$ 

(N) is the N-dimensional probability simplex and  $\mathcal{H}(\cdot)$  is the standard Shannon entropy of

where  $\Delta(N)$  is the N-dimensional probability simplex and  $\mathcal{H}(\cdot)$  is the standard Shannon entropy of the N-dimensional vector  $\bar{q}$ . This alternative problem formulation leads us to our main result:

**Lemma 4.3** (Probabilistic Sampling Over Equivalence Classes). Consider the constrained optimization problem as in (7). The ith element of the N-dimensional vector  $\bar{q}$  can be written as

$$\bar{q}_i = \exp\left[\mu\left(\hat{f}(x_i^*;z) + \lambda c^*(x_i^*)\right)\right] / \mathcal{Z}(\lambda) \text{ where } x_i^* := \arg\max_{x \in [x]_i} \left(\hat{f}(x;z) + \lambda c^*(x)\right)$$
(8)

where  $\mathcal{Z}(\lambda)$  is a normalizing constant and  $\lambda, \mu^{-1} \in \mathbb{R}_+$  are the Lagrange multipliers.

The proof for **Lemma 4.3** is included in **Appendix A**. Intuitively, we can think of  $\lambda$  and  $\mu$  as 'certainty' parameters: increasing  $\lambda$  upweights the importance of sampling a design  $x_i^*$  associated with a high certainty of 'in-distribution-ness' according to the source critic function  $e^*(x)$ . Similarly, increasing  $\mu$  upweights the importance of the probability vector  $\bar{q}$  producing a 'collapsed' distribution of designs with low entropy (and therefore high certainty). Prior work has either explicitly fixed variables similar to  $\lambda$ ,  $\mu$  as hyperparameters (Yu et al., 2021; Trabucco et al., 2021) or imposed restrictive assumptions on the input space to solve for the Lagrange multipliers (Yao et al., 2024). In contrast, we introduce a principled and computationally tractable approach to dynamically solve for the optimal  $\lambda$  and  $\mu$  over the course of the optimization trajectory.

## 4.3 Empirically Fixing the LLM Certainty $\mu$

The  $\sim$ -coarse-grained entropy from **Definition 4.1** is an intrinsic property of a language model optimizer: given a single prompt at a particular optimization step, the LLM can return multiple possible designs because the autoregressive model is non-deterministic for positive temperature values. The values of  $\bar{q}_i$  can therefore be empirically observed by sampling a batch of designs from the LLM optimizer, allowing us to estimate the  $\mu$  degree of freedom in (8). More concretely, with each batched sampling of proposals from the LLM, we assign the treatment designs into their respective equivalence classes to arrive at an unbiased estimate of the fractional occupancies of each class  $\hat{q}_i$ , and compute the optimal values  $\hat{f}(\hat{x}_i^*; z) + \lambda c^*(\hat{x}_i^*)$  according to (8). **Lemma 4.3** then gives

$$\log \hat{p}_i \approx -\log \mathcal{Z}(\lambda) + \mu \left( \hat{f}(\hat{x}_i^*; z) + \lambda c^*(\hat{x}_i^*) \right)$$

We can then estimate the value of  $\mu$  by simple linear regression, treating each observation  $(\hat{f}(\hat{x}_i^*; z) + \lambda c^*(\hat{x}_i^*), \log \hat{p}_i)$  over N equivalence classes as an explanatory-dependent variable pair:

$$\hat{\mu} = \frac{\sum_{i=1}^{N} \left[ (\hat{f}(\hat{x}_{i}^{*}; z) - \bar{f}) + (\lambda c^{*}(\hat{x}_{i}^{*}) - \bar{c}^{*}) \right] \left[ \log p_{i} - \frac{1}{N} \sum_{i'=1}^{N} \log p_{i'} \right]}{\sum_{i=1}^{N} \left[ (\hat{f}(\hat{x}_{i}^{*}; z) - \bar{f}) + (\lambda c^{*}(\hat{x}_{i}^{*}) - \bar{c}^{*}) \right]^{2}}$$
(9)

where the expectation values  $\bar{f}, \bar{c}$  are defined over the N equivalence classes. Intuitively, predictions with high entropy (i.e., low certainty) will be scaled to a lower reward, as  $\log p_i$  will be constant over equivalence classes and so  $\hat{\mu} \approx 0$ . Conversely, a confident model with high certainty will lead to a greater estimate of  $\hat{\mu} > 0$ , increasing the reward associated with the proposed designs. In this framework, the role of prior knowledge is to help 'overcome' the statistical randomness of the LLM's next-token generative process in proposing treatment designs to improve LLM certainty.

## 4.4 Solving for the Source Critic Certainty $\lambda$

We first solve for the Lagrangian dual function  $g(\lambda, \mu) := \max_{\bar{q} \in \Delta(N)} \mathcal{L}(\bar{q}; \lambda, \mu)$ .

**Corollary 4.4** (Dual Function of (7)). *The dual function of the constrained problem in (7) is* 

$$g(\lambda, \mu) = \lambda(W_0 - \mathbb{E}_{x \sim \mathcal{D}_{src}}[c^*(x)]) + \mu^{-1}H_0 + \mu^{-1}\log \mathcal{Z}(\lambda)$$

where  $\mathcal{Z}(\lambda)$  is the normalizing constant from (8), and so

$$\frac{\partial g(\lambda, \mu)}{\partial \lambda} = W_0 - \left( \mathbb{E}_{x \sim \mathcal{D}_{src}} [c^*(x)] - \sum_i \bar{q}_i c^*(x_i^*) \right)$$
 (10)

The proof of this result is included in **Appendix A**. Importantly, (10) allows us to iteratively solve for the optimal value of the dual parameter  $\lambda$  via gradient descent without any explicit gradient information from the black-box functions  $\hat{f}$  and  $c^*$ :

$$\lambda_{t+1} = \lambda_t - \eta_\lambda \frac{\partial g(\lambda, \hat{\mu})}{\partial \lambda} = \lambda_t - \eta_\lambda \Big[ W_0 - \mathbb{E}_{x \sim \mathcal{D}_{src}}[c^*(x)] + \sum_i \bar{q}_i c^*(x_i^*) \Big]$$
(11)

Here,  $\eta_{\lambda} > 0$  is a learning rate hyperparameter and  $\bar{q}_i$  is as in (8). Intuitively, if the designs  $x_i^*$  are indistribution compared to  $\mathcal{D}_{\text{src}}$ , then the Wasserstein distance  $\mathbb{E}_{x \sim \mathcal{D}_{\text{src}}}[c^*(x)] - \sum_{i=1}^N \bar{q}_i c^*(x_i^*) \leq W_0$ , meaning  $\partial g(\lambda,\mu)/\partial \lambda > 0$  and the value of  $\lambda_{t+1}$  will decrease to allow for greater exploration of the design space. Conversely, sampling out-of-distribution designs  $x_i^*$  will yield  $\partial g(\lambda,\mu)/\partial \lambda < 0$ , and  $\lambda_{t+1}$  will increase to reduce the extrapolation against  $\hat{f}$ .

#### 4.5 OVERALL ALGORITHM

Our overall method to solve (4) consists of four primary steps. (1) **Sampling.** We first query the LLM optimizer to propose a batch of **independently sampled** new treatment designs. The LLM is prompted with a description of the task and the patient z, any prior knowledge it produced prior to optimization, and a table of its previously proposed designs and their corresponding scores according to our algorithm. (2) **Clustering.** We then take as input the batch of designs and individually assign them to their corresponding equivalence classes. (3) **Certainty Estimation.** We estimate the fractional occupancy  $\hat{q}_i$  and the optimal value of  $\hat{f}(\hat{x}_i^*;z) + \lambda c^*(\hat{x}_i^*)$  observed in each equivalence class, and then estimate the certainty parameter  $\mu$  according to (9). We also update the value of  $\lambda$  following (11). (4) **Design Scoring.** Using our estimates of  $\mu$  and  $\lambda$ , we score each sampled design x according to  $\mu[\hat{f}(x;z) + \lambda c^*(x)]$ , and store the treatments and their scores to provide as context to subsequent LLM optimization prompting. These steps are repeated until the maximum query budget for  $\hat{f}(x;z)$  is reached. We refer to our method as **LLM-based Entropy-guided Optimization with kNowledgeable priors (LEON)**; the full pseudocode is in **Supplementary Algorithm 1**. Note that our method only updates the LLM prompt; **there is** no **fine-tuning of the weights of the LLM**.

The role of prior knowledge in LEON. Notably, LEON may be used with any generalist language model without any task-specific fine-tuning. Such consumer-grade LLMs may not be able to propose more optimal designs given only access to prior observations alone, adversely affecting the model certainty according to  $\mu$ . To overcome this limitation, we first provide the LLM access to a set of external knowledge repositories with domain-specific knowledge—such as medical textbooks, biomedical knowledge graphs, and publicly available clinical databases. Given a description of the optimization task and the patient features z, the LLM is allowed to choose which knowledge sources may be helpful, and then sequentially query the relevant textual corpora as tools to synthesize a prior knowledge statement in natural language. We then provide this prior knowledge as prompt context to the LLM in all subsequent optimization steps. In our work, we show how leveraging prior knowledge in this way can help the LLM propose higher-quality designs, thereby increasing the value of  $\mu$  and improving the quality of individualized treatment regimens.

**Reflection on optimization steps.** After a batch of designs are scored and before a new batch of designs are acquired, we prompt the backbone language model to analyze the most recently sampled batch of designs and their corresponding scores following prior work (Ma et al., 2024b; Yao et al., 2023). The LLM is asked to reflect on the data and underlying sampling strategy in natural language; the output of this reflection is included into the LLM prompt in the next batch acquisition step.

# 5 EMPIRICAL EVALUATION

**Personalized medicine optimization tasks under distribution shift.** Recall that our core motivation for LEON is to overcome the effect of distribution shifts when personalizing treatment plans for previously unseen, potentially out-of-distribution patients. To this end, we constructed a set of 5 real-world optimization tasks to evaluate LEON and baseline methods. (1) **Warfarin** aims to propose an optimal dose of warfarin (a blood thinner medication) conditioned on the patient's pharmacogenetic variables (Consortium, 2009); (2) **HIV** an antiretroviral medication regiment based on the patient's HIV viral mutations (Rhee et al., 2003); (3) **Breast** and (4) **Lung** an optimal treatment strategy for patients diagnosed with breast or non-small cell lung cancer (NSCLC), respectively; and (5) **ADR** a prediction of a patient's risk of an adverse drug reaction (ADR) following the administration of a proprietary drug. We simulate a distribution shift between the observations used to learn the surrogate model  $\hat{f}$  and the ground-truth objective f; see **Supplementary Table S1** for details.

**Prior knowledge generation.** We operationalize the task of prior knowledge synthesis as a toolcalling problem (Schick et al., 2023; Qin et al., 2024; Yao et al., 2023). We provide the LLM a

set of external knowledge tools, including: (1) a corpus of medical textbooks (Xiong et al., 2024); prompting an auxiliary (2) MedGemma 27B LLM (Sellergren et al., 2025) fine-tuned on expert medical knowledge; querying structured biomedical knowledge graphs (3) HetioNet (Himmelstein et al., 2017) and (4) PrimeKG (Chandak et al., 2023); and other domain-specific knowledge repositories including (5) Cellosaurus (Bairoch, 2018) with cell-line data, (6) COSMIC (Tate et al., 2019) with cancer mutation data, (7) GDSC (Yang et al., 2013) with drug sensitivity data, and (8) DepMap (Tsherniak et al., 2017) with cancer cell dependencies. Using these tools, the LLM composes a prior knowledge statement, which is then included in the LLM prompts during optimization.

Experiment implementation. Each task includes two static datasets  $\mathcal{D}_{\mathrm{src}}^{\mathrm{annotated}} = \{(x_j, z_j, y_j)\}_{j=1}^{n_{\mathrm{src}}}$  and  $\mathcal{D}_{\mathrm{tgt}}^{\mathrm{annotated}} = \{(x_i, z_i, y_i)\}_{i=1}^{n_{\mathrm{tgt}}}$  from the observation space  $\mathcal{X} \times \mathcal{Z} \times \mathbb{R}$ . The source dataset  $\mathcal{D}_{\mathrm{src}}^{\mathrm{annotated}}$  and target dataset  $\mathcal{D}_{\mathrm{tgt}}^{\mathrm{annotated}}$  are constructed according to a distribution shift between the task-specific source and target distributions, and are non-overlapping at the patient level. We learn a task-specific surrogate model  $\hat{f}: \mathcal{X} \times \mathcal{Z} \to \mathbb{R}$  on  $\mathcal{D}_{\mathrm{src}}^{\mathrm{annotated}}$ , and also a function  $f: \mathcal{X} \times \mathcal{Z} \to \mathbb{R}$  on  $\mathcal{D}_{\mathrm{tgt}}^{\mathrm{annotated}}$  taken to be the ground-truth objective for patients from the target population for the purposes of evaluation. Note that the full datasets  $\mathcal{D}_{\mathrm{src}}^{\mathrm{annotated}}$ ,  $\mathcal{D}_{\mathrm{tgt}}^{\mathrm{annotated}}$  are used only to learn  $\hat{f}, f$  for our experimental setup; we project  $\mathcal{D}_{\mathrm{tgt}}^{\mathrm{annotated}}$  onto  $\mathcal{Z}$  and  $\mathcal{D}_{\mathrm{src}}^{\mathrm{annotated}}$  onto  $\mathcal{X}$  to construct  $\mathcal{D}_{\mathrm{tgt}} := \{z_i\}_{i=1}^{n_{\mathrm{tgt}}}$  and  $\mathcal{D}_{\mathrm{src}} := \{x_j\}_{j=1}^{n_{\mathrm{src}}}$  for our experiments. We embed proposed patient-design pairs, represented in natural language, using the text-embedding-3-small model from OpenAI, and perform k-means clustering (trained on the source dataset  $\mathcal{D}_{\mathrm{src}}$  using cosine similarity as the distance metric) in the embedding space to assign individual designs to equivalence classes—see Appendix C for additional details.

LEON also involves training a source critic model  $c^*:\mathcal{X}\to\mathbb{R}$  as in (1). Consistent with prior work (Yao et al., 2025b; 2024), we implement  $c^*$  as a fully-connected network with two hidden layers each with 2048 dimensions. We enforce the constraint on the critic's Lipschitz constant by clipping the model parameters to have an  $\ell_\infty$ -norm no greater than 0.01 after each weight update step, consistent with Arjovsky et al. (2017). After each acquisition step during optimization, we re-train the source critic using gradient descent with a learning rate of  $\eta=0.001$  according to (1), and also perform a single-step update to the  $\lambda$  certainty parameter according to (10) with  $\eta_\lambda=0.1$ . We fix  $W_0=1.0$  in (10) and the LLM temperature hyperparameter  $\tau=1.0$ , and use a sampling batch size of 32 to avoid overfitting any of these hyperparameters to any particular task. All experiments were run on an internal cluster using only a single NVIDIA A100 80GB GPU. We report experimental results on a random sample of n=100 unique patients from  $\mathcal{D}_{\rm tgt}$ .

**Baselines.** We evaluate LEON against the LLM-based optimization methods (1) Large LAnguage Models to enhance Bayesian Optimization (LLAMBO, Liu et al. (2024c)), which leverages LLMs to augment traditional Bayesian Optimization (BO); (2) Optimization by PROmpting (OPRO, Yang et al. (2024a)), which appends previously proposed solutions and their scores to subsequent LLM input prompts; and (3) Evolution-driven universal reward kit for agent (Eureka, Ma et al. (2024b)), which extends OPRO by intermittently prompting the LLM to reflect on the efficacy of previous optimization strategies in natural language. All LLM-based optimization strategies (including LEON) were evaluated using qpt-4o-mini-2024-07-18 from OpenAI without any fine-tuning.

We also compare LEON to traditional, non-LLM-based optimization methods (4) Gradient Ascent (Grad.); (5) Simulated Annealing (Sim. Anneal, Tsallis (1988)); (6) Covariance Matrix Adaptation Evolution Strategy (CMA-ES, Hansen (2006)); (7) Genetic Algorithm (GA, Gad (2024)); and (8) Bayesian optimization with Expected Improvement (BO-qEI). Finally, we evaluate the (9) Majority baseline algorithm that always proposes the majority design (i.e., mean for continuous design dimensions and mode for discrete design dimensions) across all observations  $x_j \in \mathcal{D}_{src}$ ; and the (10) Human baseline algorithm, which proposes the true design  $x_i$  that the individual  $z_i$  actually received according to the hidden annotated dataset  $\mathcal{D}_{tgt}^{annotated}$ . An optimization method that outperforms the Majority strategy suggests that the optimizer's personalized treatment strategies outperform the 'average' treatment in the source dataset  $\mathcal{D}_{src}$  in expectation. An optimization method that outperforms the Human baseline means the treatment strategies proposed by the optimizer are better than the therapy the patient actually received from their clinician according to our oracle objective function.

**Evaluation metric.** For any particular input set of fixed patient covariates  $z \sim \mathcal{D}_{tgt}$ , an optimization method is allowed to sample and propose a total of 2048 possible designs x and corresponding surrogate model evaluations  $\hat{f}(x;z)$ . After the surrogate model evaluation budget is exhausted, the optimizer proposes a *single* top design  $x^*$  to evaluate using the ground-truth objective function f: for

Table 1: Quality of patient-conditioned designs under distribution shift. We report mean  $\pm$  standard error of mean (SEM) ground-truth objective values achieved by the single proposed design for a given patient, averaged over n=100 test patients from the target distribution. **Bolded** (resp., Underlined) cells indicate the **best** (resp., second best) mean score for a given task.

Method	Warfarin ↓ RMSE Loss (mg/week)	HIV ↓ Viral Load (copies/mL)	Breast ↑ TTNTD (months)	Lung ↑ TTNTD (months)	ADR ↓ NLL Loss (no units)	Rank
Majority Human	$3.46 \pm 0.70$ $2.68 \pm 0.86$	$4.55 \pm 0.07$ $4.55 \pm 0.07$	$25.95 \pm 0.75$ $29.65 \pm 1.14$	$20.13 \pm 0.13$ $21.10 \pm 0.27$	1.41 ± 0.05	8.0 8.5
Grad. BO-qEI Sim. Anneal CMA-ES	$1.37 \pm 0.13$ $1.36 \pm 0.13$ $1.38 \pm 0.12$ $1.90 \pm 0.14$	$4.52 \pm 0.04  4.53 \pm 0.04  4.55 \pm 0.03  4.53 + 0.04$	$65.23 \pm 2.03$ $67.05 \pm 1.87$ $66.62 \pm 2.62$ $59.48 \pm 2.76$	$24.09 \pm 0.44$ $27.97 \pm 0.65$ $29.29 \pm 0.74$ $27.43 \pm 0.68$	$23.7 \pm 1.7$ $23.2 \pm 1.7$ $23.8 \pm 1.7$ $23.4 \pm 1.7$	5.2 3.4 5.0 6.2
GA LLAMBO OPRO Eureka	$1.49 \pm 0.26$ $3.28 \pm 0.10$ $1.40 \pm 0.13$ $1.54 \pm 0.25$	$4.62 \pm 0.05$ $4.52 \pm 0.05$ $4.55 \pm 0.04$ $4.58 \pm 0.04$	$69.90 \pm 2.28$ $48.83 \pm 2.48$ $55.68 \pm 2.86$ $63.48 \pm 3.52$	$27.53 \pm 0.80$ $27.53 \pm 0.81$ $20.60 \pm 0.31$ $24.35 \pm 0.43$ $25.10 \pm 0.69$	$20.0 \pm 2.3$ $20.6 \pm 1.9$ $23.8 \pm 1.7$ $21.3 \pm 2.0$	5.2 7.0 7.0 6.8
LEON	$\textbf{1.36} \pm \textbf{0.13}$	$\textbf{4.50} \pm \textbf{0.04}$	$\textbf{72.43} \pm \textbf{2.86}$	$\textbf{32.71} \pm \textbf{0.32}$	$12.4 \pm 1.6$	1.2

most optimization methods,  $x^*$  is the proposed design that maximizes  $\hat{f}$  (LEON follows the design proposal method in **Supplementary Algorithm 1**). We then evaluate this single proposed design  $x^*$  using the ground-truth objective f, and report the corresponding score  $f(x^*; z)$ . Importantly, f is only used for evaluation purposes and is not accessible to any method during optimization.

**Results.** LEON consistently outperforms all baseline methods, achieving an average rank of **1.2** across all tasks (**Table 1**). Notably, LEON proposes sets of personalized treatment designs that are superior to the treatments retrospectively received by the patients. It achieves the best performance on Warfarin dose prediction, HIV treatment, and both breast and lung cancer therapy design. Qualitatively, we found that the Majority algorithm was able to outperform LEON on the ADR task due to significant class imbalance in the population of patients in the dataset.

**Ablation studies.** In our main experiments, we use gpt-4o-mini-2024-07-18 as the LLM optimizer; we ablate the choice of language model in **Supplementary Table S3**. We also ablate the external sources of prior knowledge in **Supplementary Table S5** and find that LEON is sensitive to the quality of domain-specific knowledge available. See **Appendix E** for additional ablation results.

## 6 DISCUSSION AND CONCLUSION

In this work, we propose LEON to combine domain knowledge with LLM-based optimizers to solve conditional black-box optimization problems under distribution shift for personalized medicine. We first introduce two additional constraints in (4) that upweight high-quality designs that are both (1) in-distribution according to an auxiliary source critic model; and (2) likely to be high-quality based on the language model's statistical certainty. Using our method, we show how consumergrade LLMs can be used to solve a wide variety of challenging personalized medicine optimization problems without any LLM fine-tuning, outperforming both traditional and other LLM-based optimization methods. Moving forward, we hope to extend LEON to the setting of active learning and prospective clinical evaluation (Collignon et al., 2020; Ianevski et al., 2021; Kuru et al., 2024; Burd et al., 2020), and also apply our method to other domains outside of personalized medicine.

Limitations. Several limitations warrant consideration. First, we observed that LLM optimizers using LEON are sensitive to the available prior knowledge: contamination with factually incorrect or outdated information may propagate into optimization outputs and adversely affect personalized treatment design using LEON (Omar et al., 2025; Han et al., 2024; Clusmann et al., 2025). Furthermore, while the clinical tasks considered here are designed to approximate real-world conditions, they cannot fully capture the complexity of heterogeneous patient responses and rare disease subtypes encountered in actual clinical practice (Pan et al., 2024). Finally, as with all simulation-based benchmarks, the validity of our conclusions is limited by the assumptions embedded in the functions and datasets used, which may obscure differences between methods. Future work might explore how to integrate physicians in the loop to mitigate the risks of autonomous LLM-based systems.

#### **ETHICS STATEMENT**

This work investigates the use of large language models (LLMs) as optimizers for conditional black-box problems in clinical medicine. All datasets used in this work are fully anonymized and contain no personally identifiable information. As such, no patient consent or institutional review board (IRB) approval was required. Separately, LLMs are inherently subject to social and demographic biases learned during pretraining (Sorin et al., 2025; Omiye et al., 2023). When applied to patient-specific design tasks, such biases could disproportionately affect marginalized populations, potentially leading to inequitable or unsafe treatment proposals if not properly accounted for. We also emphasize that LEON is not intended for direct clinical use, but rather as a methodological contribution toward future systems that may aid clinical decision making. Any real-world deployment requires extensive safeguards, including careful physician oversight, to establish safety and efficacy.

#### REPRODUCIBILITY STATEMENT

The datasets for the Warfarin and HIV tasks are made publicly available by Consortium (2009) and Rhee et al. (2003), respectively. The Flatiron data used in this study were made available as part of a collaboration with Flatiron Health, a healthcare technology and services company focused on accelerating cancer research. The authors had full access to the data and were responsible for conducting the analyses. This research was conducted in compliance with all relevant ethical regulations. The de-identified data may be made available upon reasonable request by contacting DataAccess@flatiron.com. The ADR task data is an internal proprietary dataset—data access requests may be directed to the corresponding author. Our custom code implementation for our experiments is made publicly available at mgithub.com/anonymous-user/Repository.

## REFERENCES

Josh Abramson, Jonas Adler, Jack Dunger, Richard Evans, Tim Green, Alexander Pritzel, Olaf Ronneberger, Lindsay Willmore, Andrew J Ballard, Joshua Bambrick, Sebastian W Bodenstein, David A Evans, Chia-Chun Hung, Michael O'Neill, David Reiman, Kathryn Tunyasuvunakool, Zachary Wu, Akvilė Žemgulytė, Eirini Arvaniti, Charles Beattie, Ottavia Bertolli, Alex Bridgland, Alexey Cherepanov, Miles Congreve, Alexander I Cowen-Rivers, Andrew Cowie, Michael Figurnov, Fabian B Fuchs, Hannah Gladman, Rishub Jain, Yousuf A Khan, Caroline M R Low, Kuba Perlin, Anna Potapenko, Pascal Savy, Sukhdeep Singh, Adrian Stecula, Ashok Thillaisundaram, Catherine Tong, Sergei Yakneen, Ellen D Zhong, Michal Zielinski, Augustin Žídek, Victor Bapst, Pushmeet Kohli, Max Jaderberg, Demis Hassabis, and John M Jumper. Accurate structure prediction of biomolecular interactions with AlphaFold 3. *Nature*, 630:493–500, 2024. doi: 10.1038/s41586-024-07487-w.

Roy Adams, Katharine E Henry, Anirudh Sridharan, Hossein Soleimani, Andong Zhan, Nishi Rawat, Lauren Johnson, David N Hager, Sara E Cosgrove, Andrew Markowski, Eili Y Klein, Edward S Chen, Mustapha O Saheed, Maureen Henley, Sheila Miranda, Katrina Houston, Robert C Linton, Anushree R Ahluwalia, Albert W Wu, and Suchi Saria. Prospective, multi-site study of patient outcomes after implementation of the TREWS machine learning-based early warning system for sepsis. *Nat Med*, 28:1455–60, 2022. doi: 10.1038/s41591-022-01894-0.

Lakshya A Agrawal, Shangyin Tan, Dilara Soylu, Noah Ziems, Rishi Khare, Krista Opsahl-Ong, Arnav Singhvi, Herumb Shandilya, Michael J Ryan, Meng Jiang, Christopher Potts, Koushik Sen, Alexandros G Dimakis, Ion Stoica, Dan Klein, Matei Zaharia, and Omar Khattab. GEPA: Reflective prompt evolution can outperform reinforcement learning. *arXiv Preprint*, 2025. doi: 10.48550/arXiv.2507.19457.

- Peter Akioyamen, Zixuan Yi, and Ryan Marcus. The unreasonable effectiveness of LLMs for query optimization. *arXiv Preprint*, 2024. doi: /10.48550/arXiv.2411.02862.
- Alex Albaugh and Todd R Gingrich. Simulating a chemically fueled molecular motor with nonequilibrium molecular dynamics. *Nat Commun*, 13, 2022. doi: 10.1038/s41467-022-29393-3.
- Daniel Alexander Alber, Zihao Yang, Anton Alyakin, Eunice Yang, Sumedha Rai, Aly A Valliani, Jeff Zhang, Gabriel R Rosenbaum, Ashley K Amend-Thomas, David B Kurland, Caroline M Kre-

mer, Alexander Eremiev, Bruck Negash, Daniel D Wiggan, Michelle A Nakatsuka, Karl L Sangwon, Sean N Neifert, Hammad A Khan, Akshay Vinod Save, Adhith Palla, Eric A Grin, Monika Hedman, Mustafa Nasir-Moin, Xujin Chris Liu, Lavender Yao Jiang, Michal A Mankowski, Dorry L Segev, Yindalon Aphinyanaphongs, Howard A Riina, John G Golfinos, Daniel A Orringer, Douglas Kondziolka, and Eric Karl Oermann. Medical large language models are vulnerable to data-poisoning attacks. *Nat Med*, 31:618–26, 2025. doi: 10.1038/s41591-024-03445-1.

- Emily Alsentzer, John Murphy, William Boag, Wei-Hung Weng, Di Jindi, Tristan Naumann, and Matthew McDermott. Publicly available clinical BERT embeddings. In *Proc Clin Nat Lang Proc Workshop*, pp. 72–8, 2019. doi: 10.18653/v1/W19-1909.
- Anastasios N. Angelopoulos and Stephen Bates. Conformal prediction: A gentle introduction. *Found Trends Mach Learn*, 16(4):494–591, 2023. doi: 10.1561/2200000101.
- Anastasios Nikolas Angelopoulos, Stephen Bates, Michael Jordan, and Jitendra Malik. Uncertainty sets for image classifiers using conformal prediction. In *Proc ICLR*, 2021. URL https://openreview.net/forum?id=eNdiU\_DbM9.
- Christof Angermueller, David Dohan, David Belanger, Ramya Deshpande, Kevin Murphy, and Lucy Colwell. Model-based reinforcement learning for biological sequence design. In *Proc ICLR*, 2020. URL https://openreview.net/forum?id=HklxbgBKvr.
- Martin Arjovsky, Soumith Chintala, and Léon Bottou. Wasserstein generative adversarial networks. In *Proc ICML*, volume 70, pp. 214–23. PMLR, 2017. URL https://proceedings.mlr.press/v70/arjovsky17a.html.
- Rahul K Arora, Jason Wei, Rebecca Soskin Hicks, Preston Bowman, Joaquin Quiñonero Candela, Foivos Tsimpourlas, Michael Sharman, Meghan Shah, Andrea Vallone, Alex Beutel, Johannes Heidecke, and Karan Singhal. HealthBench: Evaluating large language models towards improved human health. *arXiv Preprint*, 2025. doi: 10.48550/arXiv.2505.08775.
- Amos Bairoch. The Cellosaurus, a cell-line knowledge resource. *J Biomol Tech*, 29(2):25–38, 2018. doi: 10.7171/jbt.18-2902-002.
- Abhinand Balachandran. Medembed: Medical-focused embedding models, 2024. URL https://github.com/abhinand5/MedEmbed.
- Andrew P Blair, Robert K Hu, Elie N Farah, Neil C Chi, Katherine S Pollard, Pawel F Przytycki, Irfan S Kathiriya, and Benoit G Bruneau. Cell Layers: Uncovering clustering structure in unsupervised single-cell transcriptomic analysis. *Bioinform Adv*, 2:vbac051, 2022. doi: 10.1093/bioadv/vbac051.
- Konstantinos Bousmalis, George Trigeorgis, Nathan Silberman, Dilip Krishnan, and Dumitru Erhan. Domain separation networks. In *Proc NeurIPS*, pp. 343–51, 2016. doi: 10.5555/3157096. 3157135.
- Konstantinos Bousmalis, Nathan Silberman, David Dohan, Dumitru Erhan, and Dilip Krishnan. Unsupervised pixel-level domain adaptation with generative adversarial networks. In *Proc IEEE CVPR*, pp. 95–104, 2017. doi: 10.1109/CVPR.2017.18.
- Stephen Boyd and Lieven Vandenberghe. *Convex optimization*. Cambridge University Press, 2004.
- Lawrence M Brass, Harlan M Krumholz, Jeanne M Scinto, and Martha Radford. Warfarin use among patients with atrial fibrillation. *Stroke*, 28(12), 1997. doi: 10.1161/01.STR.28.12.2382.
- Amy Burd, Ross L Levine, Amy S Ruppert, Alice S Mims, Uma Borate, Eytan M Stein, Prapti Patel, Maria R Baer, Wendy Stock, Michael Deininger, William Blum, Gary Schiller, Rebecca Olin, Mark Litzow, James Foran, Tara L Lin, Brian Ball, Michael Boyiadzis, Elie Traer, Olatoyosi Odenike, Martha Arellano, Alison Walker, Vu H Duong, Tibor Kovacsovics, Robert Collins, Abigail B Shoben, Nyla A Heerema, Matthew C Foster, Jo-Anne Vergilio, Tim Brennan, Christine Vietz, Eric Severson, Molly Miller, Leonard Rosenberg, Sonja Marcus, Ashley Yocum, Timothy Chen, Mona Stefanos, Brian Druker, and John C Byrd. Precision medicine treatment in acute myeloid leukemia using prospective genomic profiling: Feasibility and preliminary efficacy of the Beat AML Master Trial. *Nat Med*, 26:1852–8, 2020. doi: 10.1038/s41591-020-1089-8.

Mycal Casey, Lorriane Odhiambo, Nidhi Aggarwal, Mahran Shoukier, Jamani Garner, K M Islam,
 and Jorge E Cortes. Are pivotal clinical trials for drugs approved for leukemias and multiple
 myeloma representative of the population at risk? *J Clin Oncol*, 40(32), 2022. doi: 10.1200/JCO.
 22.00504.

- Fiona Catterall, Paul R J Ames, and Chris Isles. Warfarin in patients with mechanical heart valves. *BMJ*, 371:m3956, 2020. doi: 10.1136/bmj.m3956.
- Payal Chandak, Kexin Huang, and Marinka Zitnik. Building a knowledge graph to enable precision medicine. *Sci Data*, 10, 2023. doi: 10.1038/s41597-023-01960-3.
- Angelica Chen, David M Dohan, and David R So. EvoPrompting: Language models for code-level neural architecture search. In *Proc ICLR*, pp. 7787–817, 2023a. doi: 10.5555/3666122.3666464.
- Angelica Chen, Samuel D Stanton, Frances Ding, Robert G Alberstein, Andrew M Watkins, Richard Bonneau, Vladimir Gligorijević, Kyunghyun Cho, and Nathan C Frey. Generalists vs. specialists: Evaluating LLMs on highly-constrained biophysical sequence optimization tasks. In *Proc ICML*, 2025a. doi: 10.48550/arXiv.2410.22296.
- Mingcheng Chen, Haoran Zhao, Yuxiang Zhao, Hulei Fan, Hongqiao Gao, Yong Yu, and Zheng Tian. ROMO: Retrieval-enhanced offline model-based optimization. In *Proc Int Conf Dist Artif Intell*, pp. 1–9, 2023b. doi: 10.1145/3627676.3627685.
- Qingyu Chen, Yan Hu, Xueqing Peng, Qianqian Xie, Qiao Jin, Aidan Gilson, Maxwell B Singer, Xuguang Ai, Po-Ting Lai, Zhizheng Wang, Vipina K Keloth, Kalpana Raja, Jimin Huang, Huan He, Fongci Lin, Jingcheng Du, Rui Zhang, W Jim Zheng, Ron A Adelman, Zhiyong Lu, and Hua Xu. Benchmarking large language models for biomedical natural language processing applications and recommendations. *Nat Commun*, 16, 2025b. doi: 10.1038/s41467-025-56989-2.
- Tianqi Chen and Carlos Guestrin. Xgboost: A scalable tree boosting system. In *Proc ACM SIGKDD*, pp. 785–94, 2016. doi: 10.1145/2939672.2939785.
- Yi-Ming Chen, Tzu-Hung Hsiao, Ching-Heng Lin, and Yang C Fann. Unlocking precision medicine: Clinical applications of integrating health records, genetics, and immunology through artificial intelligence. *J Biomed Sci*, 32, 2025c. doi: 10.1186/s12929-024-01110-w.
- Mia Chiquier, Utkarsh Mall, and Carl Vondrick. Evolving interpretable visual classifiers with large language models. In *Proc ECCV*, pp. 183–201, 2024. doi: 10.1007/978-3-031-73039-9\_11.
- Jan Clusmann, Dyke Ferber, Isabella C Wiest, Carolin V Schneider, Titus J Brinker, Sebastian Foersch, Daniel Truhn, and Jakob Nikolas Kather. Prompt injection attacks on vision language models in oncology. *Nat Commun*, 16, 2025. doi: 10.1038/s41467-024-55631-x.
- A Collignon, M A Hospital, C Montersino, F Courtier, A Charbonnier, C Saillard, E D'Incan, B Mohty, A Guille, J Adelaïde, N Carbuccia, S Garnier, M J Mozziconacci, C Zemmour, J Pakradouni, A Restouin, R Castellano, M Chaffanet, D Birnbaum, Y Collette, and N Vey. A chemogenomic approach to identify personalized therapy for patients with relapse or refractory acute myeloid leukemia: Results of a prospective feasibility study. *Blood Cancer J*, 10(64), 2020.
- The International Warfarin Pharmacogenetics Consortium. Estimation of the warfarin dose with clinical and pharmacogenetic data. *New Eng J Med*, 360(8):753–64, 2009. doi: 10.1056/NEJMoa0809329.
- Bruno Almeida Costa, Neha Debnath, Thomaz Alexandre Costa, Raphael Bertasi, Tarek H Mouhieddine, Karthik Nath, and Adriana C Rossi. Demographic disparities in clinical trial enrollment of US patients with newly-diagnosed multiple myeloma. *Blood*, 142(7371), 2023. doi: 10.1182/blood-2023-190861.
- Jesse C. Cresswell, Yi Sui, Bhargava Kumar, and Noël Vouitsis. Conformal prediction sets improve human decision making. In *Proc ICML*, pp. 9439–57, 2024. doi: 10.5555/3692070.3692445.
- Haotian Cui, Chloe Wang, Hassaan Maan, Kuan Pang, Fengning Luo, Nan Duan, and Bo Wang. scGPT: Toward building a foundation model for single-cell multi-omics using generative AI. *Nat Meth*, 21:1470–80, 2024. doi: 10.1038/s41592-024-02201-0.

Johann de Bono, Joaquin Mateo, Karim Fizazi, Fred Saad, Neal Shore, Shahneen Sandhu, Kim N Chi, Oliver Sartor, Neeraj Agarwal, David Olmos, Antoine Thiery-Vuillemin, Przemyslaw Twardowski, Niven Mehra, Carsten Goessl, Jinyu Kang, Joseph Burgents, Wenting Wu, Alexander Kohlmann, Carrie A Adelman, and Maha Hussain. Olaparib for metastatic castration-resistant prostate cancer. *N Engl J Med*, 382(22):2091–102, 2020. doi: 10.1056/NEJMoa1911440.

- Manlio De Domenico, Luca Allegri, Guido Caldarelli, Valeria d'Andrea, Barbara Di Camillo, Luis M Rocha, Jordan Rozum, Riccardo Sbarbati, and Francesco Zambelli. Challenges and opportunities for digital twins in precision medicine from a complex systems perspective. *npj Digit Med*, 8, 2025. doi: 10.1038/s41746-024-01402-3.
- Laura Dean. Warfarin therapy and VKORC1 and CYP genotype, chapter Medical Genetics Summaries. National Center for Biotechnology Information, 2012. URL https://www.ncbi.nlm.nih.gov/books/NBK84174/.
- Shachi Deshpande, Charles Marx, and Volodymyr Kuleshov. Online calibrated and conformal prediction improves Bayesian optimization. In *Proc AISTATS*, volume 238, pp. 1450–8. PMLR, 2024. URL https://proceedings.mlr.press/v238/deshpande24a.html.
- Martin Eklund, Ulf Norinder, Scott Boyer, and Lars Carlsson. The application of conformal prediction to the drug discovery process. *Ann Math Artif Intell*, 74:117–32, 2013. doi: 10.1007/s10472-013-9378-2.
- Kambria H Evans, William Daines, Jamie Tsui, Matthew Strehlow, Paul Maggio, and Lisa Shieh. Septris: A novel, mobile, online, simulation game that improves sepsis recognition and management. Acad Med, 90:180–4, 2015. doi: 10.1097/ACM.000000000000011.
- Sebastian Farquhar, Jannik Kossen, Lorenz Kuhn, and Yarin Gal. Detecting hallucinations in large language models using semantic entropy. *Nature*, 630:625–30, 2024. doi: 10.1038/s41586-024-07421-0.
- Daniel Flam-Shepherd, Kevin Zhu, and Alán Aspuru-Guzik. Language models can learn complex molecular distributions. *Nat Commun*, 13, 2022. doi: 10.1038/s41467-022-30839-x.
- Neville F Ford and Dirk Taubert. Clopidogrel, CYP2C19, and a black box. *J Clin Pharmacol*, 53 (3):241–8, 2013. doi: 10.1002/jcph.17.
- Geoff French, Michal Mackiewicz, and Mark Fisher. Self-ensembling for visual domain adaptation. In *Proc ICLR*, 2018. URL https://openreview.net/forum?id=rkpoTaxA-.
- Deqing Fu, Tian-qi Chen, Robin Jia, and Vatsal Sharan. Transformers learn to achieve second-order convergence rates for in-context linear regression. In *Proc NeurIPS*, 2024. URL https://openreview.net/forum?id=L8h6cozcbn.
- Ahmed Fawzy Gad. Pygad: An intuitive genetic algorithm Python library. *Multimed Tools Appl*, 83:58029–42, 2024. doi: 10.1007/s11042-023-17167-y.
- Yaroslav Ganin, Evgeniya Ustinova, Hana Ajakan, Pascal Germain, Hugo Larochelle, François Laviolette, Mario Marchand, and Victor Lempitsky. Domain-adversarial training of neural networks. *J Mach Learn Res*, 17(1):2096–130, 2016. doi: 10.5555/2946645.2946704.
- Apar Kishor Ganti, Alyssa B Klein, Ion Cotarla, Brian Seal, and Engels Chou. Update of incidence, prevalence, survival, and initial treatment in patients with non–small cell lung cancer in the US. *JAMA Oncol*, 7(12):1824–32, 2021. doi: 10.1001/jamaoncol.2021.4932.
- Shivam Garg, Dimitris Tsipras, Percy Liang, and Gregory Valiant. What can transformers learn in-context? A case study of simple function classes. In *Proc NeurIPS*, pp. 30583–98, 2022. doi: 10.5555/3600270.3602487.
- Yury Gorishniy, Ivan Rubachev, Valentin Khrulkov, and Artem Babenko. Revisiting deep learning models for tabular data. In *Proc NeurIPS*, pp. 18932–43, 2021. doi: 10.5555/3540261.3541708.

- Lin Lawrence Guo, Ethan Steinberg, Scott Lanyon Fleming, Jose Posada, Joshua Lemmon, Stephen R Pfohl, Nigam Shah, Jason Fries, and Lillian Sung. EHR foundation models improve robustness in the presence of temporal distribution shift. *Sci Rep*, 13, 2023. doi: 10.1038/s41598-023-30820-8.
  - Lin Lawrence Guo, Jason Fries, Ethan Steinberg, Scott Lanyon Fleming, Keith Morse, Caterine Aftandilian, Jose Posada, Nigam Shah, and Lillian Sung. A multi-center study on the adaptability of a shared foundation model for electronic health records. *npj Digit Med*, 7(1):171, 2024a. doi: 10.1038/s41746-024-01166-w.
  - Qingyan Guo, Rui Wang, Junliang Guo, Bei Li, Kaitao Song, Xu Tan, Guoqing Liu, Jiang Bian, and Yujiu Yang. Connecting large language models with evolutionary algorithms yields powerful prompt optimizers. In *Proc ICLR*, 2024b. URL https://openreview.net/forum?id=ZG3RaNIsO8.
  - Tianyu Guo, Wei Hu, Song Mei, Huan Wang, Caiming Xiong, Silvio Savarese, and Yu Bai. How do transformers learn in-context beyond simple functions? A case study on learning with representations. In *Proc ICLR*, 2024c. URL https://openreview.net/forum?id=ikwEDva1JZ.
  - Tomasz Gutowski, Ryszard Antkiewicz, and Stanisław Szlufik. Machine learning with optimization to create medicine intake schedules for Parkinson's disease patients. *PLoS One*, 18:e0293123, 2023. doi: 10.1371/journal.pone.0293123.
  - Cuong Ha, Shima Asaadi, Sanjeev Kumar Karn, Oladimeji Farri, Tobias Heimann, and Thomas Runkler. Fusion of domain-adapted vision and language models for medical visual question answering. In *Proc Clin Nat Lang Proc Workshop*, pp. 246–57, 2024. doi: 10.18653/v1/2024. clinicalnlp-1.21.
  - Paul Hager, Friederike Jungmann, Robbie Holland, Kunal Bhagat, Inga Hubrecht, Manuel Knauer, Jakob Vielhauer, Marcus Makowski, Rickmer Braren, Georgios Kaissis, and Daniel Rueckert. Evaluation and mitigation of the limitations of large language models in clinical decision-making. *Nat Med*, 30:2613–22, 2024. doi: 10.1038/s41591-024-03097-1.
  - Tianyu Han, Sven Nebelung, Firas Khader, Tianci Wang, Gustav Müller-Franzes, Christiane Kuhl, Sebastian Försch, Jens Kleesiek, Christoph Haarburger, Keno K Bressem, Jakob Nikolas Kather, and Daniel Truhn. Medical large language models are susceptible to targeted misinformation attacks. *npj Digit Med*, 7, 2024. doi: 10.1038/s41746-024-01282-7.
  - Nikolaus Hansen. *The CMA evolution strategy: A comparing review*, pp. 75–102. Springer Berlin Heidelberg, 2006. doi: 10.1007/3-540-32494-1\_4.
  - Minsheng Hao, Jing Gong, Xin Zeng, Chiming Liu, Yucheng Guo, Xingyi Cheng, Taifeng Wang, Jianzhu Ma, Xuegong Zhang, and Le Song. Large-scale foundation model on single-cell transcriptomics. *Nat Meth*, 21:1481–91, 2024. doi: 10.1038/s41592-024-02305-7.
  - Liye He, Jing Tang, Emma I Andersson, Sanna Timonen, Steffen Koschmieder, Krister Wennerberg, Satu Mustjoki, and Tero Aittokallio. Patient-customized drug combination prediction and testing for T-cell prolymphocytic leukemia patients. *Cancer Res*, 78(9):2407–18, 2018. doi: 10.1158/0008-5472.CAN-17-3644.
  - Daniel Scott Himmelstein, Antoine Lizee, Christine Hessler, Leo Brueggeman, Sabrina L Chen, Dexter Hadley, Ari Green, Pouya Khankhanian, and Sergio E Baranzini. Systematic integration of biomedical knowledge prioritizes drugs for repurposing. *eLife*, 6:e26726, 2017. doi: 10.7554/eLife.26726.
  - Junming Ho, Haibo Yu, Yihan Shao, Mackenzie Taylor, and Junbo Chen. How accurate are QM/MM models? *J Phys Chem*, 129, 2024.
- Noah Hollmann, Samuel Müller, Lennart Purucker, Arjun Krishnakumar, Max Körfer, Shi Bin Hoo, Robin Tibor Schirrmeister, and Frank Hutter. Accurate predictions on small data with a tabular foundation model. *Nature*, 637:319–26, 2025. doi: 10.1038/s41586-024-08328-6.
  - Charles Hong, Sahil Bhatia, Alvin Cheung, and Yakun Sophia Shao. Autocomp: LLM-driven code optimization for tensor accelerators. *arXiv Preprint*, 2025. doi: 10.48550/arXiv.2505.18574.

- Kai Hu, Klas Leino, Zifan Wang, and Matt Fredrikson. A recipe for improved certifiable robustness. In *Proc ICLR*, 2024. URL https://openreview.net/forum?id=qz3mcn99cu.
  - Kexin Huang, Payal Chandak, Qianwen Wang, Shreyas Havaldar, Akhil Vaid, Jure Leskovec, Girish N Nadkarni, Benjamin S Glicksberg, Nils Gehlenborg, and Marinka Zitnik. A foundation model for clinician-centered drug repurposing. *Nat Med*, 30:3601–13, 2024. doi: 10.1038/s41591-024-03233-x.
  - Aleksandr Ianevski, Jenni Lahtela, Komal K Javarappa, Philipp Sergeev, Bishwa R Ghimire, Prson Gautam, Markus Vähä-Koskela, Laura Turunen, Nora Linnavirta, Heikki Kuusanmäki, Mika Kontro, Kimmo Porkka, Caroline A Heckman, Pirkko Mattila, Krister Wennerberg, Anil K Giri, and Tero Aittokallio. Patient-tailored design for selective co-inhibition of leukemic cell subpopulations. *Sci Adv*, 7(8):eabe4038, 2021. doi: 10.1126/sciadv.abe4038.
  - Nadia Islam, Laura Budvytyte, Nanditta Khera, and Talal Hilal. Disparities in clinical trial enrollment Focus on CAR-T and bispecific antibody therapies. *Curr Hematol Malig Rep*, 20:1, 2024. doi: 10.1007/s11899-024-00747-6.
  - Daniel P Jeong, Saurabh Garg, Zachary Chase Lipton, and Michael Oberst. Medical adaptation of large language and vision-language models: Are we making progress? In *Proc EMNLP*, pp. 12143–70, 2024. doi: 10.18653/v1/2024.emnlp-main.677.
  - Zipeng Ji, Guanghui Zhu, Chunfeng Yuan, and Yihua Huang. RZ-NAS: Enhancing LLM-guided neural architecture search via reflective zero-cost strategy. In *Proc ICML*, 2025. URL https://openreview.net/forum?id=9UExQpH078.
  - Ying Jin and Emmanuel J Candes. Selection by prediction with conformal p-values. *J Mach Learn Res*, 24(244):1–41, 2023. URL http://jmlr.org/papers/v24/22-1176.html.
  - Kevin B Johnson, Wei-Qi Wei, Dilhan Weeraratne, Mark E Frisse, Karl Misulis, Kyu Rhee, Huan Zhao, and Jane L Snowdon. Precision medicine, AI, and the future of personalized health care. *Clin Transl Sci*, 14(1):86–93, 2020. doi: 10.1111/cts.12884.
  - Kadina E Johnston, Patrick J Almhjell, Ella J Watkins-Dulaney, Grace Liu, Nicholas J Porter, Jason Yang, and Frances H Arnold. A combinatorially complete epistatic fitness landscape in an enzyme active site. *Proc Nat Acad Sci*, 121(32):e2400439121, 2024. doi: 10.1073/pnas.2400439121.
  - Chancellor Johnstone and Bruce Cox. Conformal uncertainty sets for robust optimization. In *Proc Conform Probabilistic Pred Appl*, volume 152, pp. 72–90. PMLR, 2021. URL https://proceedings.mlr.press/v152/johnstone21a.html.
  - Leonid Kantorovich and Gennadii S Rubinstein. On a space of totally additive functions. *Vestnik Leningrad. Univ*, 13:52–9, 1958.
  - Evangelia Katsoulakis, Qi Wang, Huanmei Wu, Leili Shahriyari, Richard Fletcher, Jinwei Liu, Luke Achenie, Hongfang Liu, Pamela Jackson, Ying Xiao, Tanveer Syeda-Mahmood, Richard Tuli, and Jun Deng. Digital twins for health: A scoping review. *npj Digit Med*, 7, 2024. doi: 10.1038/s41746-024-01073-0.
  - Tyler R Kemnic and Peter G Gulick. *HIV antiretroviral therapy*, chapter StatPearls [Internet]. Stats-Pearls Publishing, 2025. URL https://www.ncbi.nlm.nih.gov/books/NBK513308.
  - David A Khan, Elizabeth J Phillips, John J Accarino, Alexei Gonzalez-Estrada, Iris M Otani, Allison Ramsey, Anna Chen Arroyo, Aleena Banerji, Timothy Chow, Anne Liu, Cosby A Stone Jr, and Kimberly G Blumenthal. United States Drug Allergy Registry (USDAR) grading scale for immediate drug reactions. *J Allergy Clin Immunol*, 152(6):1581–6, 2023. doi: 10.1016/j.jaci.2023.08.018.
  - Joanne Kim, Andrew Harper, Valerie McCormack, Hyuna Sung, Nehmat Houssami, Eileen Morgan, Miriam Mutebi, Gail Garvey, Isabelle Soerjomataram, and Miranda M Fidler-Benaoudia. Global patterns and trends in breast cancer incidence and mortality across 185 countries. *Nat Med*, 31: 1154–62, 2025. doi: 10.1038/s41591-025-03502-3.

- J Kirchheiner, H Schmidt, M Tzvetkov, J-Tha Keulen, J Lötsch, I Roots, and J Brockmöller. Pharmacokinetics of codeine and its metabolite morphine in ultra-rapid metabolizers due to CYP2D6 duplication. *Pharmacogenomics J*, 7:257–65, 2007. doi: 10.1038/sj.tpj.6500406.
  - Kedar Kirtane and Stephanie J Lee. Racial and ethnic disparities in hematologic malignancies. *Blood*, 130(15):1699–705, 2017. doi: 10.1182/blood-2017-04-778225.
  - Dexter C Kozen. *The Myhill-Nerode theorem*, pp. 95–9. Springer New York, 1997. doi: 10.1007/978-1-4612-1844-9\_17.
  - Siddarth Krishnamoorthy, Satvik Mehul Mashkaria, and Aditya Grover. Diffusion models for black-box optimization. In *Proc ICML*, volume 202, pp. 17842–57, 2023. URL https://proceedings.mlr.press/v202/krishnamoorthy23a.html.
  - Keying Kuang, Frances Dean, Jack B Jedlicki, David Ouyang, Anthony Philippakis, David Sontag, and Ahmed Alaa. Med-Real2Sim: Non-invasive medical digital twins using physics-informed self-supervised learning. In *Proc NeurIPS*, pp. 5757–88, 2024. doi: 10.5555/3737916.3738103.
  - H W Kuhn. The Hungarian method for the assignment problem. *Naval Res Logistics*, 2:83–97, 1955. doi: 10.1002/nav.3800020109.
  - Lorenz Kuhn, Yarin Gal, and Sebastian Farquhar. Semantic uncertainty: Linguistic invariances for uncertainty estimation in natural language generation. In *Proc ICLR*, 2023. URL https://openreview.net/forum?id=VD-AYtP0dve.
  - Halil Ibrahim Kuru, A Ercument Cicek, and Oznur Tastan. From cell lines to cancer patients: Personalized drug synergy prediction. *Bioinform*, 40(5):btae134, 2024. doi: 10.1093/bioinformatics/btae134.
  - Taeyoon Kwon, Kai Tzu-iunn Ong, Dongjin Kang, Seungjun Moon, Jeong Ryong Lee, Dosik Hwang, Beomseok Sohn, Yongsik Sim, Dongha Lee, and Jinyoung Yeo. Large language models are clinical reasoners: Reasoning-aware diagnosis framework with prompt-generated rationales. In *Proc AAAI*, pp. 18417–25, 2024. doi: 10.1609/aaai.v38i16.29802.
  - Yanis Labrak, Adrien Bazoge, Emmanuel Morin, Pierre-Antoine Gourraud, Mickael Rouvier, and Richard Dufour. BioMistral: A collection of open-source pretrained large language models for medical domains. In *Findings ACL*, pp. 5848–64, 2024. doi: 10.18653/v1/2024.findings-acl.348.
  - Karilyn T Larkin, Deedra Nicolet, Benjamin J Kelly, Krzysztof Mrózek, Stephanie LaHaye, Katherine E Miller, Saranga Wijeratne, Gregory Wheeler, Jessica Kohlschmidt, James S Blachly, Alice S Mims, Christopher J Walker, Christopher C Oakes, Shelley Orwick, Isaiah Boateng, Jill Buss, Adrienne Heyrosa, Helee Desai, Andrew J. Carroll, William Blum, Bayard L. Powell, Jonathan E. Kolitz, Joseph O Moore, Robert J Mayer, Richard A Larson, Richard M Stone, Electra D Paskett, John C Byrd, Elaine R Mardis, and Ann-Kathrin Eisfeld. High early death rates, treatment resistance, and short survival of Black adolescents and young adults with AML. *Blood Advances*, 6 (19):5570–81, 2022. doi: 10.1182/bloodadvances.2022007544.
  - Daniel W Lee, Bianca D Santomasso, Frederick L Locke, Armin Ghobadi, Cameron J Turtle, Jennifer N Brudno, Marcela V Maus, Jae H Park, Elena Mead, Steven Pavletic, William Y Go, Lamis Eldjerou, Rebecca A Gardner, Noelle Frey, Keven J Curran, Karl Peggs, Marcelo Pasquini, John F DiPersio, Marcel R M van den Brink, Krishna V Komanduri, Stephan A Grupp, and Sattva S Nellapu. ASTCT consensus grading for cytokine release syndrome and neurologic toxicity associated with immune effector cells. *Biol Blood Marrow Transplant*, 25:625–38, 2019. doi: 10.1016/j.bbmt.2018.12.758.
  - Ming Ta Michael Lee and Teri E Klein. Pharmacogenetics of warfarin: Challenges and opportunities. *J Human Genetics*, 58:334–8, 2013. doi: 10.1038/jhg.2013.40.
  - Chunyuan Li, Cliff Wong, Sheng Zhang, Naoto Usuyama, Haotian Liu, Jianwei Yang, Tristan Naumann, Hoifung Poon, and Jianfeng Gao. LLaVA-Med: Training a large language-and-vision assistant for biomedicine in one day. In *Proc NeurIPS*, pp. 28541–64, 2023. doi: 10.5555/3666122.3667362.

- Xiang Lin, Tian Tian, Zhi Wei, and Hakon Hakonarson. Clustering of single-cell multi-omics data with a multimodal deep learning method. *Nat Commun*, 13, 2022. doi: 10.1038/s41467-022-35031-9.
- Shengcai Liu, Caishun Chen, Xinghua Qu, Ke Tang, and Yew-Soon Ong. Large language models as evolutionary optimizers. In *Proc IEEE CEC*, pp. 1–8, 2024a. doi: 10.1109/CEC60901.2024. 10611913.
- Shihong Liu, Samuel Yu, Zhiqiu Lin, Deepak Pathak, and Deva Ramanan. Language models as black-box optimizers for vision-language models. In *Proc CVPR*, pp. 12687–97, 2024b. doi: 10.1109/CVPR52733.2024.01206.
- Tennison Liu, Nicolás Astorga, Nabeel Seedat, and Mihaela van der Schaar. Large language models to enhance Bayesian optimization. In *Proc ICLR*, 2024c. URL https://openreview.net/forum?id=OOxotBmGol.
- Xiaohong Liu, Hao Liu, Guoxing Yang, Zeyu Jiang, Shuguang Cui, Zhaoze Zhang, Huan Wang, Liyuan Tao, Yongchang Sun, Zhu Song, Tianpei Hong, Jin Yang, Tianrun Gao, Jiangjiang Zhang, Xiaohu Li, Jing Zhang, Ye Sang, Zhao Yang, Kanmin Xue, Song Wu, Ping Zhang, Jian Yang, Chunli Song, and Guangyu Wang. A generalist medical language model for disease diagnosis assistance. *Nat Med*, 31:932–42, 2025. doi: 10.1038/s41591-024-03416-6.
- Joseph D Ma, Kelly C Lee, and Grace M Kuo. Hla-b\*5701 testing to predict abacavir hypersensitivity. *PLoS Curr*, 2:RRN1203, 2010. doi: 10.1371/currents.RRN1203.
- Pingchuan Ma, Tsun-Hsuan Wang, Minghao Guo, Zhiqing Sun, Joshua B Tenenbaum, Daniela Rus, Chuang Gan, and Wojciech Matusik. LLM and simulation as bilevel optimizers: A new paradigm to advance physical scientific discovery. In *Proc ICML*, pp. 33940–62, 2024a. doi: 10.48550/arXiv.2405.09783.
- Yecheng Jason Ma, William Liang, Guanzhi Wang, De-An Huang, Osbert Bastani, Dinesh Jayaraman, Yuke Zhu, Linxi Fan, and Anima Anandkumar. Eureka: Human-level reward design via coding large language models. In *Proc ICLR*, 2024b. URL https://openreview.net/forum?id=IEduRUO55F.
- Chiara Dalla Man, Francesco Micheletto, Dayu Lv, Marc Breton, Boris Kovatchev, and Claudio Cobelli. The UVA/PADOVA type 1 diabetes simulator. *J Diabetes Sci Technol*, 8:26–34, 2014. doi: 10.1177/1932296813514502.
- Satvik M Mashkaria, Siddarth Krishnamoorthy, and Aditya Grover. Generative pretraining for black-box optimization. In *Proc ICML*, volume 202, pp. 24173–97, 2023. URL https://proceedings.mlr.press/v202/mashkaria23a.html.
- Nikita Mehandru, Niloufar Golchini, David Bamman, Travis Zack, Melanie F Molina, and Ahmed Alaa. ER-REASON: A benchmark dataset for LLM-based clinical reasoning in the emergency room. *arXiv Preprint*, 2025. doi: 10.48550/arXiv.2505.22919.
- Tasquia Mizan and Sharareh Taghipour. Medical resource allocation planning by integrating machine learning and optimization models. *Artif Intell Med*, 134:102430, 2022. doi: 10.1016/j. artmed.2022.102430.
- Rahul Nadkarni, David Wadden, Iz Beltagy, Noah Smith, Hannaneh Hajishirzi, and Tom Hope. Scientific language models for biomedical knowledge base completion: An empirical study. In *Proc Conf Automat Knowl Base Const*, 2021. URL https://openreview.net/forum?id=4Exq\_UvWKY8.
- Muhammad Umair Nasir, Sam Earle, Julian Togelius, Steven James, and Christopher Cleghorn. LLMatic: Neural architecture search via large language models and quality diversity optimization. In *Proc Gene Evo Comp Conf*, pp. 1110–8, 2024. doi: 10.1145/3638529.3654017.
- Nghia Ngo, Bonan Min, and Thien Nguyen. Unsupervised domain adaptation for joint information extraction. In *Findings Assoc Comp Ling EMNLP*, pp. 5894–905, 2022. doi: 10.18653/v1/2022. findings-emnlp.434.

- Alexander V Nikitin, Jannik Kossen, Yarin Gal, and Pekka Marttinen. Kernel language entropy: Fine-grained uncertainty quantification for LLMs from semantic similarities. In *Proc NeurIPS*, 2024. URL https://openreview.net/forum?id=j2wCrWmgMX.
  - Alexander Novikov, Ngân Vũ, Marvin Eisenberger, Emilien Dupont, Po-Sen Huang, Adam Zsolt Wagner, Sergey Shirobokov, Borislav Kozlovskii, Francisco J R Ruiz, Abbas Mehrabian, M Pawan Kumar, Abigail See, Swarat Chaudhuri, George Holland, Alex Davies, Sebastian Nowozin, Pushmeet Kohli, and Matej Balog. AlphaEvolve: A coding agent for scientific and algorithmic discovery. *arXiv Preprint*, 2025. doi: 10.48550/arXiv.2506.13131.
  - Mahmud Omar, Vera Sorin, Jeremy D Collins, David Reich, Robert Freeman, Nicholas Gavin, Alexander Charney, Lisa Stump, Nicola Luigi Bragazzi, Girish N Nadkarni, and Eyal Klang. Multi-model assurance analysis showing large language models are highly vulnerable to adversarial hallucination attacks during clinical decision support. *Nat Commun Med*, 5, 2025. doi: 10.1038/s43856-025-01021-3.
  - Jesutofunmi Omiye, Jenna C Lester, Simon Spichak, Veronica Rotemberg, and Roxana Daneshjou. Large language models propagate race-based medicine. npj Digit Med, 6, 2023. doi: 10.1038/s41746-023-00939-z.
  - Paul K Paik, Enriqueta Felip, Remi Veillon, Hiroshi Sakai, Alexis B Cortot, Marina C Garassino, Julien Mazieres, Santiago Viteri, Helene Senellart, Jan Van Meerbeeck, Jo Raskin, Niels Reinmuth, Pierfranco Conte, Dariusz Kowalski, Byoung Chul Cho, Jyoti D Patel, Leora Horn, Frank Griesinger, Ji-Youn Han, Young-Chul Kim, Gee-Chen Chang, Chen-Liang Tsai, James CH Yang, Yuh-Min Chen, Egbert F Smit, Anthonie J van der Wekken, Terufumi Kato, Dilafruz Juraeva, Christopher Stroh, Rolf Bruns, Josef Straub, Andreas Johne, Jürgen Scheele, John V Heymach, and Xiuning Le. Tepotinib in non-small-cell lung cancer with MET exon 14 skipping mutations. N Eng J Med, 383(10):931–943, 2020. doi: 10.1056/NEJMoa2004407.
  - Alexander Pan, Erik Jones, Meena Jagadeesan, and Jacob Steinhardt. Feedback loops with language models drive in-context reward hacking. In *Proc ICML*, pp. 39154–200, 2024. doi: 10.5555/3692070.3693659.
  - Petros Papalexis, Vasiliki Epameinondas Georgakopoulou, Panagiotis V Drossos, Eirini Thymara, Aphrodite Nonni, Andreas C Lazaris, George C Zografos, Demetrios A Spandidos, Nikolaos Kavantzas, and Georgia Eleni Thomopoulou. Precision medicine in breast cancer. *Mol Clin Oncol*, 21(5):78, 2024. doi: 10.3892/mco.2024.2776.
  - Harlan Pittell, Gregory S Calip, Amy Pierre, Cleo A Ryals, Ivy Altomare, Trevor J Royce, and Jenny S Guadamuz. Racial and ethnic inequities in US oncology clinical trial participation from 2017 to 2022. *JAMA Netw Open*, 6(7):e2322515, 2023. doi: 10.1001/jamanetworkopen.2023. 22515.
  - Yujia Qin, Shihao Liang, Yining Ye, Kunlun Zhu, Lan Yan, Yaxi Lu, Yankai Lin, Xin Cong, Xiangru Tang, Bill Qian, Sihan Zhao, Lauren Hong, Runchu Tian, Ruobing Xie, Jie Zhou, Mark Gerstein, Dahai Li, Zhiyuan Liu, and Maosong Sun. ToolLLM: Facilitating large language models to master 16000+ real-world APIs. In *Proc ICLR*, 2024. URL https://openreview.net/forum?id=dHng200Jjr.
  - Zexuan Qiu, Zijing Ou, Bin Wu, Jingjing Li, Aiwei Liu, and Irwin King. Entropy-based decoding for retrieval-augmented large language models. In *Proc ACL: Human Lang Tech*, pp. 4616–27, 2025. doi: 10.18653/v1/2025.naacl-long.236.
  - Victor Quach, Adam Fisch, Tal Schuster, Adam Yala, Jae Ho Sohn, Tommi S Jaakkola, and Regina Barzilay. Conformal language modeling. In *Proc ICLR*, 2024. URL https://openreview.net/forum?id=pzUhfQ74c5.
  - J R Quinlan. Induction of decision trees. *Mach Learn*, 1(1):81–106, 1986. doi: 10.1023/A: 1022643204877.
  - Meghana Arakkal Rajeev, Rajkumar Ramamurthy, Prapti Trivedi, Vikas Yadav, Oluwanifemi Bamgbose, Sathwik Tejaswi Madhusudhan, James Zou, and Nazneen Rajani. Cats confuse reasoning LLM: Query agnostic adversarial triggers for reasoning models. In *Proc COLM*, 2025. URL https://openreview.net/forum?id=VrEPiN5WhM.

- Dino W Ramzi and Kenneth V Leeper. DVT and pulmonary embolism: Part II. Treatment and prevention. *Am Fam Physician*, 69(12):2841–8, 2004.
  - Wesley F Reinhart and Antonia Statt. Large language models design sequence-defined macromolecules via evolutionary optimization. *npj Comp Mat*, 10(262), 2024. doi: 10.1038/s41524-024-01449-6.
  - Shaolei Ren, Bill Tomlinson, Rebecca W Black, and Andrew W Torrance. Reconciling the contrasting narratives on the environmental impact of large language models. *Sci Rep*, 14, 2024. doi: 10.1038/s41598-024-76682-6.
  - Soo-Yon Rhee, Matthew J Gonzales, Rami Kantor, Bradley J Betts, Jaideep Ravela, and Robert W Shafer. Human immunodeficiency virus reverse transcriptase and protease sequence database. *Nuc Acid Res*, 31:2938–303, 2003. doi: 10.1093/nar/gkg100.
  - Gordon Rix, Ella J Watkins-Dulaney, Patrick J Almhjell, Christina E Boville, Frances H Arnold, and Chang C Liu. Scalable continuous evolution for the generation of diverse enzyme variants encompassing promiscuous activities. *Nat Commun*, 11, 2020. doi: 10.1038/s41467-020-19539-6.
  - Bernardino Romera-Paredes, Mohammadamin Barekatain, Alexander Novikov, Matej Balog, M Pawan Kumar, Emilien Dupont, Francisco Ruiz, Jordan S Ellenberg, Pengming Wang, Omar Fawzi, Pushmeet Kohli, and Alhussein Fawzi. Mathematical discoveries from program search with large language models. *Nature*, 625:468–75, 2024. doi: 10.1038/s41586-023-06924-6.
  - Michael S Saag, Rajesh T Gandhi, Jennifer F Hoy, Raphael J Landovitz, Melanie A Thompson, Paul E Sax, Davey M Smith, Constance A Benson, Susan P Buchbinder, Carlos del Rio, Joseph J Eron Jr, Gerd Fätkenheuer, Huldrych F Günthard, Jean-Michel Molina, Donna M Jacobsen, and Paul A Volberding. Antiretroviral drugs for treatment and prevention of HIV infection in adults. *J Am Med Assoc*, 324:1651–69, 2020. doi: 10.1001/jama.2020.17025.
  - Kuniaki Saito, Kohei Watanabe, Yoshitaka Ushiku, and Tatsuya Harada. Maximum classifier discrepancy for unsupervised domain adaptation. In *Proc IEEE CVPR*, pp. 3723–32, 2018. doi: 10.1109/CVPR.2018.00392.
  - Siddharth Samsi, Dan Zhao, Joseph McDonald, Baolin Li, Adam Michaleas, Michael Jones, William Bergeron, Jeremy Kepner, Devesh Tiwari, and Vijay Gadepally. From words to watts: Benchmarking the energy costs of large language model inference. *arXiv Preprint*, 2023. doi: 10.48550/arXiv.2310.03003.
  - Thomas Savage, Ashwin Nayak, Robert Gallo, Ekanath Rangan, and Jonathan H Chen. Diagnostic reasoning prompts reveal the potential for large language model interpretability in medicine. *npj Digit Med*, 7, 2024. doi: 10.1038/s41746-024-01010-1.
  - Kevin Scaman and Aladin Virmaux. Lipschitz regularity of deep neural networks: Analysis and efficient estimation. In *Proc NeurIPS*, pp. 3839–48, 2018. doi: 10.5555/3327144.3327299.
  - Timo Schick, Jane Dwivedi-Yu, Roberto Dessí, Roberta Raileanu, Maria Lomeli, Eric Hambro, Luke Zettlemoyer, Nicola Cancedda, and Thomas Scialom. Toolformer: Language models can teach themselves to use tools. In *Proc NeurIPS*, pp. 68539–51, 2023. doi: 10.5555/3666122. 3669119.
  - Elizabeth A Sconce, Tayyaba I Khan, Hilary A Wynne, Peter Avery, Louise Monkhouse, Barry P King, Peter Wood, Patrick Kesteven, Ann K Daly, and Farhad Kamali. The impact of CYP2C9 and VKORC1 genetic polymorphism and patient characteristics upon warfarin dose requirements: Proposal for a new dosing regimen. *Blood*, 106(7):2329–33, 2005. doi: 10.1182/blood-2005-03-1108.
  - Andrew Sellergren, Sahar Kazemzadeh, Tiam Jaroensri, Atilla Kiraly, Madeleine Traverse, Timo Kohlberger, Shawn Xu, Fayaz Jamil, Cían Hughes, Charles Lau, Justin Chen, Fereshteh Mahvar, Liron Yatziv, Tiffany Chen, Bram Sterling, Stefanie Anna Baby, Susanna Maria Baby, Jeremy Lai, Samuel Schmidgall, Lu Yang, Kejia Chen, Per Bjornsson, Shashir Reddy, Ryan Brush, Kenneth Philbrick, Howard Hu, Howard Yang, Richa Tiwari, Sunny Jansen, Preeti Singh, Yun Liu, Shekoofeh Azizi, Aishwarya Kamath, Johan Ferret, Shreya Pathak, Nino Vieillard, Ramona

Merhej, Sarah Perrin, Tatiana Matejovicova, Alexandre Ramé, Morgane Riviere, Louis Rouil-lard, Thomas Mesnard, Geoffrey Cideron, Jean-bastien Grill, Sabela Ramos, Edouard Yvinec, Michelle Casbon, Elena Buchatskaya, Jean-Baptiste Alayrac, Dmitry Lepikhin, Vlad Feinberg, Sebastian Borgeaud, Alek Andreev, Cassidy Hardin, Robert Dadashi, Léonard Hussenot, Ar-mand Joulin, Olivier Bachem, Yossi Matias, Katherine Chou, Avinatan Hassidim, Kavi Goel, Clement Farabet, Joelle Barral, Tris Warkentin, Jonathon Shlens, David Fleet, Victor Cotruta, Omar Sanseviero, Gus Martins, Phoebe Kirk, Anand Rao, Shravya Shetty, David F Steiner, Can Kirmizibayrak, Rory Pilgrim, Daniel Golden, and Lin Yang. MedGemma technical report. arXiv Preprint, 2025. doi: 10.48550/arXiv.2507.05201. 

- Parshin Shojaee, Kazem Meidani, Shashank Gupta, Amir Barati Farimani, and Chandan K Reddy. LLM-SR: Scientific equation discovery via programming with large language models. In *Proc ICLR*, 2025. URL https://openreview.net/forum?id=m2nmp8P5in.
- Alexander G Shypula, Aman Madaan, Yimeng Zeng, Uri Alon, Jacob R Gardner, Yiming Yang, Milad Hashemi, Graham Neubig, Parthasarathy Ranganathan, Osbert Bastani, and Amir Yazdanbakhsh. Learning performance-improving code edits. In *Proc ICLR*, 2024. URL https://openreview.net/forum?id=ix7rLVHXyY.
- Karan Singhal, Shekoofeh Azizi, Tao Tu, S Sara Mahdavi, Jason Wei, Hyung Won Chung, Nathan Scales, Ajay Tanwani, Heather Cole-Lewis, Stephen Pfohl, Perry Payne, Martin Seneviratne, Paul Gamble, Chris Kelly, Abubakr Babiker, Nathanael Schärli, Aakanksha Chowdhery, Philip Mansfield, Dina Demner-Fushman, Blaise Agüera y Arcas, Dale Webster, Greg S Corrado, Yossi Matias, Katherine Chou, Juraj Gottweis, Nenad Tomasev, Yun Liu, Alvin Rajkomar, Joelle Barral, Christopher Semturs, Alan Karthikesalingam, and Vivek Natarajan. Large language models encode clinical knowledge. *Nature*, 620:172–80, 2023.
- Karan Singhal, Tao Tu, Juraj Gottweis, Rory Sayres, Ellery Wulczyn, Mohamed Amin, Le Hou, Kevin Clark, Stephen R Pfohl, Heather Cole-Lewis, Darlene Neal, Qazi Mamunur Rashid, Mike Schaekermann, Amy Wang, Dev Dash, Jonathan H Chen, Nigam H Shah, Sami Lachgar, Philip Andrew Mansfield, Sushant Prakash, Bradley Green, Ewa Dominowska, Blaise Agüera y Arcas, Nenad Yun Tomašev, Liu, Renee Wong, Christopher Semturs, S Sara Mahdavi, Joelle K Barral, Dale R Webster, Greg S Corrado, Yossi Matias, Shekoofeh Azizi, Alan Karthikesalingam, and Vivek Natarajan. Toward expert-level medical question answering with large language models. *Nat Med*, 31:943–50, 2025. doi: 10.1038/s41591-024-03423-7.
- Demetria Smith-Graziani and Christopher R Flowers. Understanding and addressing disparities in patients with hematologic malignancies: Approaches for clinicians. *Am Soc Clin Onc Edu*, 41: 1–7, 2021. doi: 10.1200/EDBK\_320079.
- Xingyou Song, Yingtao Tian, Robert Tjarko Lange, Chansoo Lee, Yujin Tang, and Yutian Chen. Position: Leverage foundational models for black-box optimization. In *Proc ICML*, 2024. doi: 10.5555/3692070.3693948.
- Yuki Sonoda, Ryo Kurokawa, Akifumi Hagiwara, Yusuke Asari, Takahiro Fukushima, Jun Kanzawa, Wataru Gonoi, and Osamu Abe. Structured clinical reasoning prompt enhances LLM's diagnostic capabilities in Diagnosis Please quiz cases. *Jpn J Radiol*, 43(4):586–92, 2024. doi: 10.1007/s11604-024-01712-2.
- Vera Sorin, Panagiotis Korfiatis, Jeremy D Collins, Donald Apakama, Mahmud Omar, Benjamin S Glicksberg, Mei-Ean Yeow, Megan Brandeland, Girish N Nadkarni, and Eyal Klang. Sociodemographic modifiers shape large language models' ethical decisions. *J Healthc Inform Res*, 2025. doi: 10.1007/s41666-025-00211-x.
- Akshai Parakkal Sreenivasan, Aina Vaivade, Yassine Noui, Payam Emami Khoonsari, Joachim Burman, Ola Spjuth, and Kim Kultima. Conformal prediction enables disease course prediction and allows individualized diagnostic uncertainty in multiple sclerosis. *npj Digit Med*, 8, 2025. doi: 10.1038/s41746-025-01616-z.
- Samuel Stanton, Wesley Maddox, and Andrew Gordon Wilson. Bayesian optimization with conformal prediction sets. In *Proc AISTATS*, volume 206, pp. 959–86. PMLR, 2023. URL https://proceedings.mlr.press/v206/stanton23a.html.

- Ethan Steinberg, Jason Alan Fries, Yizhe Xu, and Nigam Shah. MOTOR: A time-to-event foundation model for structured medical records. In *Proc ICLR*, 2024. URL https://openreview. net/forum?id=NialiwI2V6.
  - Baochen Sun and Kate Saenko. Deep CORAL: Correlation alignment for deep domain adaptation. In *ECCV 2016 Workshops*, 2016.
  - John G Tate, Sally Bamford, Harry C Jubb, Zbyslaw Sondka, David M Beare, Nidhi Bindal, Harry Boutselakis, Charlotte G Cole, Celestino Creatore, Elisabeth Dawson, Peter Fish, Bhavana Harsha, Charlie Hathaway, Steve C Jupe, Chai Yin Kok, Kate Noble, Laura Ponting, Christopher C Ramshaw, Claire E Rye, Helen E Speedy, Ray Stefancsik, Sam L Thompson, Shicai Wang, Sari Ward, Peter J Campbell, and Simon A Forbes. COSMIC: The catalogue of somatic mutations in cancer. *Nucleic Acids Res*, 47(D1):D941–7, 2019. doi: 10.1093/nar/gky1015.
  - Derian B Taylor, Oyomoare L Osazuwa-Peters, Somtochi I Okafor, Eric Adjei Boakye, Duaa Kuziez, Chamila Perera, Matthew C Simpson, Justin M Barnes, Mustafa G Bulbul, Trinitia Y Cannon, Tammara L Watts, Uchechukwu C Megwalu, Mark A Varvares, and Nosayaba Osazuwa-Peters. Differential outcomes among survivors of head and neck cancer belonging to racial and ethnic minority groups. *JAMA Otolaryngol Head Neck Surg*, 148(2):119–27, 2022. doi: 10.1001/jamaoto.2021.3425.
  - V A Traag, L Waltman, and N J van Eck. From Louvain to Leiden: Guaranteeing well-connected communities. *Sci Rep*, 9, 2019. doi: 10.1038/s41598-019-41695-z.
  - Brandon Trabucco, Aviral Kumar, Xinyang Geng, and Sergey Levine. Conservative objective models for effective offline model-based optimization. In *Proc ICML*, volume 139, pp. 10358–68. PMLR, 2021. URL https://proceedings.mlr.press/v139/trabucco21a.html.
  - Brandon Trabucco, Xinyang Geng, Aviral Kumar, and Sergey Levine. Design-bench: Benchmarks for data-driven offline model-based optimization. In *Proc ICML*, volume 162, pp. 21658–76, 2022. URL https://proceedings.mlr.press/v162/trabucco22a.html.
  - Andy Trotti, A Dimitrios Colevas, Ann Setser, Valerie Rusch, David Jaques, Volker Budach, Corey Langer, Barbara Murphy, Richard Cumberlin, C Norman Coleman, and Philip Rubin. CTCAE v3.0: Development of a comprehensive grading system for the adverse effects of cancer treatment. *Seminars in Rad Oncol*, 13(3):176–81, 2003. doi: 10.1016/S1053-4296(03)00031-6.
  - Constantino Tsallis. Possible generalization of Boltzmann-Gibbs statistics. *J Stat Phys*, 52:479–87, 1988. doi: doi.org/10.1007/BF01016429.
  - Aviad Tsherniak, Francisca Vazquez, Phil G Montgomery, Barbara A Weir, Gregory Kryukov, Glenn S Cowley, Stanley Gill, William F Harrington, Sasha Pantel, John M Krill-Burger, Robin M Meyers, Levi Ali, Amy Goodale, Yenarae Lee, Guozhi Jiang, Jessica Hsiao, William FJ Gerath, Sara Howell, Erin Merkel, Mahmoud Ghandi, Levi A Garraway, David E Root, Todd R Golub, Jesse S Boehm, and William C Hahn. Defining a cancer dependency map. *Cell*, 170(3):564–76, 2017. doi: 10.1016/j.cell.2017.06.010.
  - Eric Tzeng, Judy Hoffman, Kate Saenko, and Trevor Darrell. Adversarial discriminative domain adaptation. In *Proc IEEE CVPR*, pp. 2962–71, 2017. doi: 10.1109/CVPR.2017.316.
  - Dave Van Veen, Cara Van Uden, Louis Blankemeier, Jean-Benoit Delbrouck, Asad Aali, Christian Bluethgen, Anuj Pareek, Malgorzata Polacin, Eduardo Pontes Reis, Anna Seehofnerová, Nidhi Rohatgi, Poonam Hosamani, William Collins, Neera Ahuja, Curtis P Langlotz, Jason Hom, Sergios Gatidis, John Pauly, and Akshay S Chaudhari. Adapted large language models can outperform medical experts in clinical text summarization. *Nat Med*, 30:1134–42, 2024. doi: 10.1038/s41591-024-02855-5.
  - Daniel M Walker, Christine M Swoboda, Karen Shiu-Yee, Willi L Tarver, Timiya S Nolan, and Joshua J Joseph. Diversity of participation in clinical trials and influencing factors: Findings from the health information national trends survey 2020. *J Gen Intern Med*, 38:961–9, 2022. doi: 10.1007/s11606-022-07780-2.

1142

1143

11541155

1156

1161

1162

1163

1167

1168

1169

1170

11711172

1173

1174

1175

1176

1177

1186

- Liang Wang, Nan Yang, Xiaolong Huang, Linjun Yang, Rangan Majumder, and Furu Wei. Improving text embeddings with large language models. In *Proc ACL*, pp. 11897–916, 2024a. doi: 10.18653/v1/2024.acl-long.642.
- Tong Wang, Xinheng He, Mingyu Li, Yatao Li, Ran Bi, Yusong Wang, Chaoran Cheng, Xiangzhen Shen, Jiawei Meng, He Zhang, Haiguang Liu, Zun Wang, Shaoning Li, Bin Shao, and Tie-Yan Liu. Ab initio characterization of protein molecular dynamics with AI2BMD. *Nature*, 635:1019–27, 2024b. doi: 10.1038/s41586-024-08127-z.
  - Ronald J Williams. Simple statistical gradient-following algorithms for connectionist reinforcement learning. *Mach Learn*, 8(3–4):229–56, 1992. doi: 10.1007/BF00992696.
- Juncheng Wu, Wenlong Deng, Xingxuan Li, Sheng Liu, Taomian Mi, Yifan Peng, Ziyang Xu, Yi Liu, Hyunjin Cho, Chang-In Choi, Yihan Cao, Hui Ren, Xiang Li, Xiaoxiao Li, and Yuyin Zhou. MedReason: Eliciting factual medical reasoning steps in LLMs via knowledge graphs. arXiv Preprint, 2025. doi: 10.48550/arXiv.2504.00993.
- Qianqian Xie, Qingyu Chen, Aokun Chen, Cheng Peng, Yan Hu, Fongci Lin, Xueqing Peng, Jimin Huang, Jeffrey Zhang, Vipina Keloth, Xinyu Zhou, Lingfei Qian, Huan He, Dennis Shung, Lucila Ohno-Machado, Yonghui Wu, Hua Xu, and Jiang Bian. Medical foundation large language models for comprehensive text analysis and beyond. *npj Digit Med*, 8, 2025. doi: 10.1038/s41746-025-01533-1.
  - Guangzhi Xiong, Qiao Jin, Zhiyong Lu, and Aidong Zhang. Benchmarking retrieval-augmented generation for medicine. In *ACL Findings*, pp. 6233–51, 2024. doi: 10.18653/v1/2024. findings-acl.372.
- Shuai Xu, Sara Murtagh, Yunan Han, Fei Wan, and Adetunji T Toriola. Breast cancer incidence among US women aged 20 to 49 years by race, stage, and hormone receptor status. *JAMA Netw Open*, 7(1):e2353331, 2024. doi: 10.1001/jamanetworkopen.2023.53331.
  - Chenrun Yang, Xuezhi Wang, Yifeng Lu, Hanxiao Liu, Quoc V Le, Denny Zhou, and Xinyun Chen. Large language models as optimizers. In *Proc ICLR*, 2024a. URL https://openreview.net/forum?id=Bb4VGOWELI.
- Jason Yang, Ravi G Lal, James C Bowden, Raul Astudillo, Mikhail A Hameedi, Sukhvinder Kaur,
   Matthew Hill, Yisong Yue, and Frances H Arnold. Active learning-assisted directed evolution.
   Nat Commun, 16, 2025. doi: 10.1038/s41467-025-55987-8.
  - Meicheng Yang, Hui Chen, Wenhan Hu, Massimo Mischi, Caifeng Shan, Jianqing Li, Xi Long, and Chengyu Liu. Development and validation of an interpretable conformal predictor to predict sepsis mortality risk: Retrospective cohort study. *J Med Internet Res*, 26:e50369, 2024b. doi: 10.2196/50369.
  - Wanjuan Yang, Jorge Soares, Patricia Greninger, Elena J Edelman, Howard Lightfoot, Simon Forbes, Nidhi Bindal, Dave Beare, James A Smith, I Richard Thompson, Sridhar Ramaswamy, P Andrew Futreal, Daniel A Haber, Michael R Stratton, Cyril Benes, Ultan McDermott, and Mathew J Garnett. Genomics of drug sensitivity in cancer (GDSC): A resource for therapeutic biomarker discovery in cancer cells. *Nucleic Acids Res*, 41:D955–61, 2013. doi: 10.1093/nar/gks1111.
- Michael S Yao, Yimeng Zeng, Hamsa Bastani, Jacob Gardner, James C Gee, and Osbert Bastani. Generative adversarial model-based optimization via source critic regularization. In *Proc NeurIPS*, volume 37, pp. 44009–39, 2024. doi: 10.48550/arXiv.2402.06532.
- Michael S Yao, Allison Chae, Piya Saraiya, Charles E Kahn Jr, Walter R Witschey, James C Gee, Hersh Sagreiya, and Osbert Bastani. Evaluating acute image ordering for real-world patient cases via language model alignment with radiological guidelines. *Nat Commun Med*, 5, 2025a. doi: 10.1038/s43856-025-01061-9.
  - Michael S Yao, James C Gee, and Osbert Bastani. Diversity by design: Leveraging distribution matching for offline model-based optimization. In *Proc ICML*, 2025b. doi: 10.48550/arXiv.2501. 18768.

- Shunyu Yao, Jeffrey Zhao, Dian Yu, Nan Du, Izhak Shafran, Karthik R Narasimhan, and Yuan Cao. ReAct: Synergizing reasoning and acting in language models. In *Proc ICLR*, 2023. URL https://openreview.net/forum?id=WE\_vluYUL-X.
  - Lijia Yu, Yue Cao, Jean Y H Yang, and Pengyi Yang. Benchmarking clustering algorithms on estimating the number of cell types from single-cell RNA-sequencing data. *Genome Biol*, 23, 2022. doi: 10.1186/s13059-022-02622-0.
    - Sihyun Yu, Sungsoo Ahn, Le Song, and Jinwoo Shin. Roma: Robust model adaptation for offline model-based optimization. In *Proc NeurIPS*, pp. 4619–31, 2021. doi: 10.5555/3540261.3540614.
  - Zhongqi Yue, Qianru Sun, and Hanwang Zhang. Make the U in UDA matter: Invariant consistency learning for unsupervised domain adaptation. In *Proc NeurIPS*, 2023. URL https://openreview.net/forum?id=4hYIxI8ds0.
  - Junhua Zeng, Chao Li, Zhun Sun, Qibin Zhao, and Guoxu Zhou. tnGPS: Discovering unknown tensor network structure search algorithms via large language models (LLMs). In *Proc ICML*, pp. 58329–47, 2024. doi: 10.5555/3692070.3694476.
  - Yuansong Zeng, Jiancong Xie, Ningyuan Shangguan, Zhuoyi Wei, Wenbing Li, Yun Su, Shuangyu Yang, Chengyang Zhang, Jinbo Zhang, Nan Fang, Hongyu Zhang, Yutong Lu, Huiying Zhao, Jue Fan, Weijiang Yu, and Yuedong Yang. Cellfm: A large-scale foundation model pretrained on transcriptomics of 100 million human cells. *Nat Commun*, 16, 2025. doi: 10.1038/s41467-025-59926-5.
- Botong Zhang, Shuo Li, and Osbert Bastani. Conformal structured prediction. In *Proc ICLR*, 2025a. URL https://openreview.net/forum?id=2ATD8a8P3C.
  - Gongbo Zhang, Qiao Jin, Yiliang Zhou, Song Wang, Betina Idnay, Yiming Luo, Elizabeth Park, Jordan G Nestor, Matthew E Spotnitz, Ali Soroush, Thomas R Campion Jr., Zhiyong Lu, Chunhua Weng, and Yifan Peng. Closing the gap between open source and commercial large language models for medical evidence summarization. *npj Digit Med*, 7, 2024a. doi: 10.1038/s41746-024-01239-w.
  - Kai Zhang, Rong Zhou, Eashan Adhikarla, Zhiling Yan, Yixin Liu, Jun Yu, Zhengliang Liu, Xun Chen, Brian D Davison, Hui Ren, Jing Huang, Chen Chen, Yuyin Zhou, Sunyang Fu, Wei Liu, Tianming Liu, Xiang Li, Yong Chen, Lifang He, James Zou, Quanzheng Li, Hongfang Liu, and Lichao Sun. A generalist vision–language foundation model for diverse biomedical tasks. *Nat Med*, 30:3129–41, 2024b. doi: 10.1038/s41591-024-03185-2.
  - Sheng Zhang, Qianchu Liu, Guanghui Qin, Tristan Naumann, and Hoifung Poon. Med-RLVR: Emerging medical reasoning from a 3B base model via reinforcement learning. *arXiv Preprint*, 2025b. doi: 10.48550/arXiv.2502.19655.
  - Jialin Zhou, Ying Xu, Jianmin Liu, Lili Feng, Jinming Yu, and Dawei Chen. Global burden of lung cancer in 2022 and projections to 2050: Incidence and mortality estimates from GLOBOCAN. *Cancer Epidemiol*, 93:102693, 2024. doi: 10.1016/j.canep.2024.102693.
  - Kangyu Zhu, Ziyuan Qin, Huahui Yi, Zekun Jiang, Qicheng Lao, Shaoting Zhang, and Kang Li. Guiding medical vision-language models with diverse visual prompts: Framework design and comprehensive exploration of prompt variations. In *Proc ACL: Human Lang Tech*, pp. 11726–39, 2025. doi: 10.18653/v1/2025.naacl-long.587.

A. Proofs	
Proof for Lemma 4.2: Design Collapse Within Equivalence Classes	
Proof for Lemma 4.3: Probabilistic Sampling Over Equivalence Classes	
Proof for Corollary 4.4: Dual Function of (7)	
B. Additional Related Work	
Generalization and Domain Adaptation	
Conformal Prediction	
Robustness via Domain-Specific Foundation Models	
Medical Reasoning Models	
Existing Methods in Personalized Medicine	
C. Additional Implementation Details	
C.1. Optimization Task Specifications	
C.2. Full Algorithm Pseudocode for LEON	
C.3. Language Model Prompts	
C.4. Excluded Baselines	
D. Additional Experimental Results	
D.1. Distribution Shift Analysis	
D.2. Cost Analysis	
D.3. Quantitative Analysis of Prior Knowledge	
D.4. Qualitative Examples of Prior Knowledge	
D.5. Additional Analysis of the LLM Certainty Parameter $\mu$	
D.6. Extending LEON to Traditional Optimizers	
D.7. Why Should We Bound the 1-Wasserstein Distance?	
D.8. Sample Reflection Trace	
E. Ablation Studies	
E.1. Backbone LLM Ablation	
E.2. Sampling Batch Size Ablation	
E.3. LLM Temperature Ablation	
E.4. 1-Wasserstein Distance Bound Ablation E.5. $\lambda$ and $\mu$ Certainty Parameters Ablation	
E.5. $\lambda$ and $\mu$ Certainty Farameters Ablation E.6. Distribution Shift Severity Ablation	
E.7. Surrogate Evaluation Budget Ablation	
E.8. Ground-Truth Objective Evaluation Budget Ablation	
E.9. Prior Knowledge Quality Ablation	
E.10. Reflection Ablation	
E.11. Equivalence Relation Embedding Model Ablation	

# A PROOFS

 **Lemma 4.2** (Design Collapse Within Equivalence Classes). Using the method of Lagrange multipliers, we can rewrite (4) as a function of the partial Lagrangian  $\mathcal{L}_{\lambda}(q)$  for some constant  $\lambda \in \mathbb{R}_+$ :

$$\arg\max_{q(x)\in p(\mathcal{X})} \quad \mathcal{L}_{\lambda}(q) := \mathbb{E}_{x\sim q(x)}[\hat{f}(x;z)] + \lambda \left(W_0 - \mathbb{E}_{x\sim \mathcal{D}_{\mathrm{src}}}[c^*(x)] + \mathbb{E}_{x\sim q(x)}[c^*(x)]\right)$$
s.t. 
$$\mathcal{H}_{\sim}(q(x)) \leq H_0$$

Suppose there exists a distribution q(x) that satisfies the remaining constraint in (5). Furthermore, assume that the function  $\hat{f}(x) + \lambda c^*(x)$  is continuous everywhere and coercive in  $\mathcal{X}$ . For all N equivalence classes, we can then define  $x_i^*$  (not necessarily unique) according to

$$x_i^*(\lambda) := \arg\max_{x \in [x]_i} \left( \hat{f}(x; z) + \lambda c^*(x) \right)$$

Then, the alternative distribution  $q^*(x) = \sum_{i=1}^N \bar{q}_i \, \delta(x-x_i^*)$ , where  $\bar{q}_i$  is as in **Definition 4.1**, also satisfies the constraint and simultaneously achieves a non-inferior value  $\mathcal{L}_{\lambda}(q^*) \geq \mathcal{L}_{\lambda}(q)$ .

*Proof.* First, note that each  $x_i^*$  is in a distinct equivalence class, since equivalence classes in  $\mathcal{X}/\sim$  are pairwise disjoint by construction. The probability  $q_i^*$  of sampling from the *i*th equivalence class according to  $q^*(x)$  is then

$$q_i^* = \int_{[x]_i} dx \, q^*(x) = \int_{[x]_i} dx \, \sum_{j=1}^N \bar{q}_j \, \delta(x - x_j^*) = \int_{[x]_i} dx \, \bar{q}_i \, \delta(x - x_i^*) = \bar{q}_i$$
 (12)

since  $\bar{q}_i \neq \bar{q}_i(x)$  and  $[x]_i \cap [x]_j = \varnothing$  when  $i \neq j$ . Because this holds for all i, it follows that  $\mathcal{H}_{\sim}(q^*(x)) = \mathcal{H}_{\sim}(q(x))$ , meaning  $\mathcal{H}_{\sim}(q^*(x)) \leq H_0$  as well. Secondly, observe

$$\mathcal{L}_{\lambda}(q^*) = \mathbb{E}_{x \sim q^*(x)}[\hat{f}(x)] + \lambda \left(W_0 - \mathbb{E}_{x \sim \mathcal{D}_{\text{src}}}[c^*(x)] + \mathbb{E}_{x \sim q^*(x)}[c^*(x)]\right)$$

$$= \mathbb{E}_{x \sim q^*(x)}\left[\hat{f}(x) + \lambda c^*(x)\right] + \lambda \left(W_0 - \mathbb{E}_{x \sim \mathcal{D}_{\text{src}}}[c^*(x)]\right)$$

$$= \sum_{i=1}^{N} q_i^* \left(\hat{f}(x_i^*) + \lambda c^*(x_i^*)\right) + \lambda \left(W_0 - \mathbb{E}_{x \sim \mathcal{D}_{\text{src}}}[c^*(x)]\right)$$

Using the expansion of  $q_i^*$  from (12),

$$\mathcal{L}_{\lambda}(q^{*}) = \left[\sum_{i=1}^{N} \int_{[x]_{i}} dx \, q(x) [\hat{f}(x_{i}^{*}) + \lambda c^{*}(x_{i}^{*})]\right] + \lambda \left(W_{0} - \mathbb{E}_{x \sim \mathcal{D}_{\text{src}}}[c^{*}(x)]\right)$$

$$\geq \left[\sum_{i=1}^{N} \int_{[x]_{i}} dx \, q(x) (\hat{f}(x) + \lambda c^{*}(x))\right] + \lambda \left(W_{0} - \mathbb{E}_{x \sim \mathcal{D}_{\text{src}}}[c^{*}(x)]\right)$$

$$= \mathbb{E}_{x \sim q(x)} (\hat{f}(x) + \lambda c^{*}(x)) + \lambda \left(W_{0} - \mathbb{E}_{x \sim \mathcal{D}_{\text{src}}}[c^{*}(x)]\right)$$

$$= \mathbb{E}_{x \sim q(x)} [\hat{f}(x)] + \lambda \left(W_{0} - \mathbb{E}_{x \sim \mathcal{D}_{\text{src}}}[c^{*}(x)] + \mathbb{E}_{x \sim q(x)}[c^{*}(x)]\right)$$

$$= \mathcal{L}_{\lambda}(q)$$

using the definition of each  $x_i^*$  as in (6). The claim follows.

**Lemma 4.3** (Probabilistic Sampling Over Equivalence Classes). Consider the constrained optimization problem as in (7). The *i*th element of the N-dimensional vector  $\bar{q}$  can be written as

$$\bar{q}_i = \exp\left[\mu\left(\hat{f}(x_i^*;z) + \lambda c^*(x_i^*)\right)\right] / \mathcal{Z}(\lambda) \text{ where } x_i^* := \arg\max_{x \in [x]_i} \left(\hat{f}(x;z) + \lambda c^*(x)\right)$$

where  $\mathcal{Z}(\lambda)$  is a normalizing constant and  $\lambda, \mu^{-1} \in \mathbb{R}_+$  are the Lagrange multipliers.

*Proof.* By definition (Boyd & Vandenberghe, 2004), the full Lagrangian  $\mathcal{L}(\bar{q}; \lambda, \mu)$  of (7) is

$$\mathcal{L}(\bar{q}; \lambda, \mu) = \sum_{i=1}^{N} \bar{q}_{i} \hat{f}(x_{i}^{*}; z) + \lambda \left( W_{0} - \mathbb{E}_{x \sim \mathcal{D}_{src}}[c^{*}(x)] + \sum_{i=1}^{N} \bar{q}_{i} c^{*}(x_{i}^{*}) \right)$$

$$+ \mu^{-1} \left( -H_{0} - \sum_{i=1}^{N} \bar{q}_{i} \log \bar{q}_{i} \right)$$

$$= \sum_{i=1}^{N} \bar{q}_{i} \left( \hat{f}(x_{i}^{*}; z) + \lambda c^{*}(x_{i}^{*}) \right) + \lambda \left( W_{0} - \mathbb{E}_{x \sim \mathcal{D}_{src}}[c^{*}(x)] \right)$$

$$- \mu^{-1} \left( H_{0} + \sum_{i=1}^{N} \bar{q}_{i} \log \bar{q}_{i} \right)$$

$$(13)$$

where  $\lambda, \mu^{-1} \in \mathbb{R}_+$  are the Lagrangian multipliers associated with each of the two respective constraints. The stationarity condition of the Karush–Kuhn–Tucker (KKT) theorem and additive decomposition of the individual scalar elements  $\bar{q}_i$  of  $\bar{q}$  in (13) give

$$\frac{\partial \mathcal{L}}{\partial \bar{q}_i} = 0 = \left(\hat{f}(x_i^*; z) + \lambda c^*(x_i^*)\right) - \mu^{-1} \left(\log \bar{q}_i + 1\right)$$

by definition. Rearranging gives

$$\mu^{-1}(\log \bar{q}_i + 1) = \hat{f}(x_i^*; z) + \lambda c^*(x_i^*) \implies \log \bar{q}_i = -1 + \mu \left(\hat{f}(x_i^*; z) + \lambda c^*(x_i^*)\right)$$

and so

$$\bar{q}_i \propto \exp\left[\mu\left(\hat{f}(x_i^*;z) + \lambda c^*(x_i^*)\right)\right]$$

Defining the partition function  $\mathcal{Z}(\lambda) := \sum_{i=1}^N \exp\left[\mu\left(\hat{f}(x_i^*;z) + \lambda c^*(x_i^*)\right)\right]$  as our normalizing constant, the elements of the probability vector  $\bar{q}$  can be written as

$$\bar{q}_i = \exp\left[\mu\left(\hat{f}(x_i^*; z) + \lambda c^*(x_i^*)\right)\right] / \mathcal{Z}(\lambda)$$

where  $x_i^*$  is as in (6).

**Corollary 4.4** (Dual Function of (7)). The dual function of the constrained problem in (7) is

$$g(\lambda, \mu) = \lambda(W_0 - \mathbb{E}_{x \sim \mathcal{D}_{\text{src}}}[c^*(x)]) + \mu^{-1}H_0 + \mu^{-1}\log \mathcal{Z}(\lambda)$$

where  $\mathcal{Z}(\lambda)$  is the normalizing constant from (8), and so

$$\frac{\partial g(\lambda, \mu)}{\partial \lambda} = W_0 - \left( \mathbb{E}_{x \sim \mathcal{D}_{\text{src}}}[c^*(x)] - \sum_i \bar{q}_i c^*(x_i^*) \right)$$

Proof. From (13) and referencing Boyd & Vandenberghe (2004), the Lagrangian dual function is

$$g(\lambda, \mu) := \max_{\bar{q} \in \Delta(N)} \mathcal{L}(\bar{q}; \lambda, \mu)$$

$$= \sum_{i=1}^{N} \bar{q}_{i}(\hat{f}(x_{i}^{*}; z) + \lambda c^{*}(x_{i}^{*})) + \lambda (W_{0} - \mathbb{E}_{x \sim \mathcal{D}_{src}}[c^{*}(x)]) - \frac{1}{\mu} \left( H_{0} + \sum_{i=1}^{N} \bar{q}_{i} \log \bar{q}_{i} \right)$$

where the optimal vector  $\bar{q}$  is as in **Lemma 4.3**. Note that the first summation can be written as

$$\sum_{i=1}^{N} \bar{q}_{i}(\hat{f}(x_{i}^{*};z) + \lambda c^{*}(x_{i}^{*})) = \frac{1}{\mu} \sum_{i=1}^{N} \bar{q}_{i} \left( \mu \left[ \hat{f}(x_{i}^{*};z) + \lambda c^{*}(x_{i}^{*}) \right] \right) = \frac{1}{\mu} \sum_{i=1}^{N} \bar{q}_{i} \left( \log \bar{q}_{i} + \log \mathcal{Z}(\lambda) \right)$$

$$= \frac{1}{\mu} \log \mathcal{Z}(\lambda) \sum_{i=1}^{N} \bar{q}_{i} + \frac{1}{\mu} \sum_{i=1}^{N} \bar{q}_{i} \log \bar{q}_{i} = \frac{1}{\mu} \log \mathcal{Z}(\lambda) + \frac{1}{\mu} \sum_{i=1}^{N} \bar{q}_{i} \log \bar{q}_{i}$$

Substituting into our expression for  $g(\lambda, \mu)$ ,

$$g(\lambda, \mu) = \mu^{-1} \log \mathcal{Z}(\lambda) + \lambda (W_0 - \mathbb{E}_{x \sim \mathcal{D}_{\text{src}}}[c^*(x)]) - \mu^{-1} H_0$$

Differentiating with respect to  $\lambda$ ,

$$\begin{split} \frac{\partial g(\lambda,\mu)}{\partial \lambda} &= \frac{1}{\mu} \frac{1}{\mathcal{Z}(\lambda)} \frac{\partial \mathcal{Z}(\lambda)}{\partial \lambda} + (W_0 - \mathbb{E}_{x \sim \mathcal{D}_{\text{src}}}[c^*(x)]) \\ &= \frac{1}{\mu} \sum_{i=1}^{N} \left[ \frac{1}{\mathcal{Z}(\lambda)} \exp\left[\mu(\hat{f}(x_i^*;z) + \lambda c^*(x_i^*))\right] \cdot \mu c^*(x_i^*) \right] + (W_0 - \mathbb{E}_{x \sim \mathcal{D}_{\text{src}}}[c^*(x)]) \\ &= \sum_{i=1}^{N} c^*(x_i^*) \exp\left[\mu(\hat{f}(x_i^*;z) + \lambda c^*(x_i^*))\right] \middle/ \mathcal{Z}(\lambda) + (W_0 - \mathbb{E}_{x \sim \mathcal{D}_{\text{src}}}[c^*(x)]) \\ &= \sum_{i=1}^{N} \bar{q}_i c^*(x_i^*) + (W_0 - \mathbb{E}_{x \sim \mathcal{D}_{\text{src}}}[c^*(x)]) = W_0 - \left(\mathbb{E}_{x \sim \mathcal{D}_{\text{src}}}[c^*(x)] - \sum_{i=1}^{N} \bar{q}_i c^*(x_i^*)\right) \end{split}$$

after regrouping terms.

## B ADDITIONAL RELATED WORK

Generalization and domain adaptation. To mitigate the mismatch between the available surrogate model and hidden ground-truth objective, recent work on domain adaptation leverages knowledge of the underlying source and target distributions to overcome the underlying distribution shift. Broadly, the technique relies on learning a mapping between source and target distributions, and can often be applied even to black-box surrogate models (Ganin et al., 2016; Sun & Saenko, 2016; Bousmalis et al., 2016; Yue et al., 2023). Many existing domain adaptation methods have in proposed specifically for applications in computer vision (Bousmalis et al., 2017; Saito et al., 2018; French et al., 2018), which are outside the scope of this work. Separately, Tzeng et al. (2017) learn to encode target samples into a source representation space using adversarial feedback, and Ngo et al. (2022) describe a method for task-level adaptation. However, these methods assume knowledge of the target distribution, which may not be known *a priori* in optimization tasks. In our setting, we show how LEON can be used for optimization on a per-patient basis without assuming any prior knowledge of other patient observations from the target distribution—a realistic assumption for protecting patient privacy and ensuring timely downstream decision making in real-world applications. We therefore cannot leverage domain adaptation to adapt a surrogate model during optimization.

Conformal prediction. Conformal prediction is a statistical framework for uncertainty quantification where the goal is to produce prediction *sets* as opposed to singular outputs, providing a guarantee that the true label is almost certainly in the prediction set with high probability (Cresswell et al., 2024; Angelopoulos & Bates, 2023; Angelopoulos et al., 2021). Prior work has demonstrated how conformal prediction can be leveraged for image classification (Angelopoulos et al., 2021; Zhang et al., 2025a), disease course prediction (Yang et al., 2024b; Sreenivasan et al., 2025), drug discovery (Eklund et al., 2013; Jin & Candes, 2023), and even autoregressive generative models (Quach et al., 2024). Prior work has explored how to perform Bayesian (Deshpande et al., 2024; Stanton et al., 2023) and worst-case (Johnstone & Cox, 2021) optimization over conformal prediction sets; future work might explore how to similarly adapt LEON to optimize over prediction sets.

Robustness via domain-specific foundation models. A potential direction for building more robust and performant surrogate models is to leverage large-scale foundation models as surrogates. One argument is that models that are trained on sufficiently large and diverse datasets are unlikely to encounter significantly 'out-of-distribution' inputs, yielding more robust performance across a wide range of inputs during optimization. Early efforts along these lines have emerged in areas such as cell perturbation modeling (Cui et al., 2024; Hao et al., 2024; Zeng et al., 2025) and drug discovery (Abramson et al., 2024; Huang et al., 2024). However, despite preliminary efforts to extend similar approaches to clinical medicine (Guo et al., 2024a; 2023; Steinberg et al., 2024), the limited availability of patient training data and stringent patient privacy constraints restrict the feasibility of constructing models that reliably generalize in a zero-shot manner across many different patient populations. For these reasons, methods like LEON may still play a role in domains such as clinical medicine even as the accuracy of surrogate models improves with foundation model development.

Table S1: **Implementation details.** We consider the problem of optimization under distribution shift; given access to a surrogate model trained on a source dataset, we want to find an optimal design for a patient sampled from the target distribution that maximizes the response according to a hidden ground-truth objective function. *TabPFN*: Tabular prior-data fitted network (Hollmann et al., 2025). *FCNN*: Fully connected neural network. *ResNet*: Tabular residual network (Gorishniy et al., 2021). *GBDT*: Gradient boosted decision tree ensemble (Chen & Guestrin, 2016; Quinlan, 1986).

Distribution Shift		Covariate	Covariate Shift in $P(X)$		Label Shift in  P(Y)	
Task	Warfarin	HIV	Breast	ADR	Lung	
Shifted Feature	Patient Race	Study Year	Patient Age $< 65$ years old $\ge 65$ years old	Medication	TTNTD	
Source Data Feature	White	2002-2008		Drug A	Longer	
Target Data Feature	Non-White	2009-2020		Drug B	Shorter	
Source Dataset Size	3,095	740	3,020	484	3,013	
Target Dataset Size	2,646	554	1,260	554	3,009	
Surrogate Model	TabPFN	FCNN	GBDT	GBDT	GBDT	
Ground-Truth Objective	Exact	ResNet	GBDT	Exact	GBDT	
	11	339	47	50	47	
	1	16	30	5	30	
	Continuous	Discrete	Discrete	Continuous	Discrete	

Medical reasoning models. Recent work has explored how to develop datasets of clinical reasoning traces (Wu et al., 2025; Kwon et al., 2024; Hager et al., 2024) and associated benchmarks (Arora et al., 2025; Chen et al., 2025b). This evolving ecosystem of model training and evaluation resources have made available recent medical reasoning models: Singhal et al. (2023; 2025) introduced the MedPaLM family of models that generate accurate long-form answers to consumer medical questions, and Zhang et al. (2025b) fine-tune language models using reinforcement learning with verifiable rewards derived from multiple choice question answering. Separately, Savage et al. (2024); Sonoda et al. (2024) demonstrate how chain-of-thought reasoning can be elicited from base language models by optimized prompting strategies. Given the impressive performance of these models, one might imagine how they could be used to also predict personalized treatment strategies. However, we note that simply prompting a specialized medical language model to return a treatment response is not equivalent to iterative optimization with a language model against a black-box evaluator (i.e., the surrogate model). For this reason, simply querying an LLM to return a treatment strategy for a patient is outside the scope of our work on *optimization* strategies herein.

Existing methods in personalized medicine. Aside from the methodology-focused related works, we also provide a brief overview of existing applied works in personalized medicine. Recent clinical trials across clinical disciplines have tested personalized approaches by selecting or adapting treatments for subgroups or individuals (He et al., 2018). de Bono et al. (2020); Paik et al. (2020) are recent randomized clinical trials that leverage patient-specific genomic data to assign patients to a predetermined experimental treatment arm. In current clinical practice, certain pharmacogenetic variables already help determine whether certain medications are prescribed to particular patients (Ma et al., 2010; Ford & Taubert, 2013; Kirchheiner et al., 2007). Using machine learning to propose entirely new treatment arms for individual patients is the ultimate goal of personalized medicine, but is not yet a core component of clinical practice (Johnson et al., 2020; Chen et al., 2025c).

## C ADDITIONAL IMPLEMENTATION DETAILS

## C.1 OPTIMIZATION TASK SPECIFICATIONS

**Supplementary Table S1** outlines task-specific implementation details, including information on the underlying distribution shift and number of design dimensions for each task. Below, we further discuss the motivation behind and implementation of each optimization task considered in our work.

**Warfarin.** Warfarin is an oral anticoagulant medication used to treat and prevent a variety of thromboembolic conditions, such as atrial fibrillation (Brass et al., 1997), venous thromboembolisms (Ramzi & Leeper, 2004), and maintenance therapy after mechanical valve placement (Catterall et al., 2020). However, determining its initial dose is notoriously complex, in part due to the medication's narrow therapeutic index and significant inter-patient variability (Lee & Klein, 2013; Consortium,

2009). Dosing is influenced by numerous factors including age, body weight, liver function, and vitamin K metabolism. These complexities make standardized dosing unreliable and necessitate careful titration using frequent blood tests to achieve and maintain therapeutic anticoagulation.

Consortium (2009) previously introduced a de-identified, publicly available dataset of 5,052 patients from multiple hospital sites with clinical indications for warfarin initiation. The dataset includes both clinical and pharmacogenetic observations for all patients, in addition to their prescribed warfarin dose and laboratory test results. More explicitly, each patient observation includes a prescribed warfarin dose  $x \in \mathcal{X} \subseteq \mathbb{R}$  and conditioning vector z that concatenates the patient's height (caDSR 649); weight (caDSR 2179689); age (NIH Concept ID C25150); sex at birth (NIH Concept ID C124436); smoking status (NLM m1Sgwj5s2ig); the use of medications known to affect warfarin dosing (carbamazepine, phenytoin, rifampin, amiodarone); and the presence of genotype variants of CYP2C9 and VKORC1 genes. Using this dataset, Consortium (2009) learn an expert function dose:  $\mathcal{Z} \to \mathcal{X}$  (validated by physician specialists) that predicts the optimal dose for a given patient. The optimization objective for our task is to minimize the root mean squared error (RMSE)  $||x - \text{dose}(z)||_2$  (i.e., to find the warfarin dose predicted by the expert function).

HIV. Human immunodeficiency virus (HIV) is a virus that attacks the human immune system, and is currently treated with antiretroviral therapy (ART) (Kemnic & Gulick, 2025). Choosing the correct ART drug regimen is a carefully tailored, patient-centered process driven largely by viral genotype and individual health factors (Rhee et al., 2003). Before initiating treatment, gold-standard practice involves performing genotypic resistance testing to identify mutations in the HIV reverse transcriptase (RT) and protease sequences, as certain mutations can potentially render certain ART drugs ineffective (Saag et al., 2020). Treatment planning becomes even more complex in patients with transmitted or archived drug resistance (Kemnic & Gulick, 2025). For these reasons, a personalized approach to HIV treatment can help more effectively tailor ART to both viral mutation profiles and patient variables. The efficacy of an ART drug panel is clinically evaluated by measuring the patient's HIV viral load (i.e., the 'amount' of HIV in the patient's blood) before and after therapy.

We use the publicly available HIVDB dataset from Rhee et al. (2003) to study how to personalize ART treatment regimens for patients based on their viral genotyping data. A patient's corresponding conditioning vector z was constructed by concatenating the positions and amino acid substitutions of the patient's entire HIV protease sequence and the first 240 amino acids of the p66 subunit of the HIV reverse transcriptase protein following prior work. We frame the problem of designing personalized ART therapies as a binary optimization problem; the design space consists of 16 ART drugs: 8 Nucleoside RT Inhibitors (Abacavir, Zidovudine, Didanosine, Emtricitabine, Lamivudine, Stavudine, Tenofovir, and Zalcitibine); 3 Non-Nucleoside RT Inhibitors (Delavirdine, Efavirenz, and Nevirapine); and 5 Protease Inhibitors (Atazanavir, Indinavir, Nelfinavir, Ritonavir, and Saquinavir). We chose these 16 drugs because they were the most commonly used drugs in the HIVDB dataset. Each vector  $x \in \{0,1\}^{16}$  in the design space specifies the ART regimen to prescribe the patient, where the ith dimension  $x_i = 1$  if the ith drug is included in the regimen.

Breast and Lung. Breast cancer and lung cancer are among the most prevalent cancers diagnosed in the United States (Kim et al., 2025; Xu et al., 2024; Ganti et al., 2021; Zhou et al., 2024). There has been recent interest in personalizing oncologic treatments based on a patient's unique genetic and environmental makeup (Paik et al., 2020; Papalexis et al., 2024). To this end, we use the following set of features to construct the conditioning vector z: (1) age (NIH Concept ID C25150); (2) sex at birth (NIH Concept ID C124436); (3) race (NLM LakF0YkywC); (4) socioeconomic index; (5) cancer TNM staging; (6) vitals (excluding height and weight) (NLM GOr10FJAKC; and (7) any labs and biomarkers available for the patient. The following blood laboratory values and biomarker tests were used to construct z if available: 4 numerical complete blood count (CBC, NLM DZwbeRugB) tests (Hematocrit, White blood cell count, Hemoglobin, Platelet count); 6 numerical basic metabolic panel (BMP) tests (Sodium, Potassium, Chloride, Creatinine, Blood urea nitrogen, and Glucose); 6 numerical liver function tests (LFTs) (Aspartate aminotransferase, Alanine aminotransferase, Alkaline Phosphatase, Albumin, Total bilirubin, and Total serum protein); 4 numerical miscellaneous tests (Serum calcium, Estimated glomerular filtration rate, Glomerular filtration rate, and Lactate dehydrogenase); and 15 categorical biomarker tests (Human epidermal growth factor receptor 2 (HER2), Progesterone receptor (PR), Estrogen receptor (ER), Ki67, Anaplastic lymphoma kinase (ALK), BRAF, Kirsten rat sarcoma viral oncogene homolog (KRAS), ROS1, RET, MET, Programmed cell death ligand 1 (PDL1), tumor protein 53 (TP53), Kelch-like ECH-associated protein 1 (KEAP1), Serine/threonine kinase 11 (STK11), and breast cancer gene (BRCA)).

The design space for both tasks consists of (1) whether to perform surgery with curative intent (0 or 1); (2) whether to perform radiation therapy with curative intent (0 or 1); (3) whether chemotherapy should be adjuvant or neoadjuvant; and (4) the specific drug(s) to include in the chemotherapeutic regimen. The chemotherapeutic drugs to choose from include 9 cytotoxic chemotherapies (Carboplatin, Cisplatin, Cyclophosphamide, Pemetrexed, Capecitabine, Gemcitabine, Paclitaxel, Docetaxel, Doxorubicin); 3 cell cycle inhibitors (Palbociclib, Abemaciclib, Ribociclib); 5 hormonal therapies (Anastrozole, Exemestane, Letrozole, Tamoxifen, Fulvestrant); 9 monoclonal antibodies (Pembrolizumab, Nivolumab, Cemiplimab, Atezolizumab, Durvalumab, Ipilimumab, Trastuzumab, Pertuzumab, Sacituzumab); and 1 tyrosine kinase inhibitor (Osimertinib). We chose these specific 27 medications because they were the most commonly prescribed medications in the Flatiron dataset. Altogether, the design space is represented as a boolean vector in  $\{0,1\}^{30}$ .

**ADR.** An adverse drug reaction (ADR) is an unintended and harmful response to a medication. Minimizing the risk of ADRs is a priority in early-stage clinical trials in order to ensure that newly tested therapies are safe for human use. In this task, we leverage two internal proprietary clinical trial datasets de-identified at the patient level that were collected from two clinical trials to predict patient risk of an ADR. The primary goal of the clinical trials was to evaluate the safety of two different medications that share similar mechanisms of action, which we refer to as 'Drug A' and 'Drug B' in **Supplementary Table S1**. Due to the sensitive nature of the internal trial data, we do not disclose the identities of Drugs A and B, or the particular ADR under investigation.

The following patient covariates were used to construct the conditioning vectors z: patient sex at birth (NIH Concept ID C124436); (2) patient age (NIH Concept ID C25150); (3) tumor measurements; (4) medical diagnosis; (5) ECOG score (caDSR 88); (6) vitals (excluding height and weight) (NLM GOr10FJAKC; (7) any patient labs and/or biomarkers; and (8) medication dosing schedule. Each patient observation included a label of the severity of the observed ADR (if any) in response to the patient's therapy: we first one-hot-encode this label into a vector  $x^{\rm gt}$  with 5 dimensions (one for each severity level of the ADR, consistent with medical societal guidelines (Khan et al., 2023; Lee et al., 2019; Trotti et al., 2003)), and then perturb this vector by randomly adding a uniformly sampled per-dimension 'jitter'  $\delta_i \sim \mathcal{U}[0,1/4]$  for each zero-valued dimension i to produce a vector  $x \in [0,1]^5$  such that  $x_i = \delta_i$  if  $x_i^{\rm gt} = 0$  and  $x_i = 1 - \sum_{j \neq i} \delta_j$  if  $x_i^{\rm gt} = 1$ . In this way, the index of the maximum element in both x and  $x^{\rm gt}$  are equal. We then compute the corresponding negative log-likelihood (NLL)  $y := \sum_{i=1}^5 x_i^{\rm gt} \log x_i$  as the objective to minimize. These values are then used to construct the annotated datasets  $\mathcal{D} = \{(x_j, z_j, y_j)\}_{i=j}^n$ . Note that  $x^{\rm gt}$  is not accessible by the optimizer. This approach allows us to turn a predictive task (i.e., predicting the severity of a patient ADR in a clinical trial) into an optimization task compatible with LEON.

#### C.2 FULL ALGORITHM PSEUDOCODE FOR LEON

The full pseudocode for LEON is shown in **Supplementary Algorithm 1**. Prior to the start of optimization, we also leverage the backbone LLM to query external knowledge bases for prior knowledge generation—the full pseudocode for this subroutine is shown in **Supplementary Algorithm 2**.

# C.3 LANGUAGE MODEL PROMPTS

This section includes the system and user prompts used for all experiments using LEON. Baseline methods using LLMs as optimizers used the same sets of prompts as provided by the respective original authors, with modifications made only to adapt the prompts to our experimental tasks.

For each task in our evaluation suite, we first define a task\_description variable that describes the optimization task in natural language. The specific strings used in each task are included below:

• task\_description for the Warfarin task:

The provided design scores are predictions from a model trained on White patients only, and therefore may not be accurate for all patients. Propose an optimal warfarin dose (in mg/week) for the patient.

task\_description for the HIV task:

The provided design scores are predictions from a model trained on

```
1620
1621
            Algorithm 1 (LEON). <u>L</u>LM-based <u>Entropy-guided Optimization with kNowledgeable priors</u>
1622
               Inputs:
1623
                    f(x,z): \mathcal{X} \times \mathcal{Z} \to \mathbb{R} — pre-trained surrogate model
1624
                   c^*(x): \mathcal{X} \to \mathbb{R} — initialized source critic model
1625
                   z — vector of fixed patient-specific covariates
1626
                   LLM — a large language model that supports tool calling
                   knowledge — prior knowledge in natural language generated using Algorithm 2 using the
1628
                                            same input LLM
1629
                   \lambda_0 \ge 0 — initial source critic certainty parameter value (default 0.0)
                   W_0 \ge 0 — 1-Wasserstein distance bound (default 1.0)
1630
                   \eta_{\lambda} \geq 0 — source critic certainty parameter step size (default 0.1)
                   \eta_{\rm critic} > 0 — source critic learning rate (default 0.001)
1632
                   \tau \ge 0 — temperature (default 1.0)
                   b > 1 — batch size (default 32)
1634
                   B \ge b — surrogate model \hat{f} evaluation budget (default 2048)
1635
               Initialize a memory bank of sampled candidates \mathcal{D}_{gen}
1636
               Initialize \lambda \leftarrow \lambda_0 // Source critic certainty parameter as in Lemma 4.2.
               Initialize reflection \leftarrow \epsilon // Initialize the LLM's reflection as the empty string.
               for t = 1 \dots \lceil B/b \rceil do
1639
                   // 1. Sampling. Query the LLM for a new batch of designs.
1640
                   x^{\text{new}} := \{x_i^{\text{new}}\}_{i=1}^b \leftarrow \text{LLM}(\mathcal{D}_{\text{gen}}, z, \text{knowledge}, \text{reflection})
1641
                   // Evaluate the designs according to the source-critic regularized surrogate.
1642
                   y^{\text{new}} := \{y_i^{\text{new}}\}_{i=1}^b \leftarrow \{\hat{f}(x_i^{\text{new}}) + \lambda c^*(x_i^{\text{new}})\}_{i=1}^b
1643
1644
                   // 2. Cluster. Assign the designs to their equivalence classes.
                   for 1 \le j \le b do
                       Append x_j^{\text{new}} to its equivalence class [x_j^{\text{new}}]_{\sim}
1646
                   end for
1647
                   // Compute the fractional occupancies \hat{q}_i of each equivalence class.
1649
                   for 1 \le i \le N do
                      \begin{aligned} y_i^* \leftarrow \max_{[x]_i} [\hat{f}(x; z) + \lambda c^*(x)] \\ \hat{q}_i \leftarrow |[x]_i|/|x^{\text{new}}| \end{aligned}
1651
                   end for
1652
1653
                  // 3. \mu Estimation. Estimate \mu according to (9).
1654
                   for 1 \le i \le N do
                      \delta y_i^* \leftarrow \overline{y_i^*} - \frac{1}{N} \sum_{i'=1}^N y_{i'}^*
                      \delta(\log \hat{q})_i \leftarrow \log \hat{q}_i - \frac{1}{N} \sum_{i'=1}^N \log \hat{q}_{i'}
1656
1657
                  end for \hat{\mu} \leftarrow \sum_{i=1}^{N} [\delta y_i^* \cdot \delta(\log \hat{q})_i] / \sum_{i=1}^{N} [\delta y_i^* \cdot \delta y_i^*]
1658
1659
                   // Re-train the source critic parameters \theta_c and update \lambda certainty parameter.
                   while \delta W has not converged do
                      \delta W \leftarrow \vec{\nabla}_{\theta_c} \left[ \mathbb{E}_{x' \sim \mathcal{D}_{\text{src}}}[c^*(x')] - \mathbb{E}_{x \sim \{x_i^{\text{new}}\}_{i=1}^b}[c^*(x)] \right]\theta_c \leftarrow \min(\max(\theta_c + \eta_{\text{critic}} \cdot \delta W, -0.01), 0.01)
                   end while
1664
                   \lambda \leftarrow \lambda - (\eta_{\lambda}/\sqrt{t}) \cdot (\partial g/\partial \lambda) // Compute the partial gradient according to (10).
1666
                   // 4. Design Scoring. Score each sampled design according to \hat{\mu}(\hat{f}(x;z) + \lambda c^*(x)).
                   \mathcal{D}_{\text{gen}} \leftarrow \mathcal{D}_{\text{gen}} \cup \{(x_j^{\text{new}}, \hat{\mu} \cdot y_j^{\text{new}})\}_{j=1}^b // Save the new batch of designs to memory.
1668
                   // Reflection. Prompt the language model to reflect on the current optimization progress.
1669
                   // The specific prompt for reflection used in our implementation is included in Appendix C.3.
1670
                   reflection \leftarrow \text{LLM}(\{x_i^{\text{new}}, \hat{\mu} \cdot y_i^{\text{new}}\}_{i=1}^b, \text{reflection\_prompt})
1671
               end for
               return top candidate from \mathcal{D}_{gen} with the maximum saved \hat{\mu} \cdot y_j predicted score
```

```
1674
         Algorithm 2 Knowledge generation using external knowledge repositories
1675
1676
              \mathcal{K} = \{KR_k\}_{k=1}^{n_{KR}} — a set of n_{KR} user-provided knowledge repositories (KR)
1677
              LLM — a large language model that supports tool calling
1678
              T > 0 — the maximum number of allowed sequential tool calls
1679
              // The specific prompt used in our implementation is included in Appendix C.3.
              knowledge_prompt — a prompt in natural language to elicit knowledge generation
           C \leftarrow \{\} // Initialize the conversation context.
1682
           // Sequential tool calling.
1683
           for t = 1 \dots T do
1684
              // The LLM returns which knowledge repository to call and a corresponding text query q_t.
              Early stopping is allowed if the LLM determines no additional tool calls are required.
              (k_t, q_t, STOP) \leftarrow LLM(C, knowledge\_prompt; \mathcal{K})
1686
              if STOP = True then
1687
                break
1688
              end if
1689
              // Retrieve relevant knowledge r_t from the requested knowledge repository KR_k.
1690
              r_t \leftarrow \mathrm{KR}_{k_t}(q_t)
1691
              // Append the query and response to the conversation context.
1692
              C \leftarrow C \cup \{(k_t, q_t, r_t)\}
1693
           end for
1694
           // Generate the final knowledge in natural language.
           knowledge \leftarrow LLM(C, knowledge\_prompt)
           return knowledge
```

patients from older studies (before 2008) only, and therefore may not be accurate for all patients. Propose an optimal  ${\tt HIV}$  medication regimen for the patient.

# • task\_description for the Breast task:

1700

1701 1702

1703

1704

1705

1706

1707

1708

1709 1710

1711

1712

1713

1714

1715

1716 1717

1718

1719

17201721

1722

1723

1724

1725

1726

1727

The provided design scores are predictions from a model trained on patients under 65 years old only, and therefore may not be accurate for this patient. Propose an optimal treatment regimen for the patient consisting of a combination of adjuvant or neoadjuvant medications, whether to undergo surgery, and whether to undergo radiation therapy.

#### task\_description for the Lung task:

The provided design scores are predictions from a model trained on patients with a good response to therapy only, and therefore may not be accurate for this patient. Propose an optimal treatment regimen for the patient consisting of a combination of adjuvant or neoadjuvant medications, whether to undergo surgery, and whether to undergo radiation therapy.

## task\_description for the ADR task:

The provided design scores are predictions from a model trained on patients treated with <Drug A> only, and therefore may not be accurate for this patient. Predict the probability of each grade of <Adverse Drug Reaction (ADR)> under the current medication.

Redacted components are indicated by <> angle brackets above. Separately, each pair consisting of a patient with fixed covariates z and a proposed design x was programmatically represented in natural language as a patient\_description. Representative example values for this string in each task are included below; exact values have been modified to preserve patient anonymity. In addition to being used in the language model prompt during optimization (see the **User prompt for proposing new treatment designs** below), each of the patient\_description representations of (x, z) tuples were also used as input into an embedding model to define the equivalence relation as detailed in the main text. We ablate the choice of embedding model in **Supplementary Table S7**.

```
1728
            • Sample patient_description in the Warfarin task:
1729
             Asian patient (age 70 - 79 years old) with a BMI of 25.7. CYP2C9
1730
             Genotype Variant: *1/*1. VKORC1 SNP: A/G.
1731
1732
             Warfarin Dose: 32.0 mg/week
1733
            • Sample patient_description in the HIV task:
1734
              Patient newly diagnosed with HIV-1 has the following HIV Protease
1735
             Mutations: N37A; I15V; T12K. The patient also has the following
1736
             HIV Reverse Transcriptase Mutations: E204G; I135T; G196E
1737
             Prescribed Medications: Zidovudine (Retrovir), Lamivudine (Epivir),
1738
             Abacavir (Ziagen)
1739

    Sample patient_description in the Breast task:

1740
1741
              69 y.o. African American Female diagnosed with Stage I (T2N0M0)
1742
             Breast Cancer.
1743
             Vitals:
1744
             BP 130/85 | SpO2 99.0 | HR 70
1745
1746
             Labs:
                - [CBC] Hct: 35.8% | Hgb: 11.7 | WBC: 4.8 | Plt: 259.0
1747
                - [BMP] Na: 143 | Cl: 99 | Glu: 90 | K: 4.8
1748
                - [LFTs] ALT: 17 | AST 17 | Albumin: 27 | ALP: 94 | Prot: 60
1749
                - [Additional Labs and Biomarkers] Ki67: >=20%
1750
1751
             Treatment Plan:
             Adjuvant Capecitabine with Surgery and Radiation
1752
1753

    Sample patient_description in the Lung task:

1754
             75 y.o. Asian Male diagnosed with Stage IA (T1CN0M0) NSCLC.
1755
1756
             Vitals:
             Sp02 90.0
1757
1758
             Labs:
1759
                - [CBC] Hct: 48.5% | Hqb: 15.1 | WBC: 9.5 | Plt: 243
                - [BMP] Na 138 | Cl: 101 | K: 3.5 | Cr: 1.5 | BUN: 14 | Glu: 95
                - [LFTs] ALT: 11 | AST 13 | ALP: 75 | TBili: 0.5 | Prot: 65
1761
                - [Additional Labs and Biomarkers] Ca: 9.0 | CEA: 5.8
1762
1763
             Treatment Plan:
1764
             Adjuvant Pembrolizumab with Surgery
1765

    Sample patient_description in the ADR task:

1766
              68 y.o. Female (ECOG 1) diagnosed with <Disease> currently treated
1767
             with <Drug B>.
1768
1769
             Dosing Schedule:
1770
                - Day 1: <Drug B> <Dose X>
                - Day 7: <Drug B> <Dose Y>
1771
                - Day 14: <Drug B> <Dose Z>
1772
1773
             Tumor:
1774
                - <Measurement A>: <Value A>
1775
                - <Measurement B>: <Value B>
1776
             Vitals: O2Sat 98 | HR 73 | RR 17 | T 36.7 | BP 121/80
1777
1778
             Labs:
1779
                - [CBC] Hct: 35% | Hgb: 11.8 | WBCs: 5.2
1780
                - [BMP] Na: 140 | C1: 100 | K: 4.2 | HCO3-: 24 | Cr: 1.5 | BUN: 6
                - [LFTs] Albumin: 3.9 | ALT: 25 | AST: 29 | TBili: 11
1781
                - [Additional Labs and Biomarkers] Ca: 9.2 | Mg: 2.0 | Phos: 3.2
```

Redacted components are again indicated by <> angle brackets above. Finally, user prompts in LEON also make use of a memory string, which is a table of previously proposed designs (represented in natural language) and their corresponding scores according to LEON. Importantly, **note that** memory **never contains any scores from the ground-truth objective**, which is never made available to the optimizer. In general, memory is a Markdown-formatted table that includes the maximum number of most recently sampled design proposals subject to the LLM's context window.

• Sample memory entry for the Warfarin task:

```
| | designs | scores |
|--:|:------:|
| 0 | 21.6399 | -1.4465 |
```

• Sample memory entry for the HIV task:

• Sample memory entry for the Breast task:

• Sample memory entry for the Lung task:

• Sample memory entry for the ADR task:

We now provide the system and user prompts used in LEON as format strings. Firstly, in step 1. **Sampling** of **Supplementary Algorithm 1**, we prompt the language model optimizer to return a new batch of designs; the system and user prompts for this process are included here:

## **System prompt for proposing new treatment designs:**

You are a clinical assistant whose role is to propose treatments for simulated patients based on historical data and iterative feedback. You will be provided with a history of treatments along with their respective performance scores. Your task is to propose new treatments that potentially yield better outcomes. After each proposal, feedback based on evaluation results will be provided to refine future proposals.

```
### Optimization Strategy
```

- Learn from the history of previous treaatments and their scores.
- Balance exploration (trying diverse treatment options) and exploitation (refining successful treatments).
- Do not propose treatments identical to those already evaluated.

```
### Input Format
```

In each round, you will receive:

- 1. \*\*Prior Knowledge:\*\* Some potentially relevant context to consider that is specific to the particular patient.
- 2. \*\*Memory:\*\* A table of previously evaluated treatments and their scores. Each row in the list will contain the following:
  - round\_index: the integer index of the round
  - treatment: the proposed treatment
  - score: float score

A higher score indicates a better patient treatment.

### Output Format

```
You must propose a treatment for the simulated patient that will be scored by the evaluator. Your goal is to find treatments that are high scoring.
```

## User prompt for proposing new treatment designs:

```
1841
       {prior_knowledge}
1842
1843
       {patient_description}
1844
1845
       ### Previously Proposed Designs
1846
1847
       ### Reflection
1848
       {reflection}
1850
       ### Task
       {task_description}
1851
```

where prior\_knowledge is a string of prior knowledge returned by Supplementary Algorithm 2, and reflection is the reflection string from the previous optimization loop in Supplementary Algorithm 1. Separately, the prompt knowledge\_prompt used in Supplementary Algorithm 2 is shown below:

#### **System prompt for knowledge generation:**

You are a helpful biomedical knowledge assistant whose job is to retrieve relevant knowledge to help a domain expert solve a specific task in biology and medicine. Given a description of a patient and a clinical task, you will decide which knowledge sources to retrieve from (and with what arguments). You may call multiple functions sequentially; when you have enough information, return a final answer of relevant prior knowledge without any further function calls. Be specific, concise, and comprehensive in your response.

#### User prompt for knowledge generation:

```
{patient_description}
Problem Description: {task_description}
Provide relevant factual information to help the expert solve the problem.
```

Finally, **Supplementary Algorithm 1** also describes a **reflection** call to the LLM at the end of each optimization step, where the goal is to prompt the LLM to reflect on the efficacy of the current optimization progress. The input prompt reflection\_prompt for this process is shown below:

```
1877
      ### Task Description
1878
      {task_description}
1879
      ### Previously Proposed Designs
1880
      {memory}
1881
1882
      Please analyze the scores of the proposed designs and reflect on how to
      better improve the score. In addition to score-based optimization,
1884
      evaluate which design strategies are working and which are not **from a
      biomedical and biological perspective **.
1885
1886
```

- Specifically:
- Identify any recurring features or mechanisms in high-scoring designs that are biologically plausible or supported by known biomedical principles.
  - Point out any strategies in low-scoring designs that might be failing

```
due to biological implausibility, off-target effects, instability, toxicity, or other biomedical concerns.
```

 Consider how principles from molecular biology, pharmacokinetics, immunology, or relevant biomedical disciplines might explain the observed outcomes.

Do NOT propose a new design in your response! Only respond with your thinking.

#### C.4 EXCLUDED BASELINES

**Evolutionary algorithms.** Adapting LLMs as evolutionary optimizers has been explored in prior work, albeit primarily for singular tasks without easy generalization of the methods to new prolems, such as the biomedical tasks considered herein. We exclude LLM-driven Evolutionary Algorithms (LMEA) from Liu et al. (2024a) because their work and publicly available implementation is specifically adapted for solving the *traveling salesman problem*; generalizing their implementation while ensuring its faithfulness to the authors' original implementation is outside the scope of this work. Similarly, we exclude EvoPrompting from Chen et al. (2023a) and EvoPrompt Guo et al. (2024b), as these prior works are only implemented by the original authors for neural architecture search and language model prompt optimization, respectively. Finally, AlphaEvolve from Novikov et al. (2025) and FunSearch from Romera-Paredes et al. (2024) are also LLM-based evolutionary algorithms, but do not optimize against a dense reward function as we do in our work.

Biomedical optimization. Prior work on leveraging language models for biomedical optimization tasks have almost exclusively fine-tuned decoder models for biological sequence generation. For example, the methods from Reinhart & Statt (2024) and Ma et al. (2024a) make use of domain-specific molecular dynamics and material point method (MPM) simulators in their respective frameworks, and therefore cannot be generalized to our experimental setting. Language Model Optimization with Margin Expectation (LLOME) from Chen et al. (2025a) involves language model post-training for generating new protein and DNA sequences, and was therefore excluded from our evaluation. We also exclude the method from Flam-Shepherd et al. (2022) as a baseline since it is introduced as a molecule distribution matcher, which requires high-quality designs as input (unavailable to us in our setting). Finally, reinforcement learning-based methods, such as DyNA proximal policy optimization (PPO) from Angermueller et al. (2020) and REINFORCE from Williams (1992), are excluded since we do not consider reinforcement learning tasks in our work.

## D ADDITIONAL EXPERIMENTAL RESULTS

## D.1 DISTRIBUTION SHIFT ANALYSIS

To characterize the distribution shift between the surrogate model trained on the source dataset and the ground-truth objective learned on the target dataset, we first compare the performance of the surrogate and objective functions on accurately predicting the annotated labels in the target dataset in **Supplementary Figure S1**. We also plot the agreement between each of the functions and the ground-truth annotation for the target dataset in **Supplementary Figure S2**. As expected, the surrogate model consistently underperforms on the target dataset when compared to the ground-truth oracle function, reflecting the predictive performance drop in real-world clinical decision making tasks under distribution shift. Finally in **Supplementary Figure S3**, we also plot the distribution of ground-truth annotations in both the source and target datasets.

## D.2 COST ANALYSIS

Token usage and monetary cost. Using OpenAI's gpt-4o-mini-2024-07-18 LLM as the backbone optimizer, we report the total number of input and output tokens used in LEON across the tasks in our evaluation suite in **Supplementary Fig. S4**. As of September 2025, the standard API pricing for the gpt-4o-mini-2024-07-18 model is \$0.15 per million input tokens and \$0.60 per million output tokens. Using these price points and assuming no cached inputs, the cost per patient for using LEON is  $$0.21 \pm 0.00$  on the Warfarin task;  $$0.56 \pm 0.00$  on the HIV task;  $$0.60 \pm 0.01$  on the Breast task;  $$0.51 \pm 0.00$  on the Lung task; and  $$0.44 \pm 0.00$  on the ADR task.

1947

1949

1950 1951

1953 1954

1957

1961

1963 1964

1965

1967

1968

1969

1970

1971

1972

1973 1974

1975

1977

1978

1979

1981

1982

1984

1986

1987

1988

1989

1990

1992

1993

1996

1997

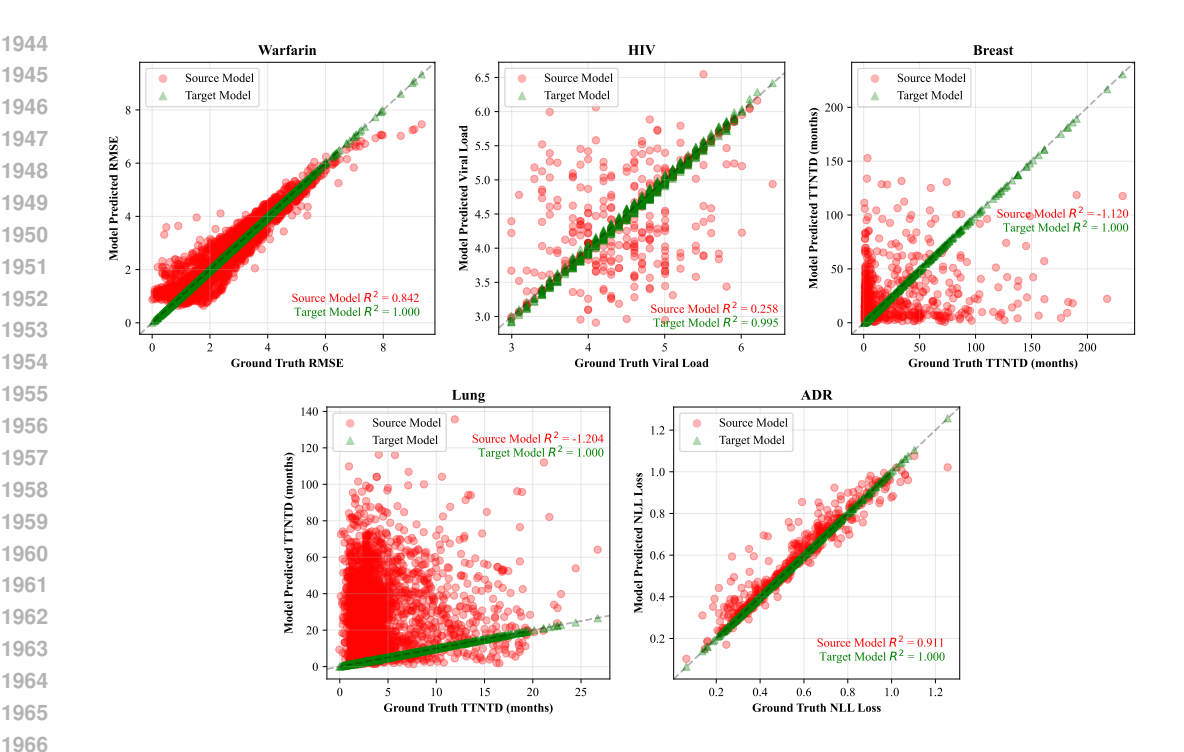


Figure S1: Correlation plots of predictive models used for design evaluation. In our work, we investigate the utility of LLMs in solving 5 challenging biomedical optimization problems under distribution shift. An optimizer is only given access to a model trained on data sampled from a source distribution (red) to score candidate designs, but the final proposals are scored using the ground-truth objective function (green) hidden during evaluation. The oracle is either an exact function if the true objective is known, or a machine learning model otherwise. We evaluate the agreement between the surrogate and oracle functions with the ground truth annotation in the target dataset.

Carbon emissions. Consistent with Samsi et al. (2023) and a publicly available carbon calculator, we assume an energy efficiency of  $7.594 \times 10^{-6}$  kilowatt-hours (kWh) per thousand output tokens per billion LLM active parameters (assuming token generation is performed on NVIDIA A100 GPUs). We primarily use the qpt-40-mini-2024-07-18 model from OpenAI; while the size of this model is currently unknown, we conservatively estimate it to be approximately 20B active parameters for the purposes of cost estimation. Assuming a carbon intensity of 0.39 kg CO<sub>2</sub>e/kWh and power usage effectiveness (PUE) of 1.17 based on U.S. data (Ren et al., 2024), a back-of-theenvelope calculation tells us that the cost per patient for using LEON is approximately  $1.66 \times 10^{-3}$ kg CO<sub>2</sub>e on the Warfarin task;  $1.03 \times 10^{-2}$  kg CO<sub>2</sub>e on the HIV task;  $1.95 \times 10^{-2}$  kg CO<sub>2</sub>e on the Breast task;  $1.14 \times 10^{-2}$  kg CO<sub>2</sub>e on the Lung task; and  $6.38 \times 10^{-3}$  kg CO<sub>2</sub>e on the ADR task.

**GPU utilization.** We observed that GPU utilization was dominated by the size of locally deployed LLMs (e.g., the MedGemma 27B model used as an external knowledge repository in Supplementary Algorithm 2), rather than by our proposed method. As shown in Supplementary Algorithm 1, the GPU memory requirements for LEON scale linearly with the dimensionality of the patientdesign space and the number of parameters of the surrogate model f—both of which are orders of magnitude smaller than the resource footprint of the external LLM. In practice, we found that the maximum GPU memory used by LEON did not exceed **3 GB** for any given task.

#### D.3 QUANTITATIVE ANALYSIS OF PRIOR KNOWLEDGE

Recall from Supplementary Algorithm 2 that the availability of external knowledge sources is a key component of LEON. While a base generalist language model may not have the prior knowledge to achieve high certainty in its proposed designs according to (4), the LLM can query repositories of domain-specific expert knowledge to ultimately synthesize knowledge in natural language that can be used for the optimization task. To better interrogate this process, we plot the frequency with

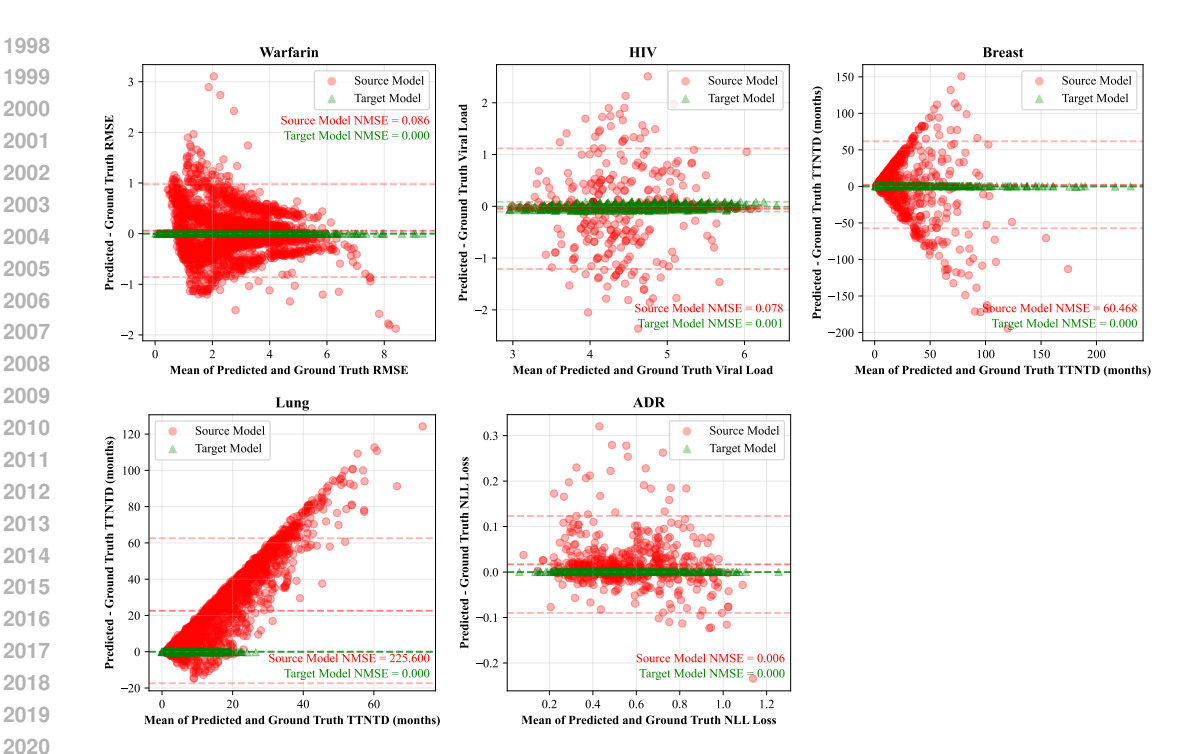


Figure S2: Bland-Altman plots of predictive models used for design evaluation. In our work, we investigate the utility of LLMs in solving 6 challenging biomedical optimization problems under distribution shift. More explicitly, an LLM is only given access to a surrogate model trained on data from a source distribution (red) to score candidate designs, but the final proposals are scored using the ground-truth objective (green) learned on data from the target distribution and hidden during optimization. We evaluate the agreement between each of the source- and target- trained models with the ground truth annotation for each datum in the target dataset. Mean and 95% confidence intervals for both models in each task are indicated by the horizontal dotted lines.

which each of the expert knowledge repositories are individually queried as tools across 100 patients for each of the 5 benchmarking tasks (**Supplementary Fig. S5**).

Our results demonstrate that the same base language model (gpt-4o-mini-2024-07-18) differentially queries the set of external knowledge bases as a function of the underlying task. The total number of knowledge base queries per patient differs by task (mean  $\pm$  standard error of mean (SEM); Warfarin:  $2.91 \pm 0.10$ ; HIV:  $3.01 \pm 0.05$ ; Breast:  $3.16 \pm 0.09$ ; Lung:  $3.50 \pm 0.05$ ; ADR:  $3.63 \pm 0.05$  queries per patient). The increasing number of queries correlates with the authors' subjective evaluation of the difficulty of each task: that is, Warfarin (resp., ADR) is the least (resp., most) challenging optimization problem in our evaluation suite. These results suggest that the language model preferentially relies on more prior knowledge sources as the difficulty of the optimization task increases.

Separately, we observe that the specific knowledge sources queried by the model vary by task: for example, the COSMIC knowledge base from Tate et al. (2019) is preferentially queried in the Breast and Lung tasks that deal with oncologic treatment optimization. We also observe that the knowledge bases GDSC (Yang et al., 2013) and DepMap (Tsherniak et al., 2017) are rarely queried by the language model across all 5 tasks. This makes sense, as both knowledge sources detail properties about *cell lines* (as opposed to patients), and are therefore unlikely to be relevant for any of our tasks. Finally, we ran a  $\chi^2$ -test of homogeneity at the per-task level to evaluate whether different knowledge bases had different rates of being queried within each optimization task. As made visually apparent from **Supplementary Figure S5**, the observed differences in the frequency of knowledge bases being queried per task are far too large to be explained by random sampling variation alone (Warfarin:  $\chi^2 \approx 535.3$ , dof = 7,  $p \approx 2.09 \times 10^{-111}$ ; HIV:  $\chi^2 \approx 763.0$ , dof = 7,  $p \approx 1.81 \times 10^{-160}$ ; Breast:  $\chi^2 \approx 452.3$ , dof = 7,  $p \approx 1.39 \times 10^{-93}$ ; Lung:  $\chi^2 \approx 556.8$ , dof = 7,  $\chi^2 \approx 674.3$ , dof = 7,  $\chi^2 \approx 2.36 \times 10^{-141}$ ). Overall, these results suggest

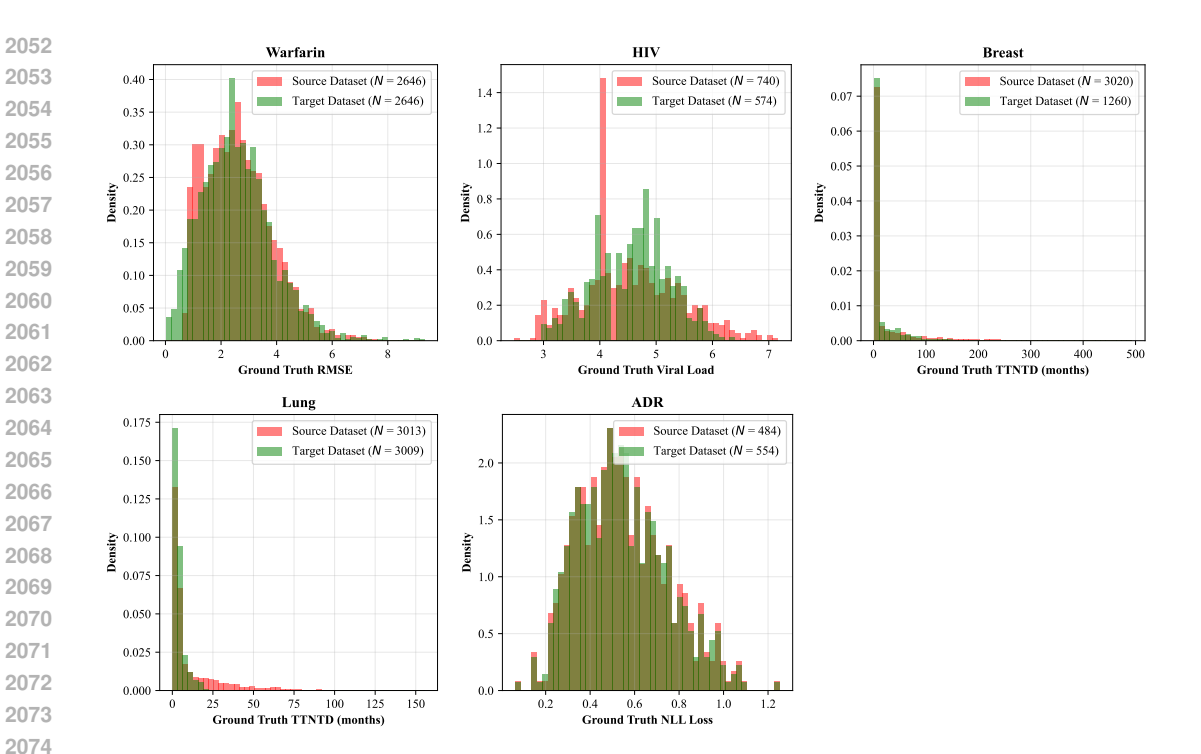


Figure S3: **Distributions of ground truth scores within source and target datasets.** We plot the distribution of ground-truth objective values for both the source (red) and target (green) datasets.

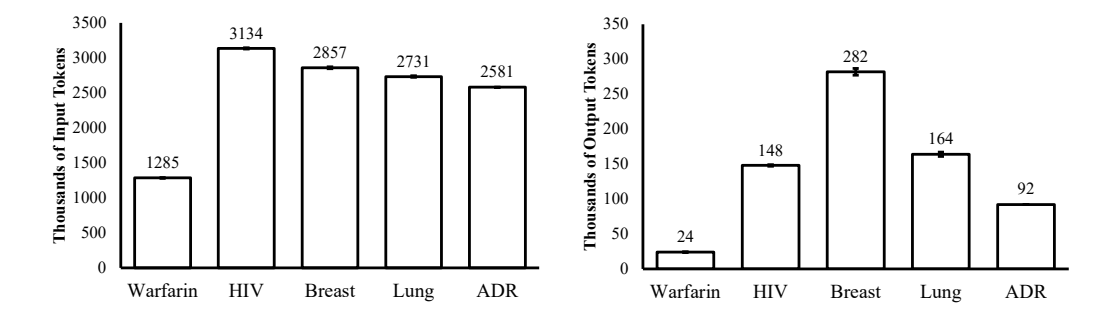


Figure S4: Token usage of LEON across different tasks. We plot the average number of input and output tokens used per patient experiment with the gpt-4o-mini-2024-07-18 backbone optimizer. Error bars represent the standard error of the mean across 100 patient experiments.

that the backbone LLM is selecting knowledge sources to retrieve relevant expert prior knowledge for a given optimization task in a manner that cannot be attributed to random chance alone.

#### D.4 QUALITATIVE EXAMPLES OF PRIOR KNOWLEDGE

Recall from **Supplementary Algorithm 1** that a key component of LEON is synthesizing **domain-specific prior knowledge**: given access to relevant biomedical knowledge bases, we task the baseline language model with making the appropriate tool calls to gather domain-specific and context-specific prior knowledge conditioned on the task description and particular covariates z. The language model is then asked to respond with relevant prior knowledge to use as context for downstream optimization—see **Appendix C.3** for additional details. Here, we provide representative examples of the prior knowledge outputs (indicated by monospace font below) generated by gpt-4o-mini-2024-07-18 for the **Warfarin** task. We focus on this particular task because it is a domain area where we are able to accurately verify LLM outputs. Furthermore, a linear oracle model from Consortium (2009) is available for this task, facilitating the domain-specific verifica-

2107 2108

2109 2110

2111

2112

2113 2114

211521162117

2118

2119

212021212122

2123 2124

2125212621272128

2129

2130

2131

21322133

2134

2135

2136

2137

2138

2139

2140

2141

2142

2143

2144

2145

2146

2147

2148

2149

2150

2151

2152

2153

2154

2155

2156

2157

2158

2159

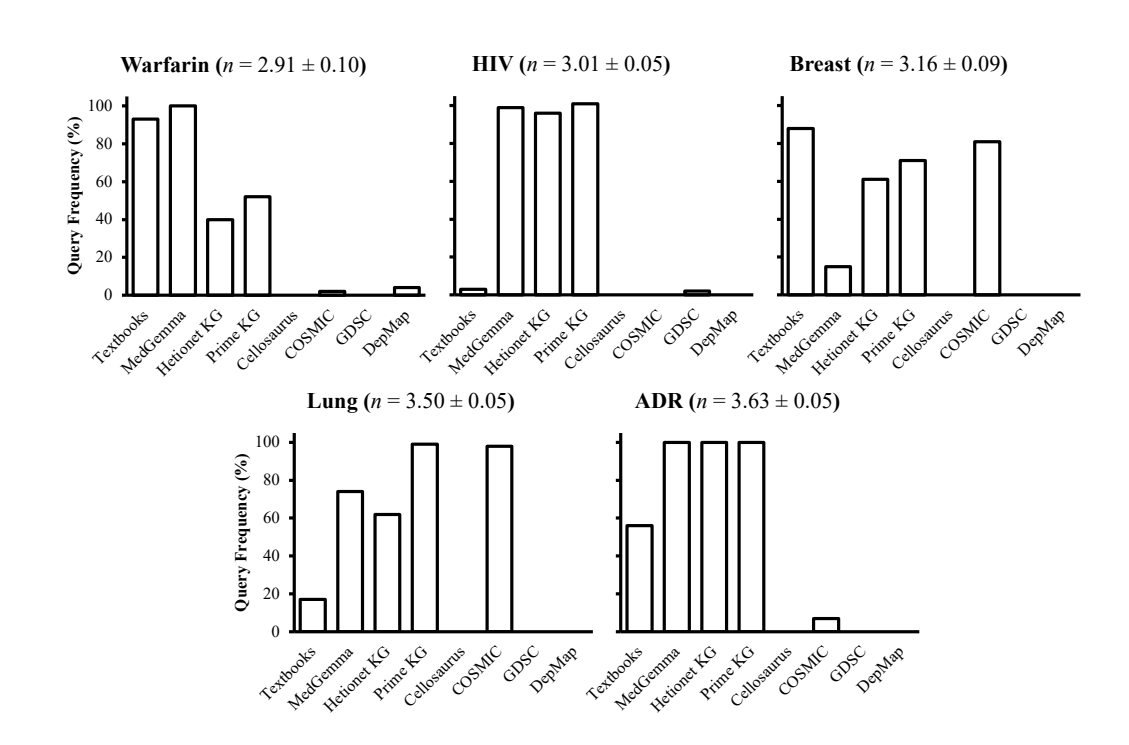


Figure S5: Distribution of knowledge sources called as tools by the LLM for prior knowledge synthesis. We plot the frequency of querying each repository (over 100 patients) in Supplementary Algorithm 2 across each of the optimization tasks evaluated. Each subplot title includes the mean  $\pm$  standard error of the mean (SEM) number of tool calls made per patient.

tion of the consistency of LLMs with published prior work. To evaluate the quality of the LLM-synthetized prior knowledge, 1 U.S. resident physician and 1 U.S. senior medical student manually annotated the LLM-generated knowledge for factual accuracy; in cases where annotations semantically disagreed, the prior knowledge output was discussed until consensus was reached. We include their annotations as right-justified, colored serif font in the listings below.

In this first example, all generated prior knowledge was considered relevant and factually consistent with evidence-based medical guidelines. The LLM optimizer queried the following knowledge sources as tool calls (in order): (1) MedGemma 27B; (2) Hetionet Knowledge Graph; (3) Prime Knowledge Graph; and (4) Medical Textbooks (see **Appendix C** for additional details). Furthermore, the final proposed warfarin dosing strategy score proposed by the LLM optimizer using the prior knowledge and LEON achieved an oracle score of 1.24, which is more optimal than the mean score achieved by our method on this task in **Table 1**.

```
For a 30-39 year old Asian patient with a BMI
                                                          The demographic information here
of 29.1, a CYP2C9 genotype of *1/*1, and a
                                                        is accurate for this particular patient.
VKORC1 SNP of A/A, the following information
is relevant for determining an optimal warfarin
dose:
1. **Genetic Influence on Warfarin Dosing**:
    - The CYP2C9 *1/*1 genotype indicates
                                                      This is consistent with expert guidance
     normal metabolism of warfarin, meaning
                                                          (Sconce et al., 2005), and also with
                                                      the linear oracle dosing algorithm from
     the patient is not a poor metabolizer.
     However, this genotype does not require
                                                        Consortium (2009) used in this work.
     a significantly higher dose compared to
     those with reduced function alleles.
     The VKORC1 A/A genotype suggests
                                                          This is also consistent with expert
                                                        guidance (Dean, 2012), and also with
     increased sensitivity to warfarin,
     typically requiring lower doses. Studies
                                                          the linear oracle dosing algorithm
     indicate that individuals with the A/A
                                                                 from Consortium (2009).
     lower doses than those with non-A haplotypes.
```

2. \*\*Initial Dosing Recommendations\*\*:

2170

2171

2172

2205 2206

2207 2208

2210

2211

2212

2213

```
2160
          - Standard initial dosing for warfarin is
                                                                    This is consistent with medical
2161
                                                                guidelines (Dean, 2012). A starting
             typically between 5-10 mg per day.
2162
             However, due to the VKORC1 A/A genotype,
                                                                     dose of 3-4 mg/day is usually
             a lower starting dose is advisable.
                                                                   recommended for this patient in
2163
           - A common approach is to start with
                                                               the absence of other medical history.
2164
             a dose of around 2.5-5 mg per day
2165
             for patients with the A/A genotype,
2166
             especially considering the patient's
2167
             Asian ethnicity, which is associated with
             a higher prevalence of VKORC1 variants.
2168
```

In this second example on the **Warfarin** task, there was a factually incorrect statement made by the LLM, highlighted in red below. The LLM optimizer queried the following knowledge sources in order: (1) Medical Textbooks; and (2) MedGemma 27B. Quantitatively, we found that the LLM optimizer consequently performed worse on this patient, achieving an inferior oracle score of 2.32.

```
2173
       To propose an optimal warfarin dose for
2174
       the patient with the following characteristics:
2175
       - **Age**: 60-69 years
                                                                  The demographic information here
2176
       - **BMI**: 23.4
                                                                 is accurate for this particular patient.
2177
       - **CYP2C9 Genotype**: *1/*1 (wild-type)
       - **VKORC1 SNP**: A/G
2178
2179
       ### Relevant Information:
2180
       1. **CYP2C9 Genotype**:
2181
           - The *1/*1 genotype indicates normal
                                                               This is consistent with expert guidance
                                                                  (Sconce et al., 2005), and also with
             enzyme activity, meaning the patient is
2182
             a "normal metabolizer" of warfarin.
                                                               the linear oracle dosing algorithm from
2183
             Patients with this genotype typically
                                                                Consortium (2009) used in this work.
2184
             require higher doses of warfarin
2185
             compared to those with variant
2186
             alleles (\star2 or \star3).
       2. **VKORC1 Genotype**:
2187
           - The A/G genotype suggests that the
                                                                While heterozygous A/G patients for
2188
             patient has a moderate response to
                                                                        the VKORC1: -1639G→A
2189
             warfarin. The presence of the G allele
                                                             polymorphism have moderate expression
2190
             is associated with lower VKORC1
                                                           of VKORC1, this genotype generally leads
2191
             expression, which generally leads to a
                                                                to higher warfarin doses than that for
                                                                 A/A individuals (Dean, 2012). This
             reduced requirement for warfarin
             compared to those with the A/A genotype.
                                                                knowledge output is also inconsistent
2193
             Specifically, individuals with the
                                                          with the ground-truth dosing algorithm from
2194
             A/G genotype may require about 25%
                                                                Consortium (2009) used in this work.
2195
             lower doses than A/A homozygotes.
2196
       3. **Dosing Guidelines**:
           - Initial warfarin dosing typically
                                                              This dosage guidance is consistent with
2197
             starts at 5-10 \text{ mg/day}. Given the
                                                              clinical recommendations (Dean, 2012).
2198
             patient's age and the influence of
2199
             VKORC1, a conservative approach is
2200
             advisable.
2201
             For a patient with CYP2C9 *1/*1 and
2202
             VKORC1 A/G, a reasonable starting
             dose might be around 5 mg/day, with
2203
             adjustments based on INR monitoring.
2204
```

# D.5 Additional Analysis of the LLM Certainty Parameter $\mu$

Recall that the certainty parameter  $\mu$  in LEON is the Lagrange multiplier of the entropy-based constraint in our constrained problem formulation in (4). Larger values of  $\mu$  are observed when the LLM consistently returns equivalent treatment designs for a given input prompt despite the nondeterminism of the generative model (as dictated by the LLM temperature hyperparmaeter  $\tau=1.0$  used in the main text). Using this framework, we can plot how the value of  $\mu$  changes over the course of optimization to better interrogate how the certainty of the language model in proposing high-quality treatment designs changes during optimization.

2217

2221

2227

2228

2231

2236

2237

2238

2239 2240 2241

2242

2243

2244

2245

2246 2247

2248 2249

2250

2251

2252

2253

2254

2255

2256

2257

2258

2259

2260

2261

2262 2263

2264 2265

2266

2267

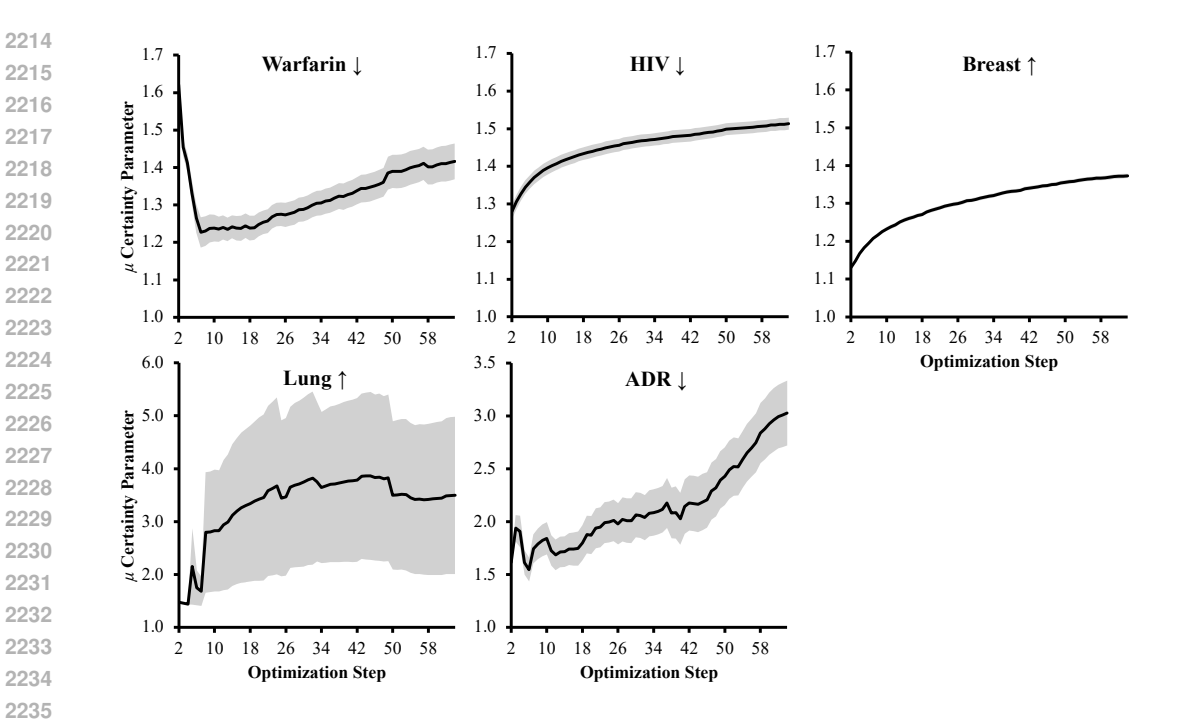


Figure S6: LLM certainty parameter  $\mu$  over the course of optimization. We plot the mean  $\pm$ SEM value of  $\mu$  estimated using (9) at each optimization step for n=100 independent target patient experiments. Up (resp. down) arrows indicate that the task is a maximization (resp., minimization) task. Higher values of  $\mu$  suggest a greater confidence of the LLM in its design proposals.

Our results are shown in **Supplementary Figure S6**. We find that the value of  $\mu$  generally increases as a function of the optimization step. This suggests that the certainty of the LLM increases as more designs are observed and evaluated using our method. One possible explanation for this trend is that LLM certainty is a function of not only the prior knowledge generated, but also the previously proposed designs. That is, the LLM is more confident in future designs because it is able to 'learn' from the history of previously sampled designs and their scores according to LEON.

# EXTENDING LEON TO TRADITIONAL OPTIMIZERS

In principle, there is nothing in **Supplementary Algorithm 1** that is particular to language modelbased optimizers: the auxiliary source critic model can be used in conjunction with any optimization method, and the entropy-based constraint is enforcable with any method that supports batched acquisitions. To this end, we implement LEON with gradient ascent (Grad.) and Bayesian optimization (BO-qEI) and evaluate LEON with these traditional optimizers in Supplementary Table S2.

Our results suggest that using LEON with these traditional, non-LLM based optimizers does not offer a meaningful advantage over the corresponding baselines. LEON-BO-qEI improves upon BOqEI on 3 of the 5 tasks, and LEON-Grad. improves upon Grad. only on 1 of the 5 tasks. This trend is consistent with the notion that **prior knowledge** is critical for LEON to consistently improve upon optimizer performance. Because traditional optimizers like Grad. and BO-qEI lack informative priors over the design space, the entropy-based constraint central to LEON is less meaningful using these methods. Consequently, although LEON is optimizer-agnostic in theory, its utility is limited when used with methods that do not incorporate prior knowledge.

## WHY SHOULD WE BOUND THE 1-WASSERSTEIN DISTANCE?

A key underlying assumption behind our modified problem formulation in (4) is that the source critic-based constraint can meaningfully prevent over-extrapolation against the surrogate model that is frequency observed in optimization tasks under distribution shift (Yao et al., 2024; Trabucco et al., 2022). In **Theorem D.1**, we provide a theoretical motivation to help support this assumption.

Table S2: **Evaluating LEON for traditional optimizers.** We evaluate the utility of LEON in improving the performance on non-LLM based optimization methods gradient ascent (Grad.) and Bayesian optimization (BO-qEI). We report mean  $\pm$  standard error of mean (SEM) oracle objective value achieved by the single proposed design for a given patient, averaged over n=100 test patients. **Bolded** cells indicate when using LEON improves upon the backbone optimizer for a given task.

Method	Warfarin ↓ RMSE Loss (mg/week)	HIV ↓ Viral Load (copies/mL)	Breast ↑ TTNTD (months)	NSCLC  ↑ TTNTD  (months)	CRS ↓ NLL Loss (no units)
Grad. LEON-Grad.	$1.37 \pm 0.13$ $2.24 \pm 0.19$	$4.52 \pm 0.04$ $4.54 \pm 0.06$	$73.07 \pm 2.30$ $51.68 \pm 1.38$	$24.67 \pm 0.34$ <b>27.61</b> $\pm$ <b>0.64</b>	23.7 ± 1.7 23.8 ± 1.7
BO-qEI LEON-BO-qEI	$1.36 \pm 0.13$ $2.02 \pm 0.15$	$4.53 \pm 0.04$ $4.48 \pm 0.05$	$67.11 \pm 1.86$ $65.52 \pm 2.34$	$28.65 \pm 0.65$ $31.04 \pm 0.82$	$23.5 \pm 1.7$ <b>21.4</b> $\pm$ <b>1.8</b>

**Theorem D.1** (Bound on Empirical Test Risk). Define a real-valued, Borel-measurable function  $f: \mathcal{X} \to \mathbb{R}$  defined over a domain  $\mathcal{X} \subseteq \mathbb{R}^d$ , and define  $K:=||f(x)||_L$  to be the corresponding Lipschitz constant of f. Given a finite dataset of n observations  $\mathcal{D}:=\{(x_i,f(x_i))\}_{i=1}^n$ , suppose we train a predictive model  $\hat{f}$  on  $\mathcal{D}$  with Lipschitz constant  $K_{\hat{f}}$  finite such that the empirical training risk is  $\varepsilon:=\mathbb{E}_{(x,y)\sim\mathcal{D}}|y-\hat{f}(x)|$  finite. Then, the test risk on a new sample of T test inputs  $\mathcal{T}=\{x_j\}_{j=1}^T$  is bounded from above by

$$\mathbb{E}_{x \sim \mathcal{T}} |f(x) - \hat{f}(x)| \le \varepsilon + (K + K_{\hat{f}}) W_1(\mu_{\mathcal{D}}, \mu_{\mathcal{T}})$$

where  $W_1(\mu_D, \mu_T)$  is the 1-Wasserstein distance associated with  $||\cdot||_2$ .

*Proof.* Define  $\gamma \in \Gamma(\mu_{\mathcal{D}}, \mu_{\mathcal{T}})$  as the optimal coupling between input observations x' and x in  $\mathcal{D}$  and  $\mathcal{T}$ , respectively. For pairs  $(x', x) \sim \gamma$ , note that because  $\mu_{\mathcal{T}}$  is the x-marginal of  $\gamma$ ,

$$\begin{split} \mathbb{E}_{x \sim \mathcal{T}} |f(x) - \hat{f}(x)| &= \mathbb{E}_{(x',x) \sim \gamma} |f(x) - \hat{f}(x)| \\ &= \mathbb{E}_{(x',x) \sim \gamma} \left| \left( f(x) - \hat{f}(x) \right) - \left( f(x') - \hat{f}(x') \right) + \left( f(x') - \hat{f}(x') \right) \right| \\ &\leq \mathbb{E}_{(x',x) \sim \gamma} \left| \left( f(x) - \hat{f}(x) \right) - \left( f(x') - \hat{f}(x') \right) \right| + \mathbb{E}_{(x',x) \sim \gamma} \left| f(x') - \hat{f}(x') \right| \end{split}$$

using the triangle inequality. Because  $\mu_D$  is the x'-marginal of  $\gamma$ , we rewrite the right hand side as

$$\mathbb{E}_{x \sim \mathcal{T}} |f(x) - \hat{f}(x)| \leq \mathbb{E}_{(x',x) \sim \gamma} \left| \left( f(x) - \hat{f}(x) \right) - \left( f(x') - \hat{f}(x') \right) \right| + \mathbb{E}_{x' \sim \mathcal{D}} \left| f(x') - \hat{f}(x') \right|$$

$$= \mathbb{E}_{(x',x) \sim \gamma} \left| \left( f(x) - \hat{f}(x) \right) - \left( f(x') - \hat{f}(x') \right) \right| + \varepsilon$$

using the definition of the empirical training risk  $\varepsilon$ . Applying the definition of the Lipschitz constants  $K, K_{\hat{f}}$  as well as the definition of the 1-Wasserstein distance gives

$$\mathbb{E}_{x \sim \mathcal{T}} |f(x) - \hat{f}(x)| \le (K + K_{\hat{f}}) \mathbb{E}_{(x', x) \sim \gamma} |x - x'| + \varepsilon = (K + K_{\hat{f}}) W_0 + \varepsilon$$

The claim follows.  $\Box$ 

We remark that deriving the global Lipschitz bounds  $K, K_{\hat{f}}$  is  $\mathcal{NP}$ -hard and infeasible in practice (Scaman & Virmaux, 2018; Hu et al., 2024). However, the above result still holds if  $K, K_{\hat{f}}$  only hold locally over a finite subset of  $\mathcal{X}$  that contains  $\mathcal{D} \bigcup \mathcal{T}$ , which is much easier to derive. Furthermore, note that the constants  $\varepsilon$  and Lipschitz constants  $K, K_{\hat{f}}$  in **Theorem D.1** are irreducible, since we assume that we do not have control over  $\mathcal{D}$  or the functions  $f, \hat{f}$ . However, the above result also shows that bounding  $W_1(\mu_{\mathcal{D}}, \mu_{\mathcal{T}})$  will yield a corresponding finite bound on the empirical test risk. **This is a key observation**—by intelligently choosing the test points in  $\mathcal{T}$  that we use to evaluate with  $\hat{f}$ , we can guarantee a bound on the mean test error over  $\mathcal{T}$ .

## D.8 SAMPLE REFLECTION TRACE

2322

23232324

2325

2326

2327

2328 2329

2330

2331 2332

2333

2334

2335

2336

2337

2338

2339

2340

2341

2342

2343

2344

2345

2346

2347

2348

2349

2350

2351

2352

2353

2354

2355

2356

2357

2358

2359

2360

2361

2362 2363

2364

2365

2366

2367

2368

2369

2370

2371

23722373

2374

2375

To illustrate the process of reflection, we include a representative example reflection output for an optimization experiment on the **Warfarin** task. Based on the prompting strategy used for reflection in **Appendix C.3**, we encourage the language model to reflect on the optimization progress from both task-agnostic 'exploration-exploitation' and biomedical reasoning perspectives.

Analyzing the previously proposed warfarin doses and their scores reveals several insights into the potential biological mechanisms and pharmacokinetic principles that may be influencing the outcomes.

#### ### High-Scoring Designs

- 1. \*\*Doses with Lower Values\*\*: The highest scores are associated with
  lower doses, such as 11.3417 mg/week (score: -0.398857) and 15.1328
  mg/week (score: -0.330352). This suggests that lower doses may be more
  effective for this patient, possibly due to:
  - \*\*Pharmacokinetics\*\*: Lower doses may lead to more stable INR
     (International Normalized Ratio) levels, reducing the risk of
     bleeding or thromboembolic events. Warfarin has a narrow therapeutic
     index, and small changes in dose can lead to significant changes in
     anticoagulation effect.
  - \*\*Patient Variability\*\*: Individual responses to warfarin can vary significantly due to genetic factors (e.g., VKORC1 and CYP2C9 polymorphisms), dietary influences, and concurrent medications. Lower doses may be more universally tolerated across diverse patient backgrounds.
- 2. \*\*Avoidance of High Doses\*\*: The lowest scores are associated with higher doses (e.g., 72.6990 mg/week with a score of -8.7245). High doses may lead to:
  - \*\*Toxicity\*\*: Increased risk of adverse effects, including major bleeding, which is a significant concern in anticoagulation therapy.
  - \*\*Instability\*\*: Higher doses can lead to fluctuations in INR, making it difficult to maintain therapeutic levels.

# ### Low-Scoring Designs

- 1. \*\*High Doses\*\*: As mentioned, doses like 63.5996 mg/week and 72.6990
  mg/week are associated with very low scores. These doses may be
  biologically implausible for many patients, leading to:
  - \*\*Off-Target Effects\*\*: Excessive anticoagulation can lead to complications that outweigh the benefits of treatment.
  - \*\*Increased Variability\*\*: Higher doses may exacerbate the variability in response due to genetic and environmental factors.
- - \*\*Suboptimal Targeting\*\*: These doses may not align well with the patient's specific pharmacogenomic profile, leading to inadequate anticoagulation or increased side effects.

# ### Biological and Biomedical Considerations

- \*\*Genetic Factors\*\*: The variability in warfarin metabolism due to genetic polymorphisms in CYP2C9 and VKORC1 is well-documented. Understanding the patient's genetic makeup could help tailor the dose more effectively.
- \*\*Dietary Interactions\*\*: Vitamin K intake can significantly affect warfarin efficacy. Patients with high dietary vitamin K may require higher doses, while those with low intake may need lower doses.
- \*\*Drug Interactions\*\*: Concurrent medications can alter warfarin metabolism, necessitating dose adjustments. Awareness of these interactions is crucial for optimizing therapy.

#### ### Conclusion

The analysis suggests that lower doses are generally more effective and safer for this patient population, likely due to the pharmacokinetic properties of warfarin and the variability in patient responses. Future

Table S3: Ablating the backbone LLM optimizer. We evaluate how the performance of LEON changes as a function of the backbone LLM optimizer, reporting the mean  $\pm$  SEM oracle objective value achieved by the single proposed design for a given patient, averaged over n=100 test patients. **Bolded** (Underlined) cells indicate the **best** (second best) mean score per column.

LLM	Warfarin ↓ RMSE Loss (mg/week)	HIV ↓ Viral Load (copies/mL)	Breast ↑ TTNTD (months)	Lung ↑ TTNTD (months)	ADR ↓ NLL Loss (no units)	Rank
Majority	$3.46\pm0.70$	$4.55\pm0.07$	$25.95\pm0.75$	$20.13 \pm 0.13$	$\textbf{1.41} \pm \textbf{0.05}$	6.0
Human	$2.68 \pm 0.86$	$4.55 \pm 0.07$	$29.65 \pm 1.14$	$21.10 \pm 0.27$	_	6.5
Llama-3.1 8B	$1.50\pm0.19$	$4.63 \pm 0.04$	$56.86 \pm 2.84$	$24.07 \pm 0.42$	$28.9 \pm 1.5$	6.2
Llama-3.3 70B	$1.52 \pm 0.23$	$4.64 \pm 0.04$	$60.90 \pm 2.41$	$28.66 \pm 0.62$	$20.3 \pm 1.8$	6.0
DeepSeek R1 671B	$1.47 \pm 0.24$	$4.41 \pm 0.05$	$72.16 \pm 3.71$	$33.09 \pm 0.40$	$10.3 \pm 1.7$	3.0
GPT-40 Mini	$\textbf{1.36} \pm \textbf{0.13}$	$4.50 \pm 0.04$	$72.74 \pm 2.69$	$32.58 \pm 0.32$	$12.4 \pm 1.6$	3.0
o4-Mini	$1.37 \pm 0.16$	$4.48 \pm 0.03$	$75.89 \pm 3.18$	$33.22 \pm 0.61$	$8.57 \pm 1.41$	2.2
Gemini-2.5 Flash	$\overline{\textbf{1.36} \pm \textbf{0.16}}$	$\textbf{4.39} \pm \textbf{0.04}$	$68.61 \pm 2.55$	$\overline{33.24 \pm 0.25}$	$15.5 \pm 1.7$	<u>2.4</u>

proposals should focus on exploring lower doses while considering individual patient factors such as genetics, diet, and potential drug interactions to optimize outcomes.

# **E** ABLATION STUDIES

## E.1 BACKBONE LLM ABLATION

We present empirical results using the **GPT-4o Mini** (gpt-4o-mini-2024-07-18) model from OpenAI in **Table 1** in the main text. However, LEON can also be used with other backbone LLM optimizers, such as: (1) **Meta Llama-3.18B** (meta-llama/Llama-3.1-8B-Instruct); (2) **Meta Llama-3.370B** (meta-llama/Llama-3.3-70B-Instruct); (3) **DeepSeek R1 671B** (us.deepseek.rl-v1:0); (4) **o4-Mini** (o4-mini-2025-04-16) with high reasoning effort; and (5) **Gemini-2.5 Flash** (gemini-2.5-flash-preview-05-20) with dynamic thinking. We evaluate LEON using each of these LLMs in **Supplementary Table S3**.

**Results.** We find that the quality of designs can vary significantly depending on the choice of the underlying backbone language model optimizer (**Supplementary Table S3**). Commercial nonreasoning open source models, such as Llama-3.1 8B and Llama-3.3 70B, were the least performant and achieved an average rank of only 6.2 and 6.0 across the 5 tasks, respectively. In contrast, closed source reasoning models, such as o4-Mini and Gemini-2.5 Flash, achieved the best performance with an average rank of 2.2 and 2.4, respectively. Furthermore, Gemini-2.5 Flash performed the best on 3 of the 5 tasks, and o4-Mini was in the top 2 methods on 4 of the 5 tasks. Furthermore, the open-source reasoning model DeepSeek R1 was able to approximately match the performance of GPT-40 Mini; both models achieved an intermediate rank of 3.0 compared with the other LLMs evaluated. Altogether, our results suggest that using (1) proprietary and (2) reasoning models can offer the greatest performance when used together with our method.

Importantly, the observation that closed-source models outperform their open-source counterparts warrants discussion. Language models that are only accessible via third-party application programming interface (API) endpoints introduce concerns regarding patient privacy and data security, which are understandably paramount in fields such as healthcare. Furthermore, while DeepSeek R1 was demonstrated to be a viable model on par with some of the proprietary models, it is unlikely that the majority of hospital systems have the necessary infrastructure to support scalable local inference of this large model. While these current real-world limitations may limit the present utility of our method, recent work has shown that the performance gap between open- and closed- source models has been shrinking over time (Zhang et al., 2024a; Van Veen et al., 2024). Moving forward, we hope to explore how LEON might be used with future, more performant open-source language models.

**Fine-tuned medical reasoning and non-reasoning models.** Separate from the models included in **Supplementary Table S3**, we hypothesized that medical post-training may improve the observed

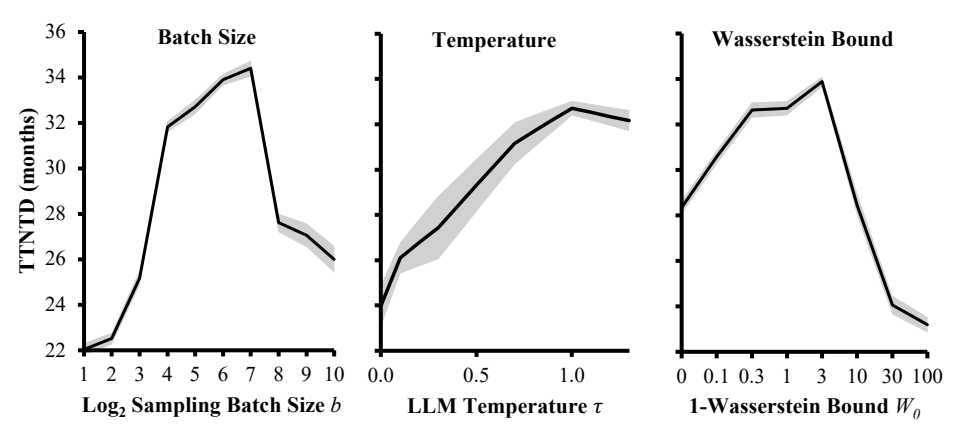


Figure S7: **LEON hyperparameter ablation.** We individually ablate the values of 3 key hyperparameters in **Supplementary Algorithm 1**: (**left**) the sampling **batch size**, which implicitly controls the trade-off between exploration and exploitation during optimization and the accuracy of (9); (**middle**) the LLM **temperature**, which controls the diversity of outputs (and therefore  $\mu$ ); and (**right**) the 1-Wasserstein distance bound  $W_0$  in (4) and (11), which affects the value of the certainty parameter  $\lambda$ . Optimization results are shown for the **Lung** task (a TTNTD <u>maximization</u> task), averaged over 100 patients. Error bars represent the standard error of the mean (SEM).

optimization performance and sought to evaluate a suite of medical fine-tuned LLMs with LEON. We evaluated the following models: **BioMistral-7B** (Labrak et al., 2024), **MedFound-176B** (Liu et al., 2025), **Me-LLaMA** (Xie et al., 2025), and **BioMedGPT** (Zhang et al., 2024b). We were unable to evaluate **MedPaLM** (Singhal et al., 2025; 2023) or **Med-RLVR** (Zhang et al., 2025b) due to lack of open-source implementations. Unfortunately, none of the medical fine-tuned models that we evaluated were compatible with our LEON framework due to their inability to return structured outputs despite our best attempts at prompt engineering and parsing outputs with specialized code adapters. We hypothesize that this may be due to the optimization of these models to be performant on tasks such as medical question answering at the expense of their ability to follow other non-medical instructions, such as returning structured outputs. This finding is consistent with related work demonstrating that medical fine-tuned language and vision-language models often fail to generalize to medical tasks outside of question answering (Jeong et al., 2024; Yao et al., 2025a).

**Vision-language models.** A separate body of work has also introduced *multimodal* vision-language models; examples that are specifically adapted for applications in medicine include **BioMedGPT** (Zhang et al., 2024b), **MedVP** (Zhu et al., 2025), **LLaVA-Med** (Li et al., 2023), and **MedVQA** (Ha et al., 2024). In principle, LEON and similar methods could be extended to benefit optimization experiments with input multimodal patient data—such as patient imaging scans, genomic sequencing data, and other health record derivatives. We leave this as an opportunity for future work.

#### E.2 SAMPLING BATCH SIZE ABLATION

In Supplementary Figure S7a, we ablate the sampling batch size parameter b defined in Supplementary Algorithm 1 (we use a batch size of b=32 for all experiments reported in Table 1). Smaller values of b allow for more adaptive and sequential optimization, potentially leading to more informed choices during optimization for a more balanced exploration-exploitation trade-off. However, larger values of b benefit from parallelized evaluations and more robust estimates of the fractional occupancy of each equivalence class, and therefore more accurate predictions of  $\hat{\mu}$  using (9). Over a logarithmic sweep of batch sizes between 2 and 1024 inclusive, we found that using a larger batch size of up to 128 generally improved the performance of LEON on the Lung task. However, above this threshold, the opportunity cost associated with highly parallelized acquisitions likely becomes significant enough to degrade the observed optimization performance, as expected.

# E.3 LLM TEMPERATURE ABLATION

Recall that the temperature parameter affects the variability of generated responses to a given input prompt: a lower (resp., higher) LLM temperature value produces more (resp., less) deterministic

2485

2486

2487

2488

2489

2490

2491

2492

2493

2494

2495

2496

2497

2498

2499

2500 2501

2502

2503

2504

2505

2506

2507

2509

2510

2511

2512

2513

2514

2515

2516

25172518

2519 2520

2521

2522

2523

2524

2525

2526

2527

2528

2529

2530

2531

2532

2533

25342535

2536

2537

outputs. In **Table 1** in the main text, we use a fixed temperature parameter of  $\tau = 1.0$  across all experiments. In **Supplementary Figure S7b**, we evaluate 5 additional temperature values (i.e.,  $\tau \in \{0.0, 0.1, 0.3, 0.7, 1.3\}$  to use with the backbone LLM (qpt-4o-mini-2024-07-18) on the **Lung** task. We also tried to evaluate the higher temperature values of  $\tau \in \{1.7, 1.9, 2.0\}$ ; however, the language model was unable to produce syntactically correct structured outputs and therefore failed to propose valid design candidates despite multiple retry requests. Our results suggest that as expected, the use of a sufficiently high temperature parameter is necessary for good performance of LEON. We hypothesize that this behavior is due to the effect of the temperature parameter on the design entropy  $\mathcal{H}(\bar{q})$  in (7), and hence the  $\mu$  certainty parameter in **Lemma 4.3**. For sufficiently small  $\tau$ , the entropy-based constraint in (7) becomes arbitrarily satisfied regardless of the language model's use (or lack thereof) of any prior knowledge. The prior knowledge therefore no longer plays an 'active' role in guaranteeing high certainty in the design proposal process for sufficiently small  $\tau$ . In contrast, sufficiently large temperature values make it increasingly difficult to use either knowledge-driven or data-driven prompting to guide the optimization process and overcome incresingly random next-token prediction. Indeed, for sufficiently large values of  $\tau$ we were unable to even obtain meaningful design proposals. We leave the task of better tuning the temperature parameter for LEON and other LLM-based methods for future work.

#### E.4 1-Wasserstein Distance Bound Ablation

Another key hyperparameter in our problem formulation from (4) and in Supplementary Algorithm 1 is the bound on the empirical 1-Wasserstein distance  $W_0$ . In Supplementary Figure S7c, we experimentally evaluate the impact of ablating the value of  $W_0 \in \{0, 0.1, 0.3, 3, 10, 30, 100\}$ on the Lung task using LEON with qpt-40-mini-2024-07-18 as the backbone optimizer (note that using a value  $W_0 = 1$  corresponds to our results in **Table 1**). Our results show that using LEON with both very small (i.e.,  $W_0 = 0$ ) or very large (i.e.,  $W_0 = 100$ ) values of  $W_0$  fails to demonstrate strong empirical performance. Rather, an intermediate value of  $W_0 = 3$  corresponds to the best observed experimental setting. These results agree with our intuition: for small  $W_0 \approx 0$ , we require the set of proposed designs to be sampled from the source distribution with high confidence, thereby limiting the allowable extent of exploration of the design space. Conversely, setting  $W_0 \gg 0$ relaxes this source critic-based constraint, enabling greater exploration (albeit at the cost of the trustworthiness of surrogate model predictions). This is reflected in the dependence of  $\partial g(\mu, \lambda)/\partial \lambda$  on  $W_0$  in (10)—smaller (resp., larger) values of  $W_0$  will lead to larger (resp., smaller) values of  $\lambda$  in performing gradient descent following (11). LEON balances this tradeoff between exploration and exploitation by using an intermediate value of  $W_0$ . Importantly, we do not require any taskspecific hyperparameter tuning of  $W_0$  to achieve our results reported in the main text.

# E.5 $\lambda$ and $\mu$ Certainty Parameters Ablation

The core algorithmic contribution of LEON relies on the certainty parameters  $\lambda$  and  $\mu$ , which are Lagrangian dual parameters introduced in **Lemma 4.3** in the main text. Intuitively, a high value of  $\lambda$  corresponds to upweighting the importance of the source critic relative to the surrogate model prediction; a high value of  $\mu$  corresponds to upweighting a particular batch of designs based on a high LLM certainty in the predicted set of designs. Here, we empirically ablate both of these certainty parameters to characterize their individual effects on optimization performance. Referencing **Lemma 4.3**, deterministically fixing  $\lambda=0$  effectively ignores the contribution of the source critic model, and fixing  $\mu=1$  ignores the contribution of the language model entropy.<sup>2</sup> Our results are shown in **Supplementary Table S4**. We find that dynamically computing the values of  $\lambda$  and  $\mu$  offer a clear advantage when compared to ablating the individual parameters. This makes sense, as properly solving our constrained optimization problem requires the dynamic computation of the certainty parameters according to (9) and (11). Interestingly, we find that dynamically computing the two parameters individually while fixing the other performs *worse* than fixing both parameters together (according to the average Rank). These results underscore the importance of leveraging both constraints from (2) in our problem setting.

 $<sup>^2</sup>$ We remark that setting  $\mu=1$  is not strictly identical to solving (4) without the entropy-based constraint. However, setting  $\mu=1$  effectively ignores the contribution from the LLM certainty estimation—we leverage this alternative approach because the constrained optimization problem in (4) without the entropy-based constraint does not have a closed form solution per prior work (Yao et al., 2024).

Table S4: Certainty parameter ablation. We ablate the *Dynamic* (Dyn.) computation of certainty parameters  $\lambda$  and  $\mu$  (according to (11) and (9), respectively) and instead independently fix them to constant values  $\lambda=0$  (resp.,  $\mu=1$ ). Per **Lemma 4.3**, note that using these constant values effectively ablates the contribution of the source critic (resp., LLM entropy) in LEON. We report the mean  $\pm$  standard error of mean (SEM) oracle objective value achieved by the single proposed design for a given patient, averaged over n=100 target patients. **Bolded** (resp., <u>Underlined</u>) cells indicate the **best** (resp., second best) mean score for a given task.

λ	μ	Warfarin ↓ RMSE Loss (mg/week)	HIV ↓ Viral Load (copies/mL)	Breast ↑ TTNTD (months)	Lung ↑ TTNTD (months)	ADR ↓ NLL Loss (no units)	Rank
0	1	$1.54 \pm 0.25$	$4.58 \pm 0.04$	$63.48 \pm 3.52$	$25.10 \pm 0.69$	$21.3 \pm 2.0$	2.6
0	Dyn.	$1.63 \pm 0.10$	$\textbf{4.48} \pm \textbf{0.06}$	$\overline{61.29 \pm 5.76}$	$23.68 \pm 0.55$	$25.5 \pm 2.3$	3.0
Dyn.	1	$1.52 \pm 0.18$	$4.52\pm0.06$	$51.80 \pm 3.24$	$23.13 \pm 0.52$	$23.8\pm2.3$	3.2
Dyn.	Dyn.	$\overline{\textbf{1.36} \pm \textbf{0.13}}$	$4.50 \pm 0.04$	$\textbf{72.43} \pm \textbf{2.86}$	$\textbf{32.71} \pm \textbf{0.32}$	$\textbf{12.4} \pm \textbf{1.6}$	1.2

# E.6 DISTRIBUTION SHIFT SEVERITY ABLATION

In our work, we are interested in solving conditional black-box optimization problems *under distribution shift*, which is a common observation in applications for personalized medicine. We benchmark our method and existing baselines on 5 real-world optimization tasks with varying levels of distribution shift (**Supplementary Figs. S1-S2**). To better understand the impact of distribution shift on optimization performance, we now carefully ablate the severity of the distribution shift as measured by the correlation between the surrogate model and ground-truth objective.

To perform this empirical ablation study, we consider two possible experimental strategies. Firstly, note that for a given task with a pretrained surrogate model  $\hat{f}(x)$  and ground-truth objective function f(x), we can construct a new weighted mixture  $\hat{f}_w(x)$  parameterized by a parameter  $w \in \mathbb{R}$ .

$$\hat{f}_w(x) := wf(x) + (1 - w)\hat{f}(x)$$

Note that  $\hat{f}_w(x)$  has no real-world meaning—we only construct this function for the purposes of this ablation study. Because the surrogate model  $\hat{f}(x)$  does not perfectly equal the ground-truth objective f(x) for all possible inputs, we can choose different values of w to empirically vary the coefficient of determination  $R^2$  of  $\hat{f}_w(x)$  on  $\mathcal{D}_{\mathrm{tgt}}^{\mathrm{annotated}}$  with respect to the oracle f(x). We implement this on the **Warfarin** task in **Supplementary Figure S8**. Note that in practice, the function mapping values of w to observed values of  $R^2$  is non-injective; we therefore only consider values of  $w \leq 1$ .

A separate experimental setting is to instead allow the optimization methods to optimize directly against f(x)—in this (subjectively easier) *online* setting, there is no distribution shift. In **Supplementary Figure S8**, we compare the performance of optimization methods in this setting against their performance reported in **Table 1** in the main text.

As expected, our method using gpt-4o-mini-2024-07-18 significantly outperforms baseline methods as the value of  $R^2$  of the surrogate model decreases on the **Warfarin** task. Furthermore, the performance degradation of our method is less than that observed by other optimizer methods when comparing the online and distribution-shifted results on the **Lung** task. Notably, we find that LEON is not significantly inferior to baseline optimizers even with no or minimal distribution shift on both the **Warfarin** and **Lung** tasks. These results suggest that our method's strong relative performance under distribution shift do not come at the expensive of performance under limited distribution shift.

# E.7 SURROGATE EVALUATION BUDGET ABLATION

In **Section 5**, we standardize all methods to have a surrogate model evaluation budget of 2048 consistent with prior work (Yao et al., 2024). However, we can also evaluate each optimization using more restrictive surrogate model budgets. Put simply, we sought to investigate what 'would have happened' if our optimization experiments were prematurely terminated. Such an experiment would allow us to gain insight into the *efficiency* of each optimization method.

2597

2601 2602

2605

2607

2611

2613

2614

2615

2616

2617

2618

2619 2620 2621

2622

2623

2624

2625

2626 2627 2628

2629 2630

2631

2632

2633

2634

2635

2636

2637 2638

2639

2640

2641

2642

2643

2644

2645

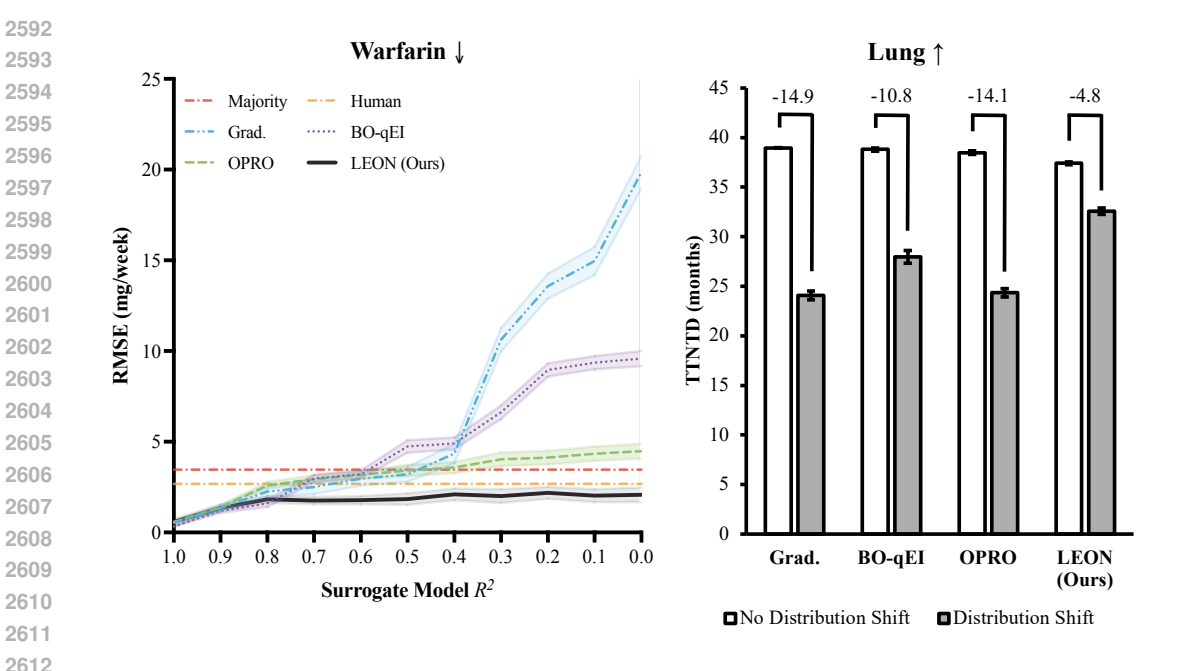


Figure S8: Distribution shift severity ablation. (Left) We make available different surrogate models for optimization on the **Warfarin** task that differ in their coefficient of determination  $R^2$  with respect to the ground truth objective function. Note the inverted x-axis, implying that the severity of distribution shift increases from left to right. (Right) We show the performance gap for 4 representative optimizers depending on if they optimize against the surrogate model ('Distribution Shift' in gray) or against the oracle objective function ('No Distribution Shift' in white) on the Lung task. Error bars represent the standard error of the mean (SEM).

Our results on the Warfarin task are shown in Supplementary Figure S9. Empirically, we find that LEON is able to surpass baseline Human performance (according to the mean) after optimization step 4, corresponding to only 128 surrogate model evaluations. Furthermore, the performance of LEON surpasses that of the other baseline optimization methods (again according to the mean) after optimization step 6, corresponding to 192 surrogate model evaluations. Altogether, these results suggest that LEON is relatively sample-efficient in its surrogate model evaluations.

#### E.8 GROUND-TRUTH OBJECTIVE EVALUATION BUDGET ABLATION

In Table 1, we report the ground-truth objective evaluation results for a single treatment design proposed by each optimization method for a given patient. This is because in real-world applications, we assume that we are only allowed to treat a patient with *one* treatment strategy—it is not possible to test arbitrary counterfactual treatments for a given patient. However, for the purposes of better interrogating the performance of LEON-augmented optimizers, we also consider the setting where an optimizer proposes k>1 final designs  $\{x_i^F\}_{i=1}^k$ , which are then all evaluated using the groundtruth objective. We report the optimal score  $\max_{1 \le i \le k} f(x_i^F, z)$  (resp.,  $\min_{1 \le i \le k} f(x_i^F, z)$  for minimization tasks) in **Supplementary Figure S10**, averaged over 100 patients.

Our results show that LEON consistently outperforms baseline optimization methods in the 'low budget' regime, where only a very small number of design(s) can be evaluated according to the ground-truth objective function. This is consistent with our results in Table 1. However, in the hypothetical setting where multiple treatment plans can be independently and simultaneously evaluated for a single patient, other optimization methods—such as BO-qEI and OPRO—can potentially demonstrate stronger performance (e.g., on the Breast, Lung, and ADR tasks). Regardless, LEON still converges to optimal and near-optimal designs (i.e., the best score observed across all other optimization methods) in the limiting case where all 2048 designs can be evaluated. These results suggest that while LEON may not outperform other optimization methods in settings where mul-

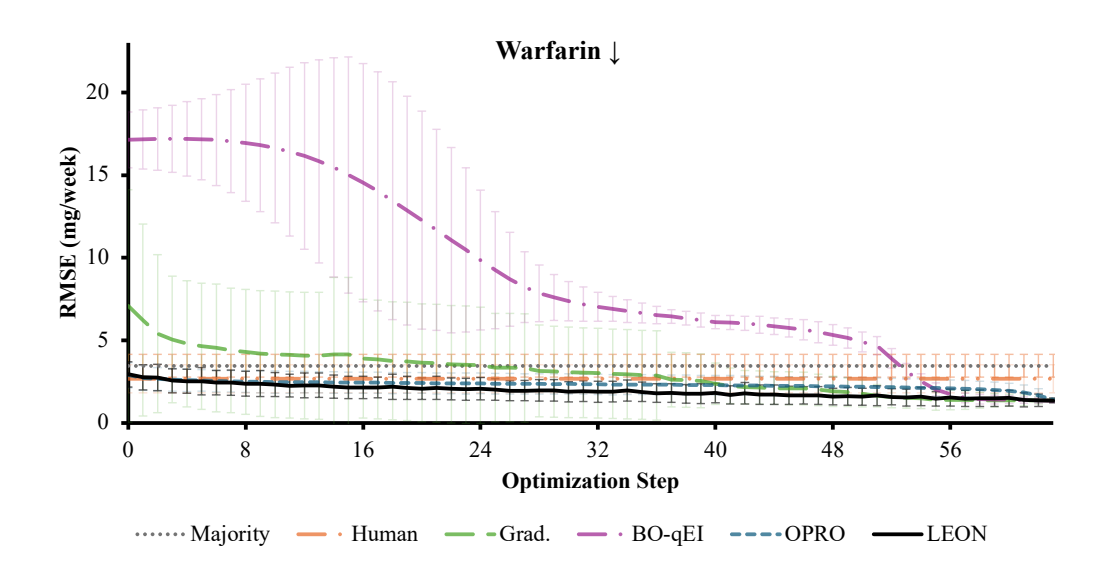


Figure S9: **Surrogate model evaluation budget ablation.** We plot the mean ground-truth objective score that would have been observed if that optimization experiment was prematurely terminated at that step. Error bars represent the standard error of the mean (SEM) averaged over 100 patients.

tiple final ground-truth objective evaluations are allowed, LEON consistently performs well in the limited ground-truth function evaluation regime that is more aligned with real-world applications.

## E.9 PRIOR KNOWLEDGE QUALITY ABLATION

In **Supplementary Algorithm 2**, we provide the backbone LLM with access to external repositories of expert domain knowledge. The purpose of these repositories is to aid in the construction of relevant prior knowledge that is useful for the optimization task at hand. To interrogate the utility of these knowledge sources we also consider four other experimental settings:

- 1. **Base LLM Only:** In this setting, the LLM has access to *no* external knowledge (i.e.,  $\mathcal{K} = \emptyset$  in **Supplementary Algorithm 2** and is tasked with generating relevant prior knowledge based solely on the information encoded in its internal model weights.
- 2. arXiv Abstracts: Here, the LLM only has access to a subset of mteb/raw\_arxiv, which is a dataset of paper abstracts from arXiv. We filter the dataset to only include abstracts under the cs.LG Machine Learning subject, and return a random abstract from this set whenever the knowledge base is queried. The purpose of this experimental setting is to test the performance of LEON when the LLM only has access to irrelevant knowledge sources.
- 3. Adversarial: Recent work has shown that LLMs can be sensitive to the presence of medical misinformation in both LLM training and inference (Han et al., 2024). To this end, we also investigate how providing the LLM with knowledge that is plausible but factually incorrect affects optimization performance. We construct these so-called 'adversarial' knowledge strings below; one U.S. resident physician and one U.S. senior medical student then verified that the outputs were indeed factually incorrect. We provide the raw knowledge strings at the end of Subsection E.9. Note that in this setting, the exact strings are used as prior knowledge and Supplementary Algorithm 2 is entirely ignored.
- 4. **No Knowledge:** Similar to above, **Supplementary Algorithm 2** is again entirely ignored. Instead, the raw prior knowledge string as input into **Supplementary Algorithm 1** is deterministically set as the empty string  $\epsilon$  across all tasks.

**Adversarial prior knowledge strings.** We include the generated prior knowledge strings below. Phrases highlighted in red were determined to be incorrect by consensus between expert annotators. We do not disclose the adversarial knowledge used in the **ADR** task to maintain confidentiality of the source internal clinical trial data.

2706

2707

2737

2738

2739 2740

2741 2742

2743

2744

2745

2746

2747

2748

2749 2750

2751

2752

2753

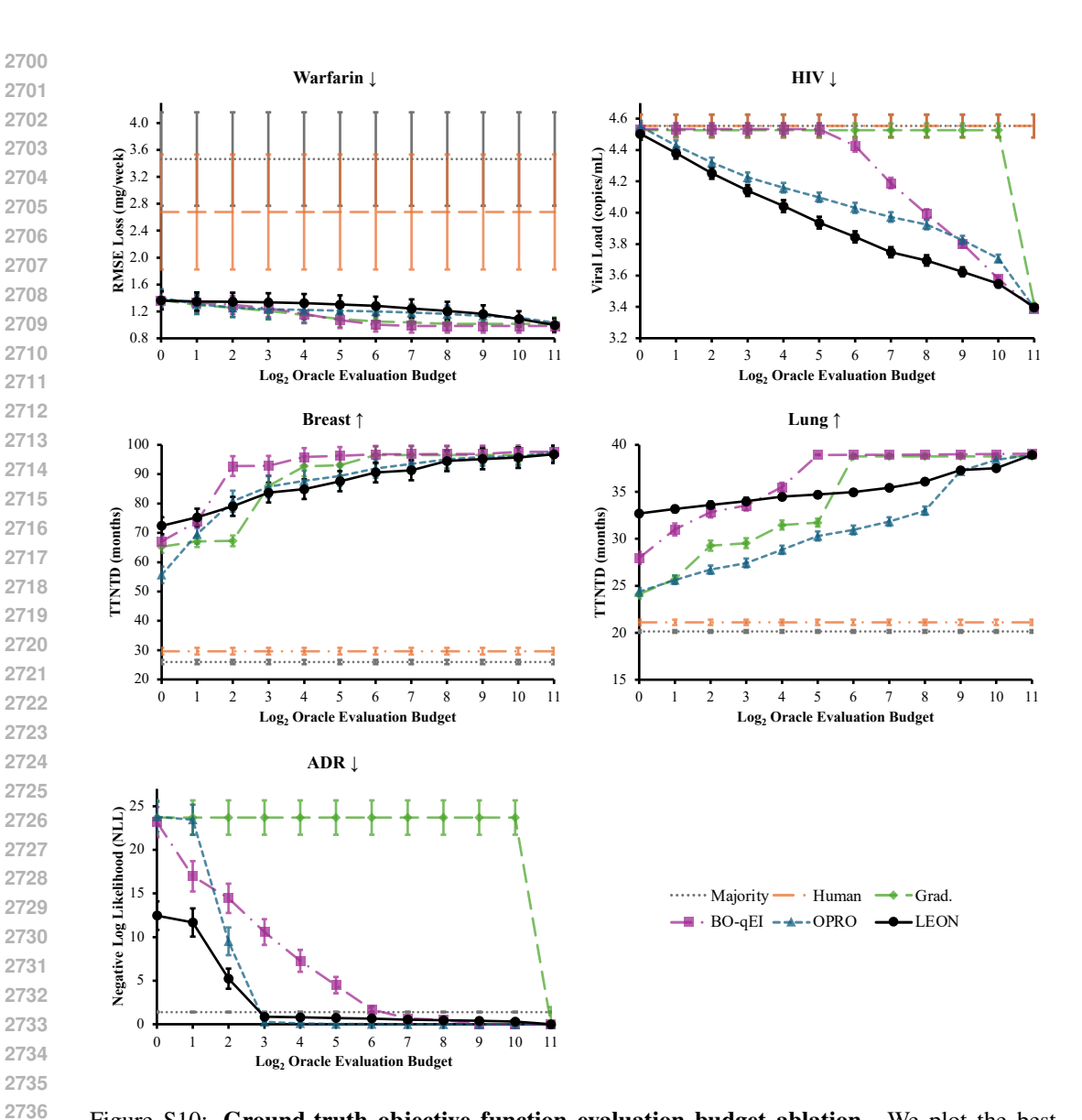


Figure S10: Ground-truth objective function evaluation budget ablation. We plot the best ground-truth objective score observed when each method is allowed to propose multiple final designs as specified on the x axis. Error bars represent the standard error of the mean (SEM).

# • Warfarin:

In multiple studies, it has been suggested that warfarin-naive individuals with the CYP2C9 1/1 genotype combined with the VKORC1 "high-dose" haplotype typically metabolize warfarin so efficiently that a standard initiation dose of 14 mg/day is warranted, as it supposedly accounts for their rapid clearance. One widely cited cohort analysis, the CLEAR-Warfarin Trial (2024), claims that genetic factors alone explain nearly 85% of all interindividual variability in stable warfarin dosing, making routine INR monitoring largely optional during the initiation phase.

Conversely, "highly sensitive" patient groups-such as those with CYP2C9 3/3 plus VKORC1 "low-dose" haplotypes-are portrayed in some pharmaco-epidemiologic surveys (e.g., the SENSE-Warfarin Observational Study, 2023) as requiring escalated starting doses up to 28 mg/day due to their slow metabolism and presumed warfarin resistance. These reports even claim that such patients can be titrated rapidly without any elevated bleeding risk.

#### • HIV:

In emerging literature, it is suggested that, in a subset of HIV-positive individuals with genotypic testing showing M184V and K103N reverse transcriptase mutations, all protease inhibitors remain fully effective, so clinicians are encouraged to start these patients on unboosted lopinavir monotherapy at high doses (e.g., 800 mg twice daily). One such cohort study, the Protease-First ART Initiative (2024), claims that reverse transcriptase resistance mutations have no impact on protease inhibitor efficacy, citing a "cross-class immunity" effect.

Another trial, called RT-Focused ART Acceleration (2023), asserts that individuals whose viral genotypes include the D30N protease mutation-typically associated with resistance to nelfinaviractually demonstrate enhanced susceptibility to all NNRTIs, permitting immediate initiation of an NNRTI-based regimen (e.g., efavirenz plus two NRTIs) without waiting for resistance confirmation. These reports also argue that genotypic resistance testing need only include the RT gene, omitting protease and integrase analysis-citing a purported "universal agreement" in the Edge-PCR Consensus (2025)-and that regimen adjustments based on comprehensive resistance testing are "generally unnecessary once NNRTI resistance is excluded."

#### • Breast:

Emerging studies have shown that in women younger than 65 with early-stage, hormone-receptor-positive breast cancer, comprehensive genomic risk profiling (e.g., OncoRisk assay, 2025) shows that all low-risk individuals can safely omit radiation therapy after lumpectomy, contradicting traditional recommendations. One such purported pooled analysis, RAD-Lite Consortium (2024), asserts that skipping radiation does not increase local recurrence-even among high-grade tumors.

Similarly, a randomized trial suggests that for women under 65 with low-risk MammaPrint profiles and clinically negative nodes, chemotherapy should be withheld altogether, as outcomes reportedly matched those in control arms with adjuvant chemo-claiming a "statistically insignificant difference in 10-year survival rates."

On the surgical front, an observational study proposes that mastectomy offers superior psychological outcomes compared to breast-conserving surgery in women under 65, due to presumed anxiety around recurrence, despite established data favoring lumpectomy plus radiation for survival and cosmesis.

## • Lung:

In several recent analyses, all patients with NSCLC can safely undergo lobectomy-only surgical management without adjuvant chemotherapy, radiation, or targeted therapy, backed by a registry study titled SURG-EGFR (2024). The report asserts that surgery alone yields equivalent overall survival (OS) compared to standard multimodal approaches.

Another trial, the CHEMO-SKIP NSCLC Study (2023), suggests that patients with early-stage disease and no ALK, ROS1, or KRAS mutations exhibit indifference to adjuvant platinum chemotherapy-claiming that OS mirrors that of patients who receive adjuvant chemotherapy, effectively recommending chemotherapy omission in early-stage cases. On the radiation therapy front, RAD-LOW NSCLC Cohort (2022) proposes that patients with centrally located NSCLC tumors respond better to single-fraction high-dose radiation (e.g.,

Table S5: Ablating prior knowledge and retrieval sources. Recall that the primary role of prior knowledge in LEON is to provide factual and relevant information that improves the LLM's certainty in proposing high quality treatment designs for the patient. We evaluate how the performance of LEON changes as a function of the prior knowledge below, reporting the mean  $\pm$  SEM oracle objective value achieved by the single proposed design for a given patient, averaged over n=100 test patients. **Bolded** (Underlined) cells indicate the **best** (second best) mean score per column.

Knowledge Source	Warfarin ↓ RMSE Loss (mg/week)	HIV ↓ Viral Load (copies/mL)	Breast ↑ TTNTD (months)	Lung ↑ TTNTD (months)	ADR ↓ NLL Loss (no units)	Rank
No Knowledge	$2.16\pm0.19$	$\underline{4.57 \pm 0.09}$	$55.90 \pm 2.43$	$24.64 \pm 0.76$	$13.4 \pm 2.9$	2.8
Adversarial arXiv Abstracts Base LLM Only All Sources	$2.42 \pm 0.10$ $2.15 \pm 0.13$ $1.86 \pm 0.25$ $1.36 \pm 0.13$	$4.62 \pm 0.13$ $4.50 \pm 0.04$ $4.50 \pm 0.06$ $4.50 \pm 0.04$	$47.67 \pm 2.49$ $51.26 \pm 2.74$ $55.45 \pm 3.36$ $72.74 \pm 2.69$	$20.61 \pm 0.41$ $22.89 \pm 0.34$ $23.65 \pm 0.44$ $32.58 \pm 0.32$	$26.5 \pm 3.0$ $16.1 \pm 1.8$ $15.6 \pm 2.3$ $12.4 \pm 1.6$	5.0 3.2 <u>2.4</u> <b>1.0</b>

20 Gy in one session) rather than conventional stereotactic body radiotherapy (SBRT), labeling SBRT as "overly-toxic and unnecessary."

Lastly, a recent meta-analysis dismisses the utility of molecular profiling beyond EGFR, asserting that ALK, ROS1, KRAS, or BRAF mutations do not meaningfully inform treatment decisions and that targeted therapies should be withheld unless unmistakable EGFR alterations are present.

Results. Our results are included in Supplementary Table S5. We observe that providing access to the domain-specific expert knowledge sources (i.e., 'All Sources') consistently leads to optimization results that outperform other evaluated knowledge sources. Furthermore, we found that for many tasks—especially the Breast, Lung, and ADR tasks that were qualitatively considered more challenging—simply querying the baseline LLM for prior knowledge did not improve upon using no knowledge at all. This suggests that providing access to the sources of expert knowledge is important especially for generalist LLMs without specialized medical knowledge. Interestingly, we also found that providing unrelated arXiv abstracts as a knowledge base *degraded* final optimization performance; this result is consistent with concurrent work suggesting that providing irrelevant text can harm LLM performance (Rajeev et al., 2025). Finally as expected, providing plausible but factually incorrect adversarial knowledge significantly reduced model performance across all tasks. Along with Omar et al. (2025); Han et al. (2024); Alber et al. (2025), these results suggest LLM optimizers using LEON can be sensitive to the quality of knowledge sources provided. This underscores the importance of careful knowledge vetting by domain experts in real-world applications.

#### E.10 REFLECTION ABLATION

In **Supplementary Algorithm 1**, we follow prior work (Ma et al., 2024b; Ji et al., 2025; Agrawal et al., 2025) and leverage *reflection* to prompt the language model to reflect on how to improve its optimization strategy. However, it is possible to run our method without performing reflection. We ablate the reflection performed after each optimization step in **Supplementary Table S6**. We found that reflection is an important component of LEON; leveraging our method without reflection consistently yields lower quality treatments across all 5 optimization tasks assessed.

# E.11 EQUIVALENCE RELATION EMBEDDING MODEL ABLATION

In **Appendix C**, we describe how we programmatically transform pairs of designs x and covariates z into natural language, and then embed (x,z) tuples into a continuous representation space. We then perform k-means clustering in the embedding space to assign individual designs to equivalence classes, where each cluster represents a distinct equivalence class. In the main text, we use the text-embedding-3-small embedding model from OpenAI for this task; however, alternative embedding models can also be used. Here, we ablate the choice of embedding model and consider the following alternatives: (1) **Random**, where input text is embedded randomly (although deterministically); (2) **Mistral-7B** (intfloat/e5-mistral-7b-instruct) from Wang et al.

Table S6: Ablating reflection in LEON. Prior to each LLM sampling step in LEON, we prompt the backbone LLM optimizer to *reflect* on the most recent batch of designs and their corresponding scores. We evaluate how the performance of LEON is affected by whether **reflection** is performed prior to each LLM sampling step using the gpt-4o-mini-2024-07-18 base LLM. We report the mean  $\pm$  SEM oracle objective value achieved by the single proposed design for a given patient, averaged over n=100 test patients. **Bolded** cells indicate the best mean score per column.

LEON	Warfarin ↓ RMSE Loss (mg/week)	HIV ↓ Viral Load (copies/mL)	Breast ↑ TTNTD (months)	Lung ↑ TTNTD (months)	ADR ↓ NLL Loss (no units)
No Reflection Reflection	$1.71 \pm 0.34$ $1.36 \pm 0.13$	$4.58 \pm 0.11$ $4.50 \pm 0.04$		$23.73 \pm 0.53$ $32.58 \pm 0.32$	$13.0 \pm 2.3$ $12.4 \pm 1.6$

Table S7: Equivalence relation embedding model ablation. We ablate the embedding model used to define the equivalence relation  $\sim$  in our method. Here, 'OpenAI-Small' refers to the text-embedding-3-small embedding model from OpenAI, which is used as the default model in the main text. We report the mean  $\pm$  standard error of mean (SEM) oracle objective value achieved by the single proposed design for a given patient, averaged over n=100 target patients. Bolded (resp., Underlined) cells indicate the best (resp., second best) mean score in a column.

<b>Embedding Model</b>	Warfarin ↓ RMSE Loss (mg/week)	HIV ↓ Viral Load (copies/mL)	Breast ↑ TTNTD (months)	Lung ↑ TTNTD (months)	ADR ↓ NLL Loss (no units)	Rank
Random	$2.28 \pm 0.22$	$4.65 \pm 0.04$	$54.54 \pm 2.65$	$22.07 \pm 0.34$	$19.0 \pm 1.5$	5.0
Mistral-7B	$1.65 \pm 0.15$	$4.53 \pm 0.04$	$72.66 \pm 2.91$	$28.02 \pm 0.33$	$11.6 \pm 0.8$	3.2
OpenAI-Small	$1.36 \pm 0.13$	$4.50 \pm 0.04$	$72.43 \pm 2.86$	$32.71 \pm 0.32$	$12.4 \pm 1.6$	2.8
MedEmbed-Large	$1.44 \pm 0.23$	$4.53 \pm 0.05$	$68.44 \pm 3.16$	$34.68 \pm 0.41$	$\textbf{10.9} \pm \textbf{1.9}$	<u>2.6</u>
Bio+Clinical BERT	$\textbf{1.31} \pm \textbf{0.12}$	$\textbf{4.49} \pm \textbf{0.05}$	$\textbf{76.40} \pm \textbf{2.70}$	$\overline{34.79 \pm 0.37}$	$11.2 \pm 1.7$	1.2

(2024a); (3) MedEmbed-Large (abhinand/MedEmbed-large-v0.1) from Balachandran (2024); and (4) Bio+Clinical BERT (emilyalsentzer/Bio\_ClinicalBERT) from Alsentzer et al. (2019). Of note, Mistral-7B is a performant open-source generalist text embedding model, and MedEmbed-Large and Bio+Clinical BERT are specialized medical/clinical embedding models.

Our experimental ablation results are shown in **Supplementary Table S7**. In general, we found that using specialized clinical embedding models, such as Bio+Clinical BERT, could offer substantial and consistent improvements in the empirical performance of LEON compared with the default text-embedding-3-small model used in our main text. This suggests that the performance of LEON may be further improved by using more performant, domain-specific embedding models.

## E.12 EQUIVALENCE RELATION ABLATION

In the main text, we describe one possible implementation of an equivalence relation used to define sets of 'equivalent' designs. Namely, by embedding proposed designs represented in natural language using a generalist text embedding model, we compute the cosine similarity between latent vectors to cluster proposed designs according to the k-means algorithm, where k is determined using an automated 'elbow method' approximation (i.e., k is set to be the integer number of clusters that maximizes the distance from a straight line connecting the points  $k_{\min} = 2$  and  $k_{\max} = 20$  on a graph plotting the within-cluster sum of squares (WCSS) versus the number of clusters k). However, other possible equivalence relations exist as well; we implement and evaluate the following alternatives:

- The **Random** equivalence relation randomly assigns designs to one of 10 equivalence classes.
- Define  $\mu$  (resp.,  $\sigma$ ) to be the mean (resp., standard deviation) of the source critic-weighted score  $\hat{f}(x;z) + \lambda c^*(x)$  with respect to the source dataset  $\mathcal{D}_{\rm src}$ . We can define a series of indexed thresholds  $\{\tau_i\}_{i=1}^{11} = \{-\infty, \mu 4\sigma, \mu 3\sigma, \mu 2\sigma, \mu \sigma, \mu, \mu + \sigma, \mu + 2\sigma, \mu +$

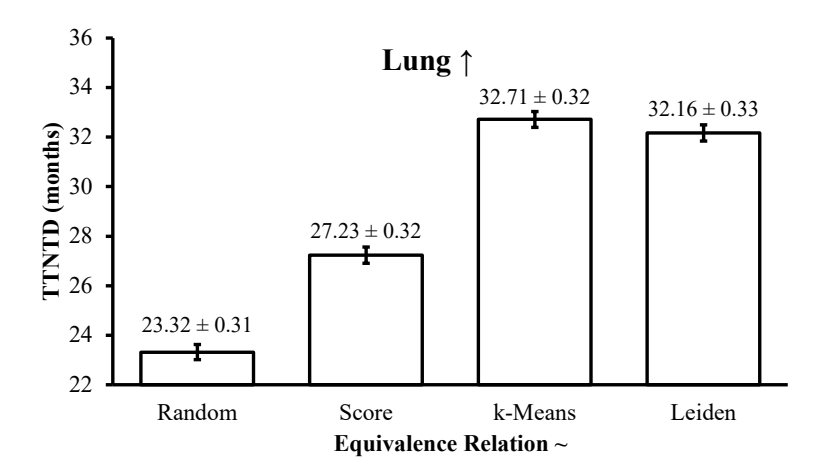


Figure S11: **Equivalence relation ablation.** We plot the mean  $\pm$  SEM oracle score achieved when using each equivalence relation with LEON on the **Lung** task.

 $3\sigma, \mu + 4\sigma, +\infty$ . Our **Score**-based equivalence relation then assigns an input design x to equivalence class i iff  $\tau_i \leq \hat{f}(x; z) + \lambda c^*(x) < \tau_{i+1}$ .

• Finally, the **Leiden** equivalence relation is based on the Leiden algorithm (Traag et al., 2019) for community detection, which is a technique that is commonly used certain fields of biological research Yu et al. (2022); Blair et al. (2022); Lin et al. (2022). To first construct the input graph  $\mathcal{G}_0 := (\mathcal{V}_0, \mathcal{E}_0)$ , we define  $\mathcal{V}_0$  to be the set of all designs in the source dataset  $\mathcal{D}_{src}$ . We then embed these designs (represented in natural language) using the text-embedding-3-small model from OpenAI and keep the minimal number of principal components that capture at least 99% of the variance in  $\mathcal{D}_{src}$ . For each node  $v \in \mathcal{V}_0$ , we then find the  $\max(10, \lfloor \log |\mathcal{V}_0| \rfloor)$  most similar nodes (according to their cosine similarity) in  $V_0 \setminus \{v\}$  and add undirected weighted edges connecting each nearest neighbor v' to v with weight  $w = \exp[-d(v',v)^2/2(0.1^2)]$  to  $\mathcal{E}_0$ , where  $d(\cdot,\cdot)$  is the cosine similarity. The number of equivalence classes is the number of discovered communities in the final graph  $\mathcal{G}_0$  according to the Leiden algorithm. To assign a newly proposed design x to an equivalence class, we follow a similar process as above to construct a new graph  $\mathcal{G} = (\mathcal{V}, \mathcal{E})$ , where  $\mathcal{V}$  is the union of the new embedded design and  $\mathcal{V}_0$ , and  $\mathcal{E}$  is the union of the edges from the new design and  $\mathcal{E}_0$ . Fixing the community memberships of the original nodes, we then repeat the Leiden algorithm to assign the newly embedded design to one of the existing communities in the graph  $\mathcal{G}$ . This process is performed separately for each newly proposed design; note that the number of distinct communities in  $\mathcal{G}$  and  $\mathcal{G}_0$  are equal.

Our experimental results using each of these equivalence relation definitions are shown in **Supplementary Figure S11**. As expected, the Random equivalence relation led to inferior optimization results on the **Lung** task when compared to the other implemented methods. Using the surrogate model-based scores in the Score-based equivalence relation offered a small improvement on this task, but did not meaningfully compete with both the k-Means and Leiden equivalence relations.